

Some pages of this thesis may have been removed for copyright restrictions.

If you have discovered material in AURA which is unlawful e.g. breaches copyright, (either yours or that of a third party) or any other law, including but not limited to those relating to patent, trademark, confidentiality, data protection, obscenity, defamation, libel, then please read our [Takedown Policy](#) and [contact the service](#) immediately

EFFECTS OF RELATIVE HUMIDITY ON
INHALATION AEROSOLS

Cheryl Vanessa Groom B.Sc.

submitted for the degree of Doctor of Philosophy
of The University of Aston in Birmingham.

September, 1981.

SUMMARY

Most drugs employed in inhalation therapy are water-soluble and when exposed to the high humidity of the respiratory tract will attempt to achieve thermodynamic equilibrium by exchange of water vapour and heat. Techniques for predicting the growth of a single water-soluble compound at 99.5% relative humidity from the physicochemical characteristics of its aqueous solution are described and results presented for several drugs currently used in inhalation therapy.

From this data, changes in particle size distributions at 99.5% relative humidity have been determined. Using a computer model of deposition in the human respiratory tract after mouth-breathing based on published data, the effect of this size change on the site and amount of deposition have been examined. Different deposition patterns are predicted for different salts of the same drug for the same original dry powder size distributions.

The techniques are not however applicable with multicomponent aerosols, for example those generated using a pressure pack. In this instance direct measurement of the size distribution under conditions of high humidity is desirable. The cascade impactor can be used to study the changes in distribution of drug amongst different aerodynamic size fractions of complex mixtures.

The design of a controlled temperature and humidity apparatus is described. The use of this apparatus has been validated using a single water-soluble model inhalation aerosol:- fluorescein disodium. The experimentally determined aerodynamic growth ratios have been compared with those predicted from the physicochemical characteristics of aqueous fluorescein disodium solutions.

The in vitro work predicts that changes in particle size due to hygroscopic growth will effect both site and amount of deposition. Chapter six is devoted to the development of a technique capable of providing information on the systemic availability of a compound administered in various inhalation aerosol formulations.

Good systemic availability ($B_f > 0.90$) has been shown for intratracheal instillations of 8.2mg to 30.5mg of fluorescein⁻ in aqueous solutions.

Keywords:

AEROSOL HUMIDITY ISO-OSMOTIC IMPACTOR BIOAVAILABILITY

To Paul

and

S.A.A

ACKNOWLEDGEMENTS

I would like to thank all the staff and students of the University of Aston in Birmingham who have assisted in this study by helpful discussion and moral support.

Special thanks are extended to my supervisor Dr. I. Gonda and to Dr. P. R. Byron and Dr. A. R. Clark of the Pharmacy Department and Dr. F. J. T. Fildes of ICI Pharmaceutical Division, Alderley Edge.

I wish to thank the Science Research Council and ICI Pharmaceutical Division for their financial support of these studies.

I would also like to thank all those who have assisted in the preparation of this thesis especially Paul Groom for the drawings and Miss Sharon Arnold for the typing.

LIST OF CONTENTS

		Page
Chapter 1	INTRODUCTION	1
Chapter 2	PREDICTION OF EQUILIBRIUM DIAMETERS OF INHALATION AEROSOL IN THE RESPIRATORY TRACT	19
2.1	Introduction	19
2.2	Experimental	23
2.2.1	Vapour pressure osmometry	23
2.2.1.1	Calibration of vapour pressure osmometer	23
2.2.1.2	Preparation of test solutions	24
2.2.1.3	Measurement of water activity	24
2.2.2	Density measurements	25
2.2.2.1	Density of dry powders	25
2.2.2.2	Density of solutions	25
2.2.3	Surface tension measurement	26
2.3	Results	28
2.3.1	Vapour pressure osmometry	28
2.3.1.1	Calibration of vapour pressure osmometer	28
2.3.1.2	Water activity of test solutions	29
2.3.2	Density results	29
2.3.2.1	Density of dry powders	29
2.3.2.2	Density of aqueous dry solutions	30
2.3.3	Surface tension measurements	30
2.3.3.1	Calibration of instrument	30
2.3.3.2	Surface tension of aqueous drug solutions	31
2.4	Calculation of growth ratios	32
2.5	Discussion	35
2.6	Tables	37
2.7	Figures	41
Chapter 3	PREDICTED DEPOSITION OF INHALATION AEROSOLS IN THE RESPIRATORY TRACT	51
3.1	Introduction	51
3.2	Size distributions of inhaled aerosols	54
3.3	Deposition model for mouth inhalation	56
3.4	Calculated deposition of inhaled aerosols	59
3.5	Discussion	61

		Page
3.6	Figures	63
Chapter 4	AEROSOL SIZING BY CASCADE IMPACTORS	72
4.1	Introduction	72
4.2	Experimental Procedures	76
4.2.1	Generation of monodisperse aerosols	76
4.2.2	Quantitative determination of fluorescein	78
4.2.2.1	Effect of pH on the absorbance of fluorescein	78
4.2.2.2	Determination of emission wavelength maximum	78
4.2.2.3	Determination of excitation wavelength maximum	79
4.2.2.4	Quantitative determination of fluorescein	79
4.2.2.5	Fluorescein recovery from the collection surfaces	86
4.2.3	Preparation of collection surfaces	81
4.2.4	Determination of collection efficiencies	81
4.3	Results	83
4.3.1	Monodisperse aerosol generation	83
4.3.2	Quantitative determination of fluorescein	83
4.3.2.1	The effect of pH on the absorbance of fluorescein	83
4.3.2.2	Determination of emission maximum	84
4.3.2.3	Determination of excitation maximum	84
4.3.2.4	Quantitative determination of fluorescein	84
4.3.2.5	Fluorescein recovery from collection surfaces	85
4.3.3	Collection efficiency of different collection surfaces	85
4.3.4	Calibration of DCI-6 impactor	86
4.4	Data Inversion	88
4.5	Expansion Humidity in the cascade impactor	91
4.6	Conclusion	94
4.7	Tables	96
4.8	Figures	101
Chapter 5	THE EFFECT OF RELATIVE HUMIDITY ON THE PARTICLE SIZE OF INHALATION AEROSOLS	118
5.1	Introduction	118
5.2	Controlled temperature and humidity apparatus	122
5.2.1	Design considerations	122

		Page
5.2.2	Final Design	125
5.3	Experimental	127
5.3.1	Prediction of equilibrium growth of fluorescein disodium aerosols from bulk solution data	127
5.3.2	Nebuliser characteristics	128
5.3.3	Fluorescein disodium aerosol size distribution with varying relative humidity	130
5.3.3.1	Humidity levels during aerosol sizing experiments	132
5.4	Results and Calculations	133
5.4.1	Predicted growth of fluorescein disodium aerosols with varying relative humidity	133
5.4.2	Nebuliser characteristics	134
5.4.3	Fluorescein disodium aerosol size distributions with varying relative humidity	136
5.5	Discussion	139
5.6	Tables	141
5.7	Figures	145
Chapter 6	DEVELOPMENT OF AN <u>IN VIVO</u> MODEL FOR OPTIMISING SYSTEMIC DRUG DELIVERY BY INHALATION AEROSOL ADMINISTRATION	155
6.1	Introduction	155
6.2	Experimental	160
6.2.1	Determination of fluorescein ⁼ (II) in plasma and urine	160
6.2.2	The pharmacokinetics of fluorescein ⁼ (II)	161
6.2.2.1	Preparation of intravenous solutions for injection	162
6.2.2.2	Intravenous dose ranging study	162
6.2.2.3	Intratracheal administration	164
6.3	Results and Discussion	165
6.3.1	Quantitative determination of fluorescein ⁼ (II) in plasma and urine	165
6.3.2	The pharmacokinetics of fluorescein ⁼ (II)	166
6.3.2.1	Linear pharmacokinetics	166
6.3.2.2	Non-linear pharmacokinetics	171
6.3.2.3	Intratracheal instillation	177

		Page
6.4	Conclusions	181
6.5	Tables	183
6.6	Figures	189
Chapter 7	DISCUSSION AND SUGGESTED FUTURE WORK	212
Appendix 1	Water activity of solutions used in calibration	216
Appendix 2	Calibration curves for the Knauer vapour pressure osmometer percentage full scale detection versus negative natural logarithm of water activity	218
Appendix 3	Description of DABRA79 -proportional power controller	219
Appendix 4	Analog computer circuitry to model two- -compartment open body model	221
Appendix 5	Publications	222
REFERENCES		255

LIST OF FIGURES

	Page
Figure 1.1 Schematic diagram of the Spinhaler (Fisons Ltd., Loughborough) powder insufflator	11
Figure 1.2 Growth ratio versus relative humidity of a hypothetical water-soluble aerosol	16
Figure 2.1 Schematic diagram of the vapour pressure osmometer	43
Figure 2.2 Saturation vapour pressure, p , versus temperature T , for solvent and solution	44
Figure 2.3 Instrumental response of the Knauer vapour pressure osmometer (sensitivity setting 16) versus the negative of the natural logarithm of water activity at 25° C for sodium chloride, potassium chloride, calcium chloride and sucrose	45
Figure 2.4 Water activity versus molality for aqueous solutions of isoprenaline hydrochloride at 37° C isoprenaline sulphate at 37° C, salbutamol sulphate at 37° C and disodium cromoglycate at 37° C and 25° C	46
Figure 2.5 Density of aqueous solutions of disodium cromoglycate, salbutamol sulphate, isoprenaline hydrochloride, and isoprenaline sulphate at 37° C	47
Figure 2.6 Calibration of surface tension apparatus, instrumental response versus surface tension.	48
Figure 2.7 Surface tension against molality at 37° C for aqueous solutions of disodium cromoglycate, isoprenaline hydrochloride, isoprenaline sulphate and salbutamol sulphate.	49
Figure 2.8 Percentage error caused by neglecting the Kelvin effect in calculation of equilibrium droplet size	50
Figure 3.1 Cumulative mass size distribution of disodium cromoglycate (DSCG). Percent undersize versus equivalent volume diameter of dry powder.	64
Figure 3.2 Cumulative mass size distribution of DSCG. Percent weight undersize versus aerodynamic diameter of the dry powder and droplets in equilibrium with 99.5% relative humidity.	65

	Page	
Figure 3.3	Cumulative mass size distribution of Isoprenaline Sulphate (courtesy of Riker Laboratories) Percent weight undersize versus equivalent volume diameter of dry powder	66
Figure 3.4	Cumulative weight versus aerodynamic diameter of Isoprenaline Sulphate of the dry powder and droplets in equilibrium with 99.5% relative humidity.	67
Figure 3.5	Cumulative weight versus aerodynamic diameter of Isoprenaline Hydrochloride of the dry powder, and droplets in equilibrium with 99.5% relative humidity	68
Figure 3.6	Model for deposition: Fraction deposited versus aerodynamic diameter, 750ml tidal volume, 15 respirations per minute for mouth breathing	69
Figure 3.7	Model for deposition: Fraction deposition versus aerodynamic diameter, 1250ml tidal volume, 15 respirations per minute for mouth breathing	70
Figure 3.8	Model for deposition: Fraction deposited versus aerodynamic diameter, 2150 ml tidal volume, 15 respirations per minute for mouth breathing	71
Figure 4.1	Schemation diagram of aerosol collection by cascade impactor a) ideal collection efficiencies and b) non-ideal collection efficiencies	103
Figure 4.2	Schematic diagram of the apparatus for determination of collection efficiencies	104
Figure 4.3	Scanning electromicrograph of fluorescein disodium particle generated using the vibrating orifice generator	105
Figure 4.4	Effect of pH on absorbance of 7.6 μ m solution of fluorescein disodium at 492nm	106
Figure 4.5	Percentage transmission of 5.5ng per ml solution of fluorescein versus emission wavelength (excitation wavelength 486nm)	107
Figure 4.6	Percentage transmission of 5.5ng per ml solution of fluorescein ⁼ versus excitation wavelength (emission wavelength 516nm)	108
Figure 4.7	Relative intensity versus concentration of fluorescein ⁼ in buffer (pH 12)	109
Figure 4.8	Collection efficiency versus aerodynamic diameter for stage 1 of DCI 5 cascade impactor	110
Figure 4.9	Collection efficiency versus aerodynamic diameter for stage 1 of DCI 6 cascade impactor	111

Figure 4.10	Collection efficiency versus aerodynamic diameter for stage 2 of DCI 6 cascade impactor	112
Figure 4.11	Collection efficiency versus aerodynamic diameter for stage 3 of DCI 6 cascade impactor	113
Figure 4.12	Collection efficiency versus aerodynamic diameter for stage 4 of DCI 6 cascade impactor	114
Figure 4.13	Collection efficiency versus aerodynamic diameter for stage 5 of DCI 6 cascade impactor	115
Figure 4.14	Collection efficiency versus aerodynamic diameter for stage 6 of DCI 6 cascade impactor	116
Figure 4.15	Mean collection efficiency versus square root of impaction parameter for DCI 6 cascade impactor	117
Figure 5.1	Temperature fluctuations in the equilibrium chamber reservoir when a bandwidth of 0.5° C is used on the proportional temperature controller	146
Figure 5.2	Schematic diagram of the controlled temperature and humidity apparatus	147
Figure 5.3	Determination of flow rate through the Bird nebuliser versus inlet gauge pressure: Schematic diagram of apparatus.	148
Figure 5.4	Water activity of aqueous fluorescein disodium solution versus concentration	149
Figure 5.5	Density of aqueous fluorescein disodium solutions at 37° C	150
Figure 5.6	Calculated aerodynamic growth ratio versus relative humidity for fluorescein disodium	151
Figure 5.7	Bird nebuliser operating characteristic: Air flow rate versus gauge pressure. Single determinations are shown	152
Figure 5.8	Bird nebuliser operating characteristics: total output versus inlet gauge pressure	153
Figure 5.9	Aerodynamic growth ratio versus relative humidity for disodium fluorescein aerosols	154
Figure 6.1	The chemical structure of fluorescein disodium (I) and fluorescein ⁻ (II)	193
Figure 6.2	Relative Intensity (Equation 6.1) versus concentration for Fluorescein ⁻ (II) in plasma and urine .	194

	Page	
Figure 6.3	Plasma concentration versus time profiles for II after iv administration as solution boli. $[Do]_{iv}$ was 0.43mg and 3.4mg	195
Figure 6.4	Plasma concentration versus time profile of II after iv administration as solution boli. $[Do]_{iv}$ was 8.2mg and 10.8mg	196
Figure 6.5	Plasma concentration versus time profile of II after iv administration as solution bolus. $[Do]_{iv}$ was 11.4mg	197
Figure 6.6	Plasma concentration versus time profiles for II after iv administration as solution boli. $[Do]_{iv}$ was 13.6mg and 13.95mg (two experiments)	198
Figure 6.7	Plasma concentration versus time profiles for II after iv administration as solution boli. $[Do]_{iv}$ was 18.0mg and 33.0mg.	199
Figure 6.8	Plasma concentration versus time profiles for II after iv administration as solution bolus. $[Do]_{iv}$ was 123mg	200
Figure 6.9	Area under iv plasma concentration $[AUC]_{iv}^{5 \rightarrow 60}$ versus time profiles (t=5 to t=60) versus $[Do]_{iv}$	201
Figure 6.10	Plasma concentration divided by dose ($C_p/[Do]_{iv}$) versus time for $[Do]_{iv} \leq 11.4mg$ (data from Figure 6.3 to 6.5).	202
Figure 6.11	Total area $[AUC]_{iv}^{0 \rightarrow \infty}$ under plasma concentration versus time profile as a function of iv dose, $[Do]_{iv}$ when $[Do]_{iv} \leq 11.4mg$	203
Figure 6.12	Cumulative amount of II excreted in urine after 18mg iv bolus.	204
Figure 6.13	Plasma concentration time profile after 0.43mg iv bolus to anaesthetised and conscious dog	205
Figure 6.14	Plasma concentration of II (linear scale) versus time profile after administration of 123mg iv bolus	206
Figure 6.15	Plasma concentration versus time profile for II after $[Do]_{it} = 8.6mg$ intratracheal instillation	207
Figure 6.16	Plasma concentration versus time profile for II after $[Do]_{it} = 19.0mg$ intratracheal instillation	208

		Page
Figure 6.17	Plasma concentration versus time profile for II after $[Do]_{it} = 28.2\text{mg}$ intratracheal instillation	209
Figure 6.18	Plasma concentration versus time profile for II after $[Do]_{it} = 30.5\text{mg}$ intratracheal instillation	210
Figure 6.19	Log-linear plot of plasma concentration versus time for II after intratracheal instillation of an aqueous bolus of 28.2mg	211

LIST OF TABLES

		Page
Table 2.1	Reference solutions used to calibrate surface tension apparatus (Handbook of Chemistry and Physics, 1978)	38
Table 2.2	Density of dry powders determined by air comparison pycnometry	39
Table 2.3	Growth ratios calculated assuming ideal solution behaviour and full ionisation or based on experimental iso-osmotic concentration at 37° C. The Kelvin effect is neglected and the results refer to the limit of large spherical particles	40
Table 3.1	Calculated deposition fractions in the head, tracheobronchial and pulmonary regions of dry particles and equilibrium droplets of disodium cromoglycate, isoprenaline hydrochloride and isoprenaline sulphate	60
Table 4.1	Characteristics of Battelle Cascade Impactors, DCI5 and DCI 6 cascade impactor; jet diameter, D_j , Reynolds number, Re ; and linear velocity V , for each stage (Hering et al, 1978)	97
Table 4.2	Operating conditions for the Berglund Lui, model 3050, vibrating orifice monodisperse aerosol generator.	98
Table 4.3	Manufacturer's calibration and experimentally obtained D_{50} values for each stage of the DCI-6 cascade impactor.	99
Table 4.4	Adiabatic perturbations in the DCI-6 cascade impactor. Transit times: t_{min} , the time taken to traverse the jet to slide distance, t_{max} , the time taken to traverse the jet length. Temperature changes: ΔT_H , the temperature change for high humidity air; ΔT_D , the temperature change for dry air	100
Table 5.1	Humidifier solutions and the relative humidity over their saturated solutions at 37° C	142
Table 5.2	Particle size distributions of fluorescein disodium aerosols exposed to varying humidity	143
Table 5.3	Measured resultant humidity levels from the mixing experiment (section 5.4.3.1).	144
Table 6.1	Best estimates for the fitted parameters k_{12} , k_{21} , k_{10} and V_1 from non linear least means square regression analysis after iv administration of II for $[Do]_{iv} \leq 11.4\text{mg}$	184

		Page
Table 6.2	Estimates for renal clearance of an 18mg iv bolus of II according to Equation 6.13	185
Table 6.3	k_{10} values estimated by analog computation of C_p versus time profiles according to Equation 6.18 for $[D_0]_{iv} \gg 11.4mg$	186
Table 6.4	Terminal slope, S^1 , values following intratracheal administration, estimated by least mean square regression of the apparently mono-exponential portions of the plasma concentration versus time profiles	187
Table 6.5	Bioavailable fraction of II after intratracheal administration of an aqueous bolus, determined using Equation 6.19	188

Chapter 1 INTRODUCTION

The term aerosol has been used in many ways, creating some degree of confusion. Initially coined to describe colloids of solid or liquid particles in a gas, the term is now frequently used to describe the 'pressurised pack' (Ansel, 1976, Sciarra, 1975). In this thesis the term 'inhalation aerosol' shall be taken to mean a dispersion of solid or liquid in a gas intended for administration to the respiratory tract.

Inhalation aerosols have long been used in respiratory medicine for the management of respiratory disease. Commonly used aerosols include water or saline droplets to 'liquify' sputum, β_2 adrenergic agonists for bronchodilation and disodium cromoglycate and steroid aerosols for prophylactic treatment of asthma. To be effective aerosols of these drugs must deposit within the respiratory tract, whether or not their subsequent pharmacological response is brought about by local concentration of the drug in the respiratory tract (e.g. salbutamol probably exerts its anti-asthmatic effect locally in the respiratory tract (Walker et al, 1972)) or by systemic concentrations after drug absorption from the respiratory tract (e.g. isoprenaline bronchodilator action may be due to circulating levels (Davies, 1975)). Deposition of aerosols within the respiratory tract is not a simple matter since the respiratory airways form an extremely efficient aerodynamic filter, which acts as an important pulmonary defence mechanism preventing naturally occurring airborne particulates from penetrating the lung (Proctor, 1964).

A number of factors influence the site and extent of deposition in the respiratory tract, these have been reviewed in detail by Morrow (1974). These include both physiological parameters, such as tidal volume, respiratory rate and residence time within the respiratory tract and particle characteristics such as particle size, shape and density.

The TASK group on Lung Dynamics (1966) recommended that data produced for aerosols of various sizes, shapes and densities be normalised by the use of the aerodynamic diameter (Da). This is defined as the 'diameter of a unit density sphere with the same settling velocity as the particle in question'. In this context unit density, do , means 1 g cm^{-3} . The aerodynamic diameter is given by

$$Da = Dv \sqrt{\frac{(dp \cdot C(Dv))}{(S_p \cdot do \cdot C(Da))}} = Dg \sqrt{\frac{(dp \cdot C(Dg))}{(do \cdot C(Da))}}$$

Equation 1.1

where the first expression is for non-spherical particles of equivalent volume diameter, Dv , and the second for spherical particles of geometric diameter, Dg , with particle density, dp . The dynamic shape factor, S_p , is the ratio of the drag force on the non-spherical particle to the drag force on a sphere of equal volume. Stöber (1972) has reviewed the theoretical and experimental aspects of determining dynamic shape factors for spheroid, isometric and cluster aggregates

The general expression for the slip correction, $C(D)$, to Stokes Law for small spherical particles of diameter, D , is (Fuchs, 1964).

$$C(D) = 1 + \frac{2L}{D} (x + ye^{-(ZD/2L)}) \quad \text{Equation 1.2}$$

where L is the mean free path of air molecules and x, y and Z material dependent constants. For particles larger than 0.3 μ m diameter, $(x + ye^{-(ZD/2L)})$ may be approximated to 1.26 (Raabe 1976). The accepted value for the mean free path of air molecules at 23 $^{\circ}$ C and 760mm Hg is 0.0653 μ m. Substituting these values into Equation 1.2 and combining the result with Equation 1.1, the following equation is obtained for the aerodynamic diameter of spherical particles greater than 0.3 μ m diameter, where the particle density is in g cm $^{-3}$ and the geometric particle diameter and aerodynamic diameter in μ m.

$$Da = 0.0823 \sqrt{(0.0068 + 0.1646 dpDg + dp Dg^2)} \quad \text{Equation 1.3}$$

From Equation 1.2 it is seen that the slip correction factor is a function of the mean free path of air molecules. Since the mean free path of gas molecules is inversely proportional to their concentration, from the ideal gas equation the mean free path of air molecules at temperature T($^{\circ}$ K) and pressure P (mm Hg) can be calculated as (Raabe, 1976)

$$L = 0.0653 \cdot \frac{760}{P} \cdot \frac{T}{296} \quad \text{Equation 1.4}$$

The slip correction factor becomes most significant for small particles, if a spherical particle of 0.3 μ m geometrical diameter and of 1.5gcm $^{-3}$ density is considered, the difference in the aerodynamic diameter of such a particle at 23 $^{\circ}$ C and 37 $^{\circ}$ C will be

less than 1%. The use of the aerodynamic diameter enables comparison to be made between deposition of different materials in the respiratory tract in most instances. However for fibrous particles the probability of interception or wall collision increases as the fibre length becomes a significant fraction of the airway diameter and thus for long thin fibres while the probability of deposition based on the particles aerodynamic diameter is low, the probability of interception may be high because of fibre length (Timbrell, 1972). The use of aerodynamic diameters is also only of limited use when deposition of submicron particles is considered. For these particles the principle mechanism for deposition is diffusion, a mechanism which is a function of the geometric diameter (cf the Stokes-Einstein Equation) of the particle rather than the aerodynamic diameter.

Air entering the respiratory tract will be conditioned until, in the pulmonary region (as defined by TASK, 1966), it is at 99.5% relative humidity, that is the saturated vapour pressure over isotonic body fluids, and at body temperature (Muir, 1972). Air temperature conditioning occurs mainly in the nasal passages and oral cavity (Walker 1961). Cole (1953) has shown that the mouth performs this function with an efficiency nearly equal to that of the nasal passages. As the inspired air is warmed, its water content will increase. By comparison of the water content and temperature of inspired air samples in the pharynx with the variation of water content of saturated air with temperature, Cole (1953) has shown that air in the pharynx is near saturation whatever temperature it has attained during its passage to the pharyngeal region. The recent calculations of Ferron (1981) have revealed that

as mass transport (in this instance of water vapour) is faster than heat transport, supersaturation of the inhaled air might occur in the trachea or first bronchus. Inhaled aerosol particles will thus be subjected to high humidity conditions almost immediately upon entry to the respiratory tract, even before inspired air has attained complete temperature conditioning.

An aerosol particle not in thermodynamic equilibrium with the surrounding atmosphere will attempt to attain the equilibrium state by condensation or evaporation of water vapour and heat exchange. An aerosol particle containing hygroscopic substances will, at equilibrium, form a droplet whose humidity is equal to the humidity of the surrounding air. As particle size is a determining factor in the site and extent of deposition in the respiratory tract, condensation growth of hygroscopic drug aerosol particles would be expected to affect the site and dose of drug deposited in the respiratory tract. Only 5 to 10% of the inhaled dose of disodium cromoglycate is absorbed (Moss, 1970) it has been suggested that this may be explained by the effects of condensation growth (Gonda and Byron, 1978). The importance of condensation growth on lung deposition clearly depends upon the rate of growth (Ferron 1977). An indication that hygroscopic particles grow sufficiently fast to affect lung deposition comes from studies with aerosol of inorganic electrolytes (Walkenhorst and Dautrebande, 1961; Wagner, 1975) and the recent work of Martonen et al (1980) has shown that isoprenaline hydrochloride particles grow at approximately the same rate as sodium chloride in the 90 - 95% relative humidity range.

The TASK group (1966) suggest that the effect of condensation growth on hygroscopic aerosols can be considered by assuming that the solution formed behaves as an ideal solution. If we consider a dry particle of a single water-soluble compound with diameter, D_o , mass, M_o and density d_o , undergoing condensation growth to form a droplet of diameter D_d , mass, M_d and density d_d , the ratio of the diameter of the equilibrium droplet to initial dry particle diameter will be

$$\frac{D_d}{D_o} = \sqrt[3]{\frac{M_d}{M_o} \cdot \frac{d_o}{d_d}} \quad \text{Equation 1.5}$$

The mass of the droplet will equal the mass of the initial dry particle plus the condensed water, M_w

$$M_d = M_o + M_w \quad \text{Equation 1.6}$$

The mass of water can be described in terms of the number of moles of water, n_w , and the molecular mass of water W_w

$$M_w = n_w W_w \quad \text{Equation 1.7}$$

and a similar expression will describe the mass of the dry particle in terms of the number of moles of solute, n_s , and the molecular mass of the solute, W_s .

$$M_o = n_s W_s \quad \text{Equation 1.8}$$

Substituting Equations 1.6, 1.7 and 1.8 into Equation 1.5 and rearranging, the following expression for the growth ratio

is obtained

$$\frac{Dd}{D_0} = \sqrt[3]{\frac{d_0}{d_d} \left(1 + \frac{ns}{nw} \cdot \frac{Ww}{Ws} \right)} \quad \text{Equation 1.9}$$

At equilibrium the fractional humidity of the droplet will equal the fractional humidity of the surrounding air, H. If surface tension effects are negligible the humidity of the droplet will equal the water activity of the solution of concentration equal to that in the droplet. Assuming ideal solution behaviour the water activity, a, will equal the mole fraction of water

$$a = \frac{nw}{nw + ins} = H \quad \text{Equation 1.10}$$

Rearranging Equation 1.10

$$\frac{nw}{ns} = \frac{iH}{1 - H} \quad \text{Equation 1.11}$$

Substituting this expression into Equation 1.9, the following equation is obtained describing the growth ratio in terms of the molecular mass of water and solute, the density of the dry particle and droplet grown from it and the humidity of the surrounding atmosphere.

$$\frac{Dd}{D_0} = \sqrt[3]{\frac{d_0}{d_d} \left(1 + \frac{Ww}{Ws} \left(\frac{iH}{(1-H)} \right) \right)} \quad \text{Equation 1.12}$$

This expression assumes that the solute concentration is below

the solubility limit, that there are negligible surface tension effects and that the solution formed behaves in an ideal manner. A similar expression incorporating a term to allow for hydrated solute molecules has been used by Ferron (1977). The accuracy of the growth ratio obtained using this expression clearly depends upon the solute forming an ideal solution. If physical data is available it is obviously preferable to use this data to determine the growth ratio. Neglecting surface tension effects the equilibrium droplet will have the same concentration as the bulk solution whose water activity is equal to the humidity over isotonic body fluids at 37° C, that is the iso-osmotic concentration, Me' . The concentration in the droplet in terms of mass of solute and water (measured in grams) can be defined by

$$Me' = \frac{Mo \cdot 1000}{Ws \cdot Mw} \quad \text{Equation 1.13}$$

The mass of water in the equilibrium droplet will equal the difference between the mass of the droplet and the dry particle

$$Mw = Md - Mo \quad \text{Equation 1.14}$$

Combining Equations 1.13 and 1.14 and substituting the result in Equation 1.5, the following expression is obtained to describe the growth ratio in terms of iso-osmotic concentration, dry particle density and droplet density.

$$\frac{Dd}{Do} = \sqrt[3]{\frac{d_o}{d_d} \left(1 + \frac{1000}{Ws \cdot Me'} \right)} \quad \text{Equation 1.15}$$

The British Pharmaceutical Codex lists the depression of freezing point of 1% solutions of a number of substances commonly used in injections. The depression of freezing point of water due to solutes in blood serum has an average value of 0.52°C . Assuming Raoult's Law to be applicable, the relationship between depression of freezing point and concentration will be linear and the concentration of drug giving a freezing point depression of 0.52°C may be easily determined. Although water activity in electrolyte solutions is relatively insensitive to temperature (Robinson and Stokes 1959a) for systems such as disodium cromoglycate-water which undergo phase transitions (Cox et al, 1971), it is advisable to take measurements at body temperature and iso-osmotic concentrations found by freezing-point depression should be treated with some suspicion. A number of techniques are available for determining iso-osmotic concentrations at body temperature. Robinson and Stokes (1959b) have reviewed techniques for determining the vapour pressure of electrolyte solutions. However, for dilute solutions very accurate pressure measurements are required. Recently vapour pressure osmometry has been used to determine osmotic behaviour of a number of electrolytes found in atmospheric aerosol (Thudium, 1978). Using this technique water activities may be determined at body temperature.

Rigorously speaking, the concentration of solute in the droplet equilibrated to 99.5% relative humidity at 37°C will not be the same as the concentration of bulk solution giving a water activity of 0.995 at 37°C , as the humidity of the droplet, h will be greater than the water activity of the

solution because of surface tension effects and is given by the Kelvin equation

$$h = a + \exp \left(\frac{4S W_w}{d_d \cdot RT \cdot Dd} \right) \quad \text{Equation 1.16}$$

where S is the surface tension of the solution, d_d its density R the universal gas constant and T the droplet temperature.

The exponential term becomes more significant for small diameters.

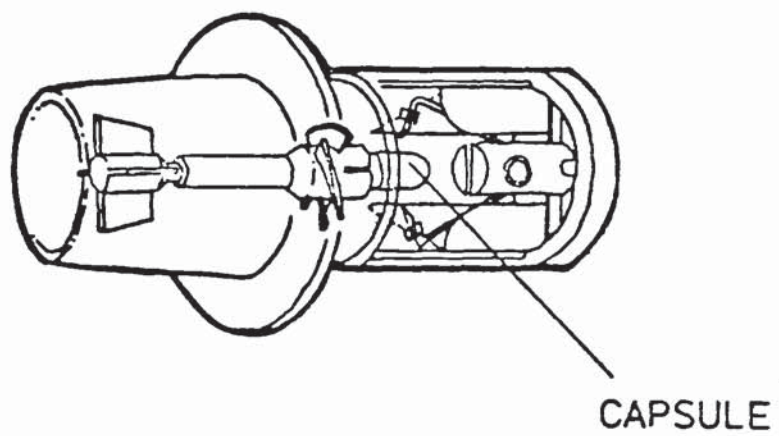
In order to investigate the likely overestimate of the growth ratio by neglecting this term data relating the surface tension of drug solutions to their concentration are required. If the exponential term is designated by E^1 Equation 1.12 becomes (Ferron, 1977)

$$\frac{Dd}{Do} = \sqrt[3]{\frac{do}{dd} \left(1 + \frac{Ww}{Ws} \left(\frac{i (H - E^1)}{1 - (H - E^1)} \right) \right)} \quad \text{Equation 1.17}$$

if surface tension effects are considered, As the exponential term includes the diameter of the droplet an explicit expression for the growth ratio is not obtainable and the growth ratio may be found in an iterative manner.

The growth ratios described (Equations 1.12, 1.15 and 1.17) are applicable to single water-soluble compounds of initially dry particles. This type of aerosol would be generated from powder insufflators such as the Spinhaler (Fisons Ltd.). The Spinhaler is a tubular plastic device which is loaded with a gelatine capsule containing the drug mix (see Figure 1.1). Two metal pins pierce the capsule to

Figure 1.1 Schematic diagram of the Spinhaler (Fisons Ltd., Loughborough) powder insufflator.



provide an escape route for the capsule contents. When the user inhales, a rotor spins the capsule and powder is thrown out into the inhaled air stream. Lactose (30 - 60µm in diameter) is mixed with micronised drug to assist dispersion, some drug will adhere to the lactose particles but most of the drug will be dispersed as single particles or aggregates of drug alone (Bell et al, 1971).

Drugs may also be administered as aerosol droplets generated using airblast or ultrasonic nebulisers. If the simplest formula of water-soluble drug in water is considered, an equation to determine the growth or shrinkage of the aerosol droplet of initial diameter, D_i can be derived. The ratio of the diameter of the equilibrium droplet, D_d , to the diameter of the initial droplet may be described in terms of the mass and density of the initial and equilibrium droplet

$$\frac{D_d}{D_i} = \sqrt[3]{\frac{M_i}{M_d} \cdot \frac{d_d}{d_i}} \quad \text{Equation 1.18}$$

where M_i and d_i are the mass and density of the initial droplet. If the mass of solute in the droplets is M_o , the initial molality, M_i' will be

$$M_i' = \frac{M_o}{W_s} \cdot \frac{1000}{(M_i - M_o)} \quad \text{Equation 1.19}$$

Combining Equations 1.14, 1.18 and 1.19 the following expression for the ratio of the diameters of the initial and equilibrium droplet

$$\frac{D_e}{D_i} = \sqrt[3]{\frac{\frac{d_i}{d_e} \left(1 - \frac{1000}{W_s M_e}\right)}{\left(1 - \frac{1000}{W_s M_i}\right)}} \quad \text{Equation 1.20}$$

Frequently however, nebuliser solutions are not of drug in water but may contain other solvents such as alcohols or glycols, and other formulating agents such as buffers, antioxidants preservatives and salts. If the nebuliser solution is formulated to be isotonic and if surface tension effects are assumed to be negligible, the droplets would be expected to neither grow or shrink. For small droplets where surface tension effect became significant the humidity above the isotonic droplet will be greater than 0.995 and some evaporation will occur.

The major domiciliary aerosol generator used in inhalation therapy is the pressure pack. The basic principles of pressurised products are extensively described by Sciarra (1975). Two types of pressurised inhalation aerosol packs are formulated. The active medicament may be dissolved in the liquified propellant usually with addition of cosolvents to assist drug solubility such as alcohols or glycols.

Alternatively the active agent may be suspended as a micronised powder in the liquid propellant system. Surfactants such as lecithin, lanolin, oleyl alcohol or cholesterol derivatives are frequently added to prevent drug agglomerations.

Lubricants such as isopropyl myristate, isopropyl palmitate allow the powder particle to flow through the valve minimising valve clogging. The moisture content in the pack can be minimised by inclusion of desiccants. Aerosols generated from pressurised packs will be polyphasic and it is not possible to determine the aerosol behaviour at high humidity

from physicochemical characteristics of the drug alone. In these instances direct measurement of the change in size distribution of the aerosol at high humidity is desirable. Hiller et al have described the changes in particle size distributions of aerosol of disodium cromoglycate (1980a), Isoprenaline hydrochloride and sulphate (1980b) and isoetharine sulphate and metaproterenol sulphate (1978) generated from commercial products at high (95%) and low (21%) humidity. The aerodynamic diameter distribution of the aerosols were measured using the single particle aerodynamic relaxation time analyser. This type of analysis will not however distinguish between aerosol particles containing the compound of interest, that is the drug, and aerosol particles void of the medicament.

It is sometimes possible however, to infer which part of the total distribution is due to drug aerosol particles. For example, powder insufflators frequently incorporate an inert excipient to improve the flow properties of the mixture and facilitate aerosol generation. The average size of the excipient particles is usually much larger than that of the drug particles.

Impaction techniques allow the collection of aerosols of various aerodynamic size fractions. Chemicals or radioactive analysis of the deposits provides a means of distinguishing the aerodynamic distribution of a particular species of interest, in this case drug. Hiller et al (1978) have suggested that the instability of water-containing particles precludes the use of impaction techniques and measurement in the suspended state is necessary in order to

assess accurately the effect of humidity on the size of inhalation aerosols. Velocity changes in the jets (Hering et al, 1978) will lead to variation in temperature in the gas stream (Fuchs, 1978). The linear velocity in an impactor jet can be calculated from the volume flow rate through the impactor and jet diameter. The largest perturbation in temperature will occur at the smallest diameter jets however, the transit time through the smallest jets will be very small. Calculations for the Delron DCI-6 cascade impactor reveal that the transition time through the last two stages will be 0.35 and 0.15 milliseconds respectively. It is unlikely that any substantial changes in particle size would occur on such a short time scale. Hochrainer and Zebel (1981) have performed similar calculations and examined this problem experimentally and agree with this viewpoint. Indeed the cascade impactor has been used as the sizing instrument in experiments examining the effect of humidity on the size distribution of propylene glycol (Davis and Bubb, 1978) and disodium cromoglycate aerosols (Byron et al 1977).

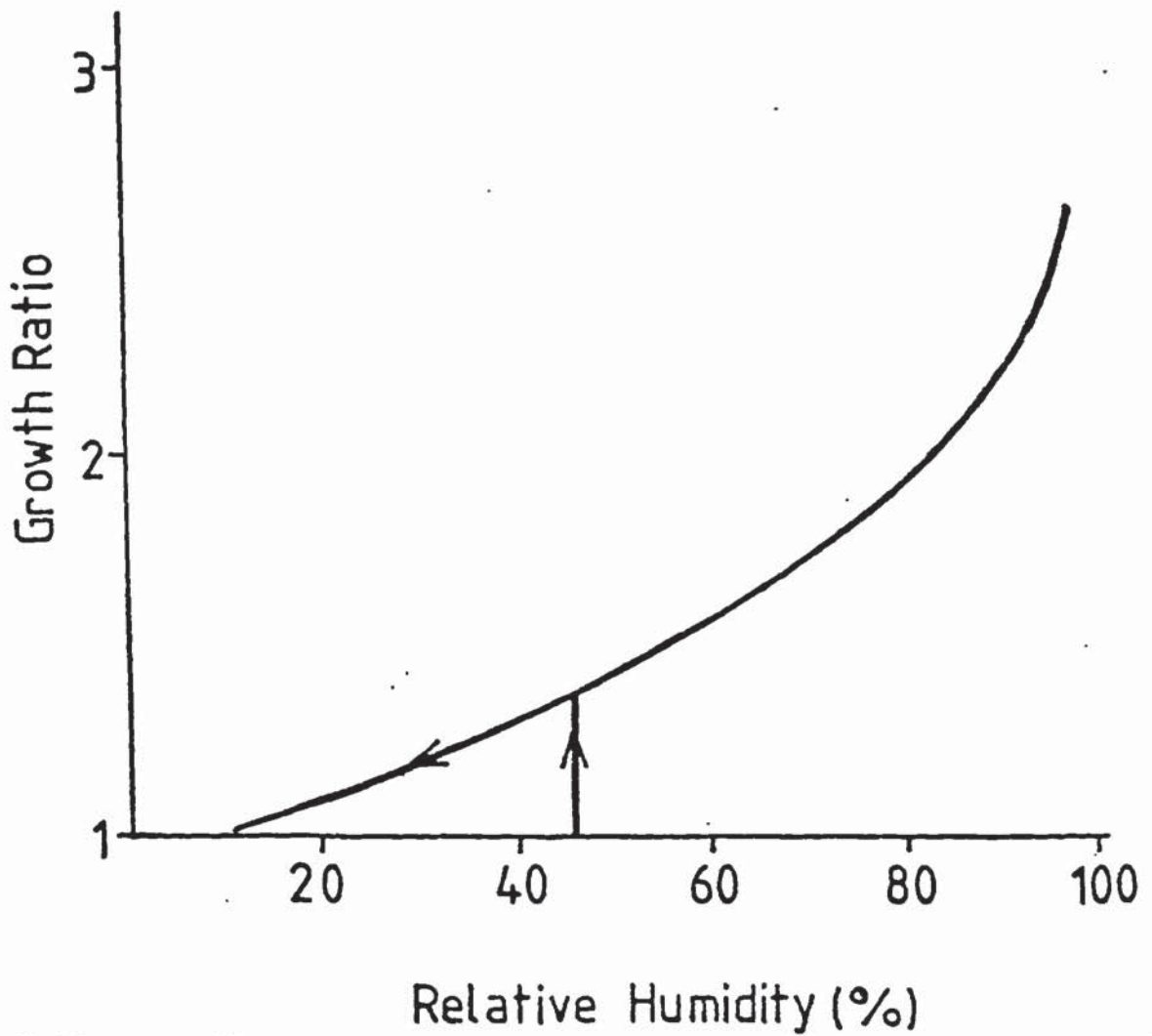
In practise it is difficult to achieve the degree of temperature control required to maintain the relative humidity experienced in the respiratory tract. For example, in order to obtain the growth ratio for a single water-soluble compound with an accuracy of 5% at 99.5% relative humidity would require temperature control within $\pm 0.015^{\circ}$ C at 37° C. (Gonda et al, 1981). Correspondingly studies on the effect of humidity on particle size distributions of aerosol are performed at sub-physiological humidity. Dry aerosols of a single water-soluble compound exposed to increasing humidity will display

a distinct humidity at which particles will start to grow. If the droplet formed is then exposed to decreasing humidity, no abrupt reduction in particle size is observed, instead a continuous reduction in size takes place as a result of the droplet becoming super-saturated. This hysteresis phenomenon is well known for inorganic salt aerosols and has been observed by a number of investigators (Orr, 1954; Tang, 1977). Figure 1.2 illustrates the effect of humidity on the size of a hypothetical single water-soluble compound. At high humidity the growth ratio shows a steep dependence on humidity. This makes accurate prediction of the growth ratio at 99.5% humidity from direct measurement at lower humidities difficult.

Atmospheric aerosols, which consist of mixtures of inorganic water-soluble materials and insoluble materials, by comparison show a continuous growth character by gradual deliquescence of water-soluble material (Winkler, 1974) but still display steep dependence at high humidities. Studies with atmospheric aerosols have indicated that the particles show reduced water absorption when water-insoluble compounds are present (Winkler, 1974; Eisner et al, 1960; Snead and Zung, 1968). Similarly, it may be expected that pharmaceutical aerosols from pressure packs, which include water-soluble components would show reduced water absorption compared with the active component alone.

As particle size is a determining factor in the site and extent of deposition in the respiratory tract, condensation growth of hygroscopic drug aerosol particles would be expected to affect the dose deposited in the respiratory tract.

Figure 1.2 Growth ratio versus relative humidity of a hypothetical water-soluble aerosol.



The magnitude of this effect may be examined using theoretical models based on the deposition patterns of non-hygroscopic aerosols.

Most pharmaceutical inhalation aerosols currently in use, are intended for local activity within the respiratory tract. However, the inhalation route would appear to offer a number of advantages as an absorption site. The surface area is approximately 30m^2 (Hatch and Gross, 1964a), providing an absorptive area comparable with that of the gastrointestinal tract. Drugs administered by the inhalation route will not be subject to large pH changes (compared with the gastrointestinal tract) nor such a large number of degradative enzymes (Gonda and Byron, 1978). The inhalation route may be useful in attaining rapid delivery of drugs designed to act systemically. Indeed this route is already used to achieve rapid onset of action of Ergotamine (Ergotamine Aerosol Inhalation, British Pharmaceutical Codex, 1979). Chapter six describes the development of a technique capable of providing information on the systemic bioavailability of a compound administered as an inhalation aerosol formulation to an experimental animal.

Chapter 2 PREDICTION OF EQUILIBRIUM DIAMETERS OF INHALATION AEROSOLS
IN THE RESPIRATORY TRACT

2.1 INTRODUCTION

In the introductory chapter expressions for the growth ratios of aerosols of single water-soluble compounds in the high humidity of the respiratory tract were described. The purpose of this chapter is to determine the physicochemical characteristics of several drugs currently used in inhalation therapy and use this data to calculate the increase in diameter of these drug aerosols in the respiratory tract.

The simplest expression for the growth ratio of dry particles to droplets in equilibrium with a humidity of 99.5% assumes that the solution formed behaves in an ideal manner and that surface tension effects are negligible. (Equation 1.12). The main advantage of this expression is that only a few compound specific parameters are required; the molecular weight of the drug, the density of the dry powder and the density of the solution formed.

In order to obtain a more exact estimate of the growth ratio knowledge of the water activity of aqueous solution of drug at 37° C is required. Vapour pressure osmometry provides a technique for the determination of water activity of solutions. This technique has been used to determine the isotonic equivalents of a number of drugs (Newburger, 1977).

Figure 2.1 is a schematic diagram of the vapour pressure osmometer. It consists of a heat insulated chamber containing a pair of thermistors which are connected to a wheatstone bridge. Using filter paper wicks and a reservoir of distilled water vapour concentration near saturation is maintained within the

chamber. Syringes containing solution and solvent are kept at approximately chamber temperature within a heated head. Droplets of solution and solvent (in this instance water) may be applied to the thermistors by lowering the syringe needles into the chamber. The wheatstone bridge is initially zeroed after applying solvent droplets approximately equal in diameter to both the test and reference thermistors. Figure 2.2a illustrates saturation vapour pressure, p , as a function of temperature, T , for pure water and for a solution. When droplets of solution and solvent are applied to the thermistors they attempt to achieve equilibrium with the vapour pressure of the chamber, p^1 , by evaporation and condensation of water vapour. The water vapour concentration within the chamber will be near to saturation vapour pressure and so little change will occur to the solvent droplet. The vapour pressure of the solution droplet will be lower than the chamber and so water vapour will condense onto the solution droplet raising its temperature to $T + \Delta T$, when the vapour pressure of the solution equals that of the chamber. The temperature difference established, ΔT , is measured by means of the thermistors. It has been shown theoretically that the temperature difference is proportional to the negative of the natural logarithm of water activity ($-\ln a$) (Thudium, 1978). The droplets applied to the thermistors are large enough for the condensing water vapour to have negligible effect on the concentration of the solution droplet (Whatley, 1966). Waste droplets of solution are washed into the chamber reservoir in the apparatus used in this study (KG Dr. Ing Herbert Knauer, West Germany) and so during a course of readings the vapour pressure of the chamber will be lowered. Figure 2.2b

may be used to illustrate the establishment of the temperature difference between the solution and solvent droplets when the vapour pressure of the chamber is less than the saturation vapour pressure. In this instance the solvent droplet will attempt to attain equilibrium by evaporation of water vapour, correspondingly the solvent droplet will cool until at the temperature of $T - \Delta T_1$ its vapour pressure equals that of the chamber. The vapour pressure of the solvent droplet, in this example, is still lower than that of the chamber. Condensation of water vapour onto the solvent droplet will occur until at a temperature of $T + \Delta T_2$ its vapour pressure equals that of the chamber. The fall in temperature of the solvent droplet plus the rise in temperature will equal the same temperature difference, ΔT , described in Figure 2.2a. This may be confirmed experimentally by determining the established temperature difference for the same solution at the beginning and at the end of a set of experimental readings.

Solutions of surface active materials might be expected to give false results using the vapour pressure osmometer because of possible effects the surface film may have affecting heat and mass transfer in an unequal manner. However, Fineman and McBain (1948) have shown that addition of a small amount of potassium laurate, sufficient to lower surface tension appreciably without appreciably lowering vapour pressure, to 0.1Molal potassium chloride solutions did not affect the temperature difference between the solution and solvent droplets. Indeed, vapour pressure osmometry has been used to determine the critical micelle concentration of aqueous solutions of detergents (Huff et al, 1951).

In order to determine the magnitude of the Kelvin effect on the growth ratio it is necessary to determine the surface tension of aqueous solutions of the compounds used in this study. The surface tension was determined using the Wilhelmy plate technique (Adamson, 1967). The basis of this technique is that a thin plate will support a meniscus whose weight, measured statically or by detachment is given by

$$m_t = m_p + S.e \quad \text{Equation 2.1}$$

where m_t and m_p are the total mass and the mass of the plate respectively; S the surface tension of the solution and e, the perimeter of the plate.

2.2 EXPERIMENTAL

2.2.1 Vapour Pressure Osmometry

2.2.1.1 Calibration of vapour pressure osmometer

The instrumental response of the vapour pressure osmometer used in this study (K G Dr. Ing Herbert Knauer, West Germany) at various sensitivity settings was calibrated against electrolytes and non-electrolyte solutions of known water activity. Data were directly available for solutions at 25° C (Robinson and Stoke, 1959a) either tabulated as water activity or in terms of osmotic coefficient. Water activity, a , may be calculated from osmotic coefficient, ϕ , by

$$-\ln a = 0.018 i M \phi \quad \text{Equation 2.2}$$

where i is the number of ions formed by the compound and M the solution concentration in moles per kg of water (Robinson and Stoke, 1959 d).

Osmotic coefficients for sodium chloride solutions of greater than 1 molal at 37° C were obtained from the data of Gibbard et al (1974). Other values were obtained by extrapolation between available data at 25° C and the nearest temperature to 37° C available in the literature. The values used in the calibration are tabulated in Appendix 1.

Solutions of known water activity were prepared from analytical grade sodium, potassium and calcium chlorides and sucrose with deionised water.

2.2.1.2 Preparation of test solutions

Disodium cromoglycate (supplied by Fisons, Pharmaceutical Division, Loughborough) was dried in a vacuum oven at 170° C for 18 hours, then allowed to cool over phosphorous pentoxide (Attiga et al, 1979). Solutions of known molality were prepared from this dried powder and deionised water.

Isoprenaline sulphate and hydrochloride were used as supplied by the manufacturer (Riker Laboratories, Loughborough). Solutions of isoprenaline salts decompose on exposure to air as indicated by the appearance of a pink coloured solution. Solutions of isoprenaline sulphate and isoprenaline hydrochloride of known molality were prepared with deionised water therefore just prior to measurement.

Only limited quantities of salbutamol sulphate (Glaxo Group Research, Ware) were available. Solutions of known molality were prepared by dilution of a 0.15 molar stock solution in deionised water.

2.2.1.3 Measurement of water activity

The apparatus was allowed to equilibrate for at least one hour before any measurements were made. The instrument was initially zeroed by placing solvent onto both reference and test thermistors. Once a constant instrumental reading was obtained, the wheatstone bridge was balanced to give a zero reading. Measurements were then made by placing droplets of solution onto the test thermistor and solvent onto the reference thermistor of similar size (approximately 4mm in diameter). The size of the droplets could be observed through

a window into the test chamber. The most dilute solutions were measured first. At least three measurements were made of instrumental response with each solution. The solution droplet was then washed from the test thermistor with several drops of the next most concentrated solution before the determination of instrumental response to that solution.

2.2.2 Density Measurements

2.2.2.1 Density of dry powders

The density of the dry powders used in this study were measured by air comparison pycnometry (Beckman, Model 930). Approximately thirty grams of each powder was accurately weighed into the sample chamber and the volume of air displaced by the powder determined. Only 2 grams of salbutamol sulphate was available for density determination and this is reflected in the accuracy of the measurements. The density of each powder was determined three times.

2.2.2.2 Density of Solutions

The density of aqueous solutions of the compounds used in this study at 37° C were determined using a specific gravity bottle. The volume of the bottle at 37° C was determined by filling the bottle with deionised water and leaving it in a water bath at 37° C for 1 hour to equilibrate. Excess solution was removed, the bottle dried externally and allowed to cool before weighing. The volume of the bottle could then be calculated from the weight of water held in the bottle and the tabulated density of water at 37° C (Robinson and Stokes, 1959).

The specific gravity bottle could then be used to determine the density of aqueous solutions of drug at 37° C in a similar manner. Each determination was made three times.

2.2.3 Surface Tension Measurements

The surface tension of aqueous solutions of the compounds used in this study were determined using the Wilhelmy plate technique (Adamson, 1967). The plate used in these studies was 10mm high, 5mm wide and 0.025mm thick and made of 99.95% pure platinum (Goodfellow metals, Cambridge). The plate was roughened slightly to enhance wetting. Before each measurement the platinum plate was cleaned by heating to red heat and used immediately it had cooled (Bewig, 1965). The cleaned plate was hung from the beam of a microbalance (CI Electronics Ltd., Mark 2B). This arrangement was counter balanced in air by a weighing pan and weights hung from the other balance arm.

Twenty five millilitres of the test liquid, which had been previously warmed to 37° C was placed in a jacketted beaker maintained at 37° C using a water circulator-heater (Chiller-Thermo Circulator, Churchill Ltd.). The beaker was placed on a movable platform which was raised until the plate was just below the surface of the liquid. The platform was then lowered slowly until the plate detached from the liquid surface. The increase in weight on the balance arm was read from an indicating meter and chart recorder. All measurements were made at least three times. The meter readings obtained were calibrated using solutions of known surface tension shown in Table 2.1 .

Test solutions were prepared with deionised water from dried disodium cromoglycate (see section 2.2.1.2) and isoprenaline sulphate, isoprenaline hydrochloride and salbutamol sulphate as supplied by the manufacturers.

- 2.3 EXPERIMENTAL RESULTS
- 2.3.1 Vapour Pressure Osmometry
- 2.3.1.1 Calibration of vapour pressure osmometer

The temperature difference between the solution and solvent droplets in the vapour pressure osmometer has been shown to be proportional to the negative of the natural logarithm of water activity (Thudium, 1978). The instrumental response (percent full scale deflection, % FSD) is directly proportional to the temperature difference. Figure 2.3 shows the instrumental response at an instrumental sensitivity setting of 16, versus $-\ln a$ for sodium, potassium and calcium chloride and sucrose at 25° C. The results could be satisfactorily described by a rectilinear plot of the form

$$\% \text{ FSD} = 3329 (-\ln a) - 0.8 \quad \text{Equation 2.3}$$

with a correlation coefficient of greater than 0.999 ($n = 57$). The theoretical relationship therefore appears to apply to 1:1 and 1:2 electrolytes and non-electrolyte solutions.

Similar rectilinear plots with correlation coefficients of greater than 0.998 ($n > 15$), were obtained at 37° C for several instrument sensitivity settings. The slope and intercepts of these calibration curves are given in Appendix 2. The calibration curves were used to determine the water activities of test solutions.

2.3.1.2 Water activity of Test solutions

The water activity (a) versus concentration (M) for aqueous solutions of isoprenaline hydrochloride, isoprenaline sulphate and salbutamol sulphate at 37° C and disodium cromoglycate at 37° C and 25° C are shown in Figure 2.4. The solid lines indicate the linear approximations used in the computation of growth ratios taking into account the Kelvin effect (section 2.4).

The water activity versus concentration plots for isoprenaline hydrochloride, isoprenaline sulphate and salbutamol sulphate could be satisfactorily described by rectilinear plots. Included on Figure 2.4 are the lines for ideal solution behaviour assuming dissociation into 2 ions, e.g. isoprenaline hydrochloride or 3 ions, c.f. disodium cromoglycate and the sulphates of isoprenaline and salbutamol. It is readily seen that all aqueous solutions of the drugs examined show apparent deviation from ideality.

The relationship between water activity and concentration for disodium cromoglycate solutions was complex. For the concentration range examined water activity appears to plateau at concentrations exceeding 0.22 Molal at 37° C and 0.13 Molal at 25° C. These transition points correspond to a phase change between solution and mixed solution and mesophase (Cox, et al, 1971)

2.3.2 Density Results

2.3.2.1 Density of dry powders

The mean and standard deviation of three determinations

of dry powder density determined by air comparison pycnometry are given in Table 2.2. The density of salbutamol sulphate could only be determined to $\pm 0.5\text{gcm}^{-3}$ as insufficient sample was available for more accurate determination.

2.3.2.2 Density of aqueous drug solutions

Figure 2.5 illustrates the density of aqueous solutions of disodium cromoglycate, isoprenaline hydrochloride, isoprenaline sulphate and salbutamol sulphate. The mean results of three determinations and the least mean square regression line are illustrated. Each determination was within 0.0002gcm^{-3} of the mean value. For the concentration range considered, the density of the aqueous solutions could be satisfactorily described by rectilinear plots of density versus concentration.

2.3.3 Surface Tension Measurement

2.3.3.1 Calibration of Instrument

Figure 2.6 shows instrumental response (Y) versus surface tension (S). The mean of three determinations is illustrated, all individual readings were within ± 1 instrumental response unit. Instrumental response versus surface tension could be satisfactorily described by a rectilinear plot. The least mean square regression line may be described by

$$Y = 1138 S + 0.15 \quad \text{Equation 2.4}$$

where S is the surface tension in Nm^{-1} .

The correlation coefficient of this line was 0.999 ($n = 24$).

This calibration line was used to determine the surface tension of test solutions.

2.3.3.2 Surface tension of aqueous drug solutions

Figure 2.7 illustrates the surface tension of drug solutions. The reproducibility in replicate determinations of surface tension by measurement of the force on the immersed plate was about 0.0001 Nm^{-1} . The solid lines in Figure 2.7 show the linear approximations used to compute the growth ratios taking into account the Kelvin effect.

It is interesting to note that the surface tension of aqueous disodium cromoglycate solutions decrease rapidly with increasing concentration above 0.13 Molal at 25° C and 0.21 Molal at 37° C, corresponding to the transition points from solution to mixed solution and mesophase (Cox, 1971). These values compare favourably with the transition points for this phase change obtained from water activity data of 0.13 Molal at 25° C and 0.22 Molal at 37° C (see Figure 2.4).

Examination of the plots of water activity versus concentration (Figure 2.4) reveals that all the compounds studied here show appreciable deviation from ideality. The experimentally determined isosmotic concentrations show greater than 10% deviation from those predicted on the basis of 'ideal' solution behaviour and full ionization. The growth ratio of an initially dry spherical particle to a droplet in equilibrium with a relative humidity of 99.5% at 37° C may be calculated assuming 'ideal' solution behaviour and full ionization using Equation 1.12 and from experimental isosmotic concentrations using Equation 1.15. Both these equations neglect surface tension and so the results refer to the limit of large spherical particles. The calculated ratios are given in Table 2.3 and reveal that the deviation from ideality observed for these compounds is sufficient to affect the growth ratio markedly.

From a deposition viewpoint it is the increase in aerodynamic diameter which is important. It is useful therefore to express the growth ratio in terms of aerodynamic diameter. As the growth ratios determined from experimental isosmotic concentrations refer to the limit of large spherical particles, it is reasonable to neglect the Cunningham slip factor in the determination of aerodynamic diameters. The aerodynamic growth ratio, $(\frac{D_d}{D_o})_a$, may be calculated from

$$\left(\frac{Dd}{Do} \right)_a = \sqrt{\frac{dd}{do}} \cdot \left(\frac{Dd}{Do} \right) \quad \text{Equation 2,5}$$

where dd and do are the densities of the equilibrium droplet and initial dry particle respectively and Dd/Do is the ratio for geometric diameters calculated from Equation 1.15. As the increase in geometric diameter due to condensation of water is accompanied by a decrease in particle density, the aerodynamic growth ratio will be less than the growth ratio in terms of geometric diameter. The calculated aerodynamic growth ratios are given in Table 2.3.

When surface tension effects are considered no single growth ratio will apply to all particle sizes. Growth ratios considering the Kelvin effect were therefore calculated for individual particle diameters using an iterative computer programme. For each drug the experimental results for surface tension, water activity and density were expressed as functions of concentration using the linear approximations shown in Figures 2.4, 2.5 and 2.7. The programme starts with the isosmotic concentration of each drug at 37° C and using the Kelvin equation calculates the humidity above the droplet. For small droplets the fractional humidity in this instance will exceed 0.995. The drug concentration is then increased in an incremental manner and the droplet humidity recalculated. When the droplet humidity is less than 0.995, the concentration is reduced to the previous value and the size of the incremental step reduced. In this manner the concentration at which a droplet of known diameter has a fractional humidity equal to

0.9950000 ± 0.0000001 is determined. The growth ratio can then be calculated using Equation 1.15 for the droplet size under consideration and the procedure repeated for the next particle size.

The magnitude of the Kelvin effect relative to aerodynamic diameter is illustrated in Figure 2.8 where $(Da)_i$ refers to the aerodynamic diameter calculated from the isosmotic concentration and $(Da)_e$, the aerodynamic diameter calculated including the Kelvin effect. It is apparent that this effect is only significant for very small particles (initially less than $1\mu\text{m}$) which are unlikely to occur in appreciable quantities in most currently employed inhalation aerosols (Byron et al, 1978; Davis, 1978; Hallworth and Andrews, 1976; Mercer et al, 1968; Ruffin et al, 1978).

The water activity of disodium cromoglycate, isoprenaline hydrochloride, isoprenaline sulphate and salbutamol sulphate in aqueous solution has been determined by vapour pressure osmometry. In all instances there was a significant deviation from 'ideal' solution behaviour. This was most marked for disodium cromoglycate which undergoes a phase transition from solution to mixed solution and mesophase. This phase change is indicated by a plateau in water activity. The concentration at which this phase change occurs has been shown to be temperature dependent (Cox et al, 1971). Furthermore, at 25° C the water activity at the plateau is higher than the value for isotonic saline, whereas the converse is true at 37° C. In the light of this observation it is advisable that determinations of iso-osmotic equivalents should be made at physiological temperatures.

The most exact expression for condensation growth ratios takes into account the increased vapour pressure above curved surfaces of small droplets, the Kelvin effect. In this instance explicit expressions for the growth ratio of all particle sizes is not possible, the growth ratio for each particle size may be found in an iterative manner.

Determination of growth ratios from the experimentally determined iso-osmotic concentrations, neglecting the Kelvin effect will lead to overestimates. For the compounds studied here this overestimation is less than 5% for particles initially greater than 1µm in diameter. Submicron particles are unlikely

to occur in appreciable quantities in most currently employed inhalation aerosols. Reasonably accurate estimates of the growth ratios can therefore be obtained from the iso-osmotic concentrations at 37° C for pharmaceutical aerosols.

2.6 TABLES

Table Captions

Table 2.1 Reference solutions used to calibrate surface tension apparatus (Handbook of Chemistry and Physics, 1978)

Table 2.2 Density of dry powders determined by air comparison pycnometry

Table 2.3 Growth ratios calculated assuming ideal solution behaviour and full ionization or based on experimental iso-osmotic concentration at 37° C. The Kelvin effect is neglected and the results refer to the limit of large spherical particles.

Table 2.1 Reference solutions used to calibrate surface tension apparatus (Handbook of Chemistry and Physics, 1978).

Solution	Temperature ° C	Surface Tension (S) mNm ⁻¹
Acetone	20	23.9
Benzene	20	28.9
20% w/w acetone in water	25	41
10% w/w acetone in water	25	48.9
5% w/w acetone in water	25	55.5
Water	40	69.6
Water	30	71.2
Water	20	72.75

Table 2.2 Density of Dry powder determined by air comparison pycnometry

Compound	Density (gcm ⁻³)
Disodium cromoglycate	1.623 ± 0.001
Isoprenaline hydrochloride	1.325 ± 0.003
Isoprenaline sulphate	1.362 ± 0.001
Salbutamol sulphate	1.50 ± 0.5 *
* insufficient sample for more accurate determination	

Table 2.3 Growth ratios calculated assuming ideal solution behaviour and full ionized (Equation 1.12) or based on experimental iso-osmotic concentration at 37° C (Equation 1.15). The Kelvin effect is neglected and the results refer to the limit of larger spherical particles.

Drug	Geometric diameter growth ratios		Aerodynamic diameter growth ratios	
	Assuming ideal solution behaviour	Calculated from iso-osmotic concentration	Assuming ideal solution behaviour	Calculated from iso-osmotic concentration
Disodium cromoglycate	3.26	2.67	2.60	2.12
Isoprenaline hydrochloride	3.40	3.28	2.97	2.85
Isoprenaline sulphate dihydrate	3.02	2.76	2.59	2.37
Salbutamol Sulphate	3.1*	2.96	2.5*	2.41

* Sample too small for greater accuracy

FIGURESFigure Captions

Figure 2.1 Schematic diagram of the vapour pressure osmometer

Figure 2.2 Saturation vapour pressure, p , versus temperature, T , for solvent and solution

Figure 2.3 Instrumental response of the Knauer vapour pressure osmometer (sensitivity setting 16) versus the negative of the natural logarithm of water activity at 25° C for sodium chloride (○), potassium chloride (●), calcium chloride (Δ) and sucrose (x).

Figure 2.4 Water activity versus molality for aqueous solutions of isoprenaline hydrochloride at 37° C (◇), isoprenaline sulphate at 37° C (◆), salbutamol sulphate at 37° C (Δ) and disodium cromoglycate at 37° C and 25° C (●). The solid lines indicate the linear approximations used to compute equilibrium diameters with the inclusion of the Kelvin effect. Also shown are the lines for ideal solution behaviour assuming dissociation into 2 ions (••••) - cf isoprenaline hydrochloride or 3 ions (.....) - cf disodium cromoglycate and sulphates of isoprenaline and salbutamol.

Figure 2.5 Density of aqueous solutions of disodium cromoglycate (○), salbutamol sulphate (x), isoprenaline hydrochloride (●) and isoprenaline sulphate (Δ) at 37° C. The solid lines illustrate the linear approximations used to determine droplet equilibrium diameters with the inclusion of the Kelvin effect. The mean of three determinations is illustrated.

Figure 2.6 Calibration of surface tension apparatus, instrumental response versus surface tension. The mean of three determinations is illustrated, individual readings were within ± 1 instrumental response limit of the mean.

Figure 2.7 Surface tension against molality at 37° C for aqueous solutions of disodium cromoglycate (●), isoprenaline hydrochloride (▲), isoprenaline sulphate (△) and salbutamol sulphate (○). The solid lines indicate linear approximations used to compute the equilibrium diameters with inclusion of the Kelvin effect.

Figure 2.8 Percentage error caused by neglecting the Kelvin effect in calculation of equilibrium droplet size: $(Da)_e$ and $(Da)_i$ - aerodynamic diameters calculated with and without the Kelvin correction respectively. Results for isoprenaline sulphate (____), isoprenaline hydrochloride(--.--), salbutamol sulphate (---) and disodium cromoglycate (-.-), all at 37° C

Figure 2.1 Schematic diagram of the Vapour Pressure Osmometer

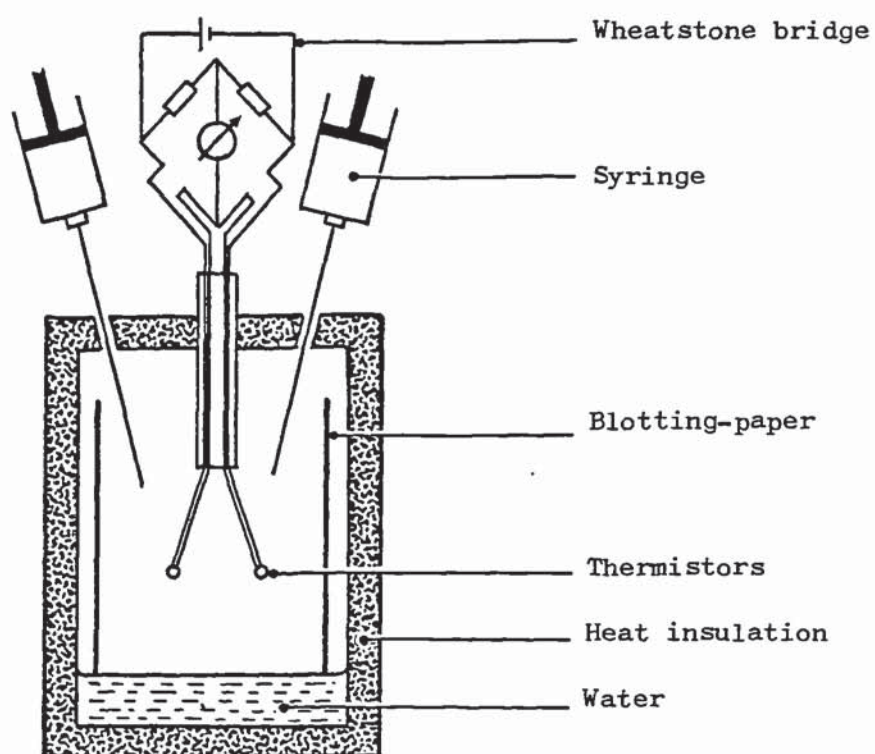
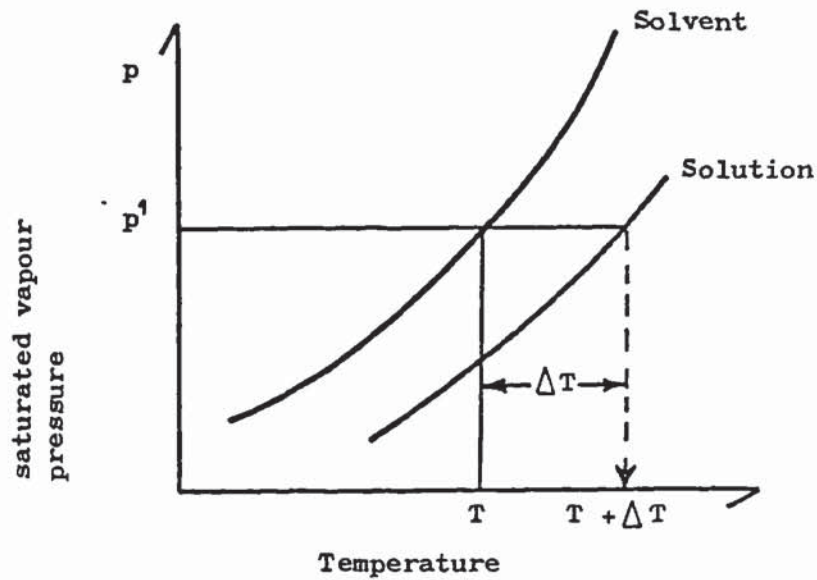


Figure 2.2: Saturation vapour pressure p , versus temperature, T , for solvent and solution.

a)



b)

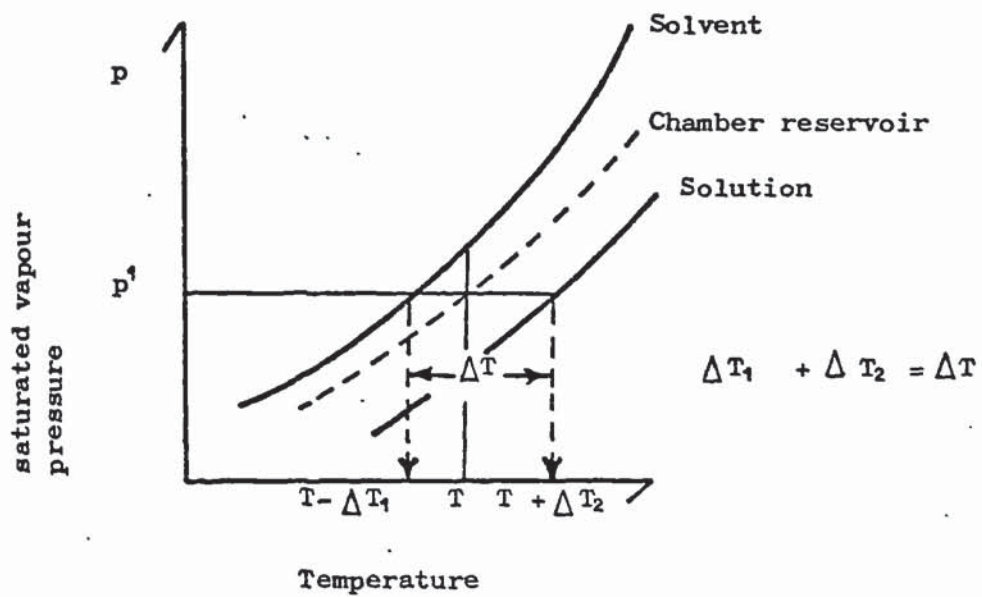


Figure 2.3 Instrumental response of the Knauer vapour pressure osmometer (sensitivity setting 16) versus the negative of the natural logarithm of water activity at 25° C for sodium chloride (O), potassium chloride (●), calcium chloride (Δ) and sucrose (x).

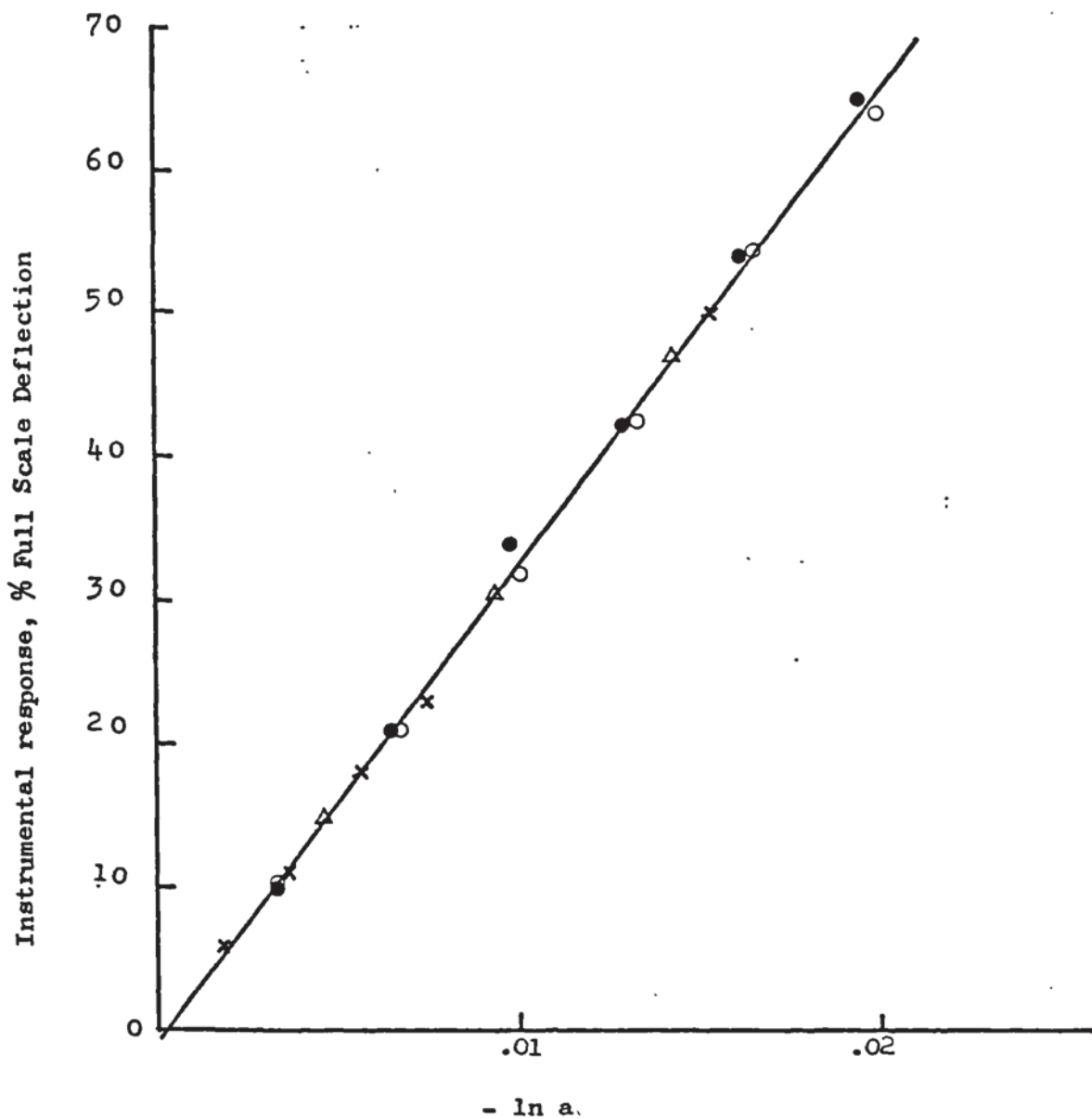


Figure 2.4 Water activity versus molality for aqueous solutions of isoprenaline hydrochloride at 37° C (\diamond), isoprenaline sulphate at 37° C (\blacklozenge), salbutamol sulphate at 37° C (Δ) and disodium cromoglycate at 37° C (\circ) and 25° C (\bullet). The solid lines indicate the linear approximations used to compute equilibrium diameters with the inclusion of the Kelvin effect. Also shown are the lines for ideal solution behaviour assuming dissociation into 2 ions (.....) - cf isoprenaline hydrochloride, or 3 ions (.....) - cf disodium cromoglycate and sulphates of isoprenaline and salbutamol.

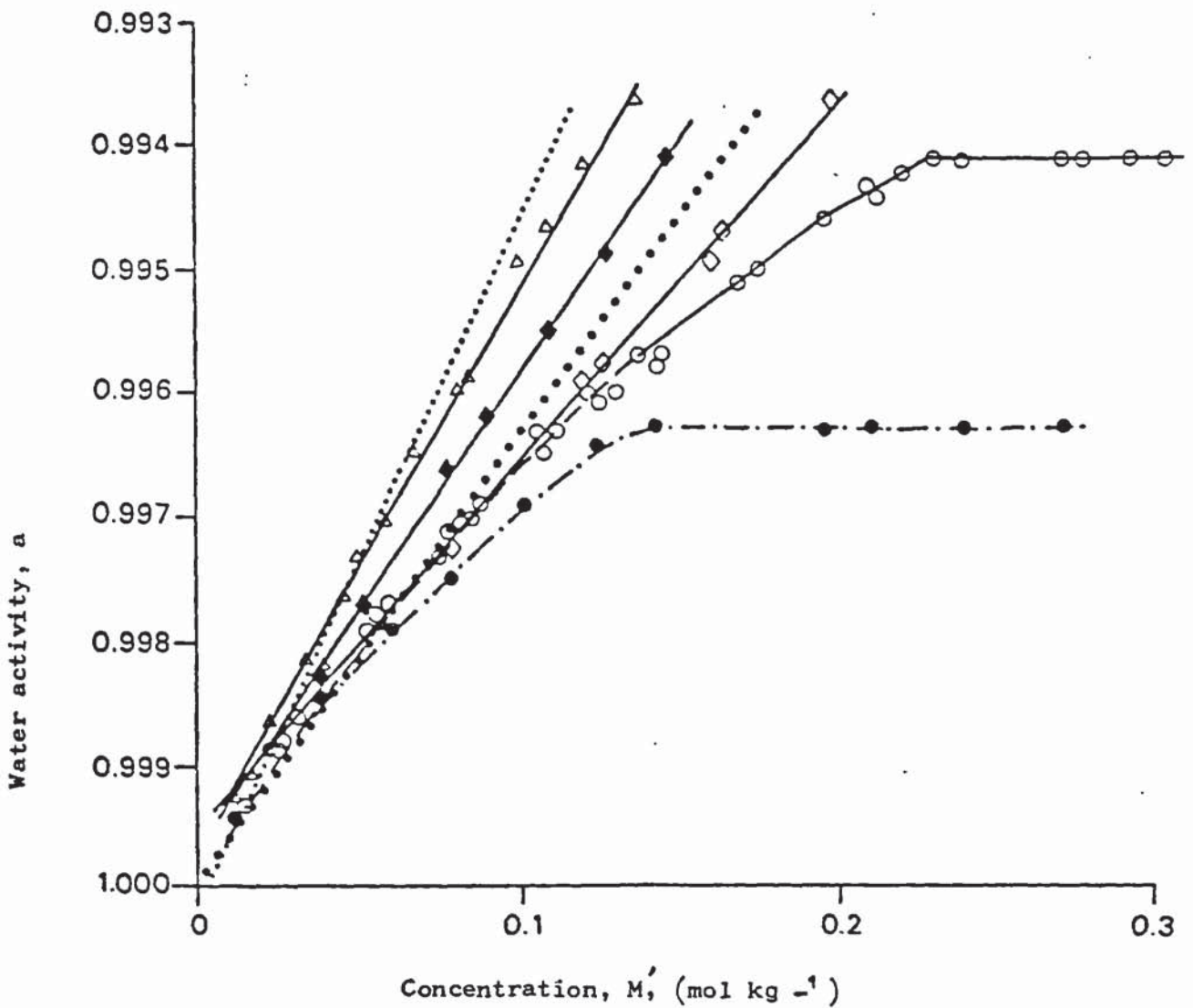


Figure 2.5 : Density of aqueous solutions of Disodium cromoglycate (O), salbutamol sulphate (x) isoprenaline hydrochloride (●) and isoprenaline sulphate (Δ) at 37°C. The solid lines illustrate the linear approximations used to determine droplet equilibrium diameters with the inclusion of the Kelvin effect. The mean of three determinations is illustrated.

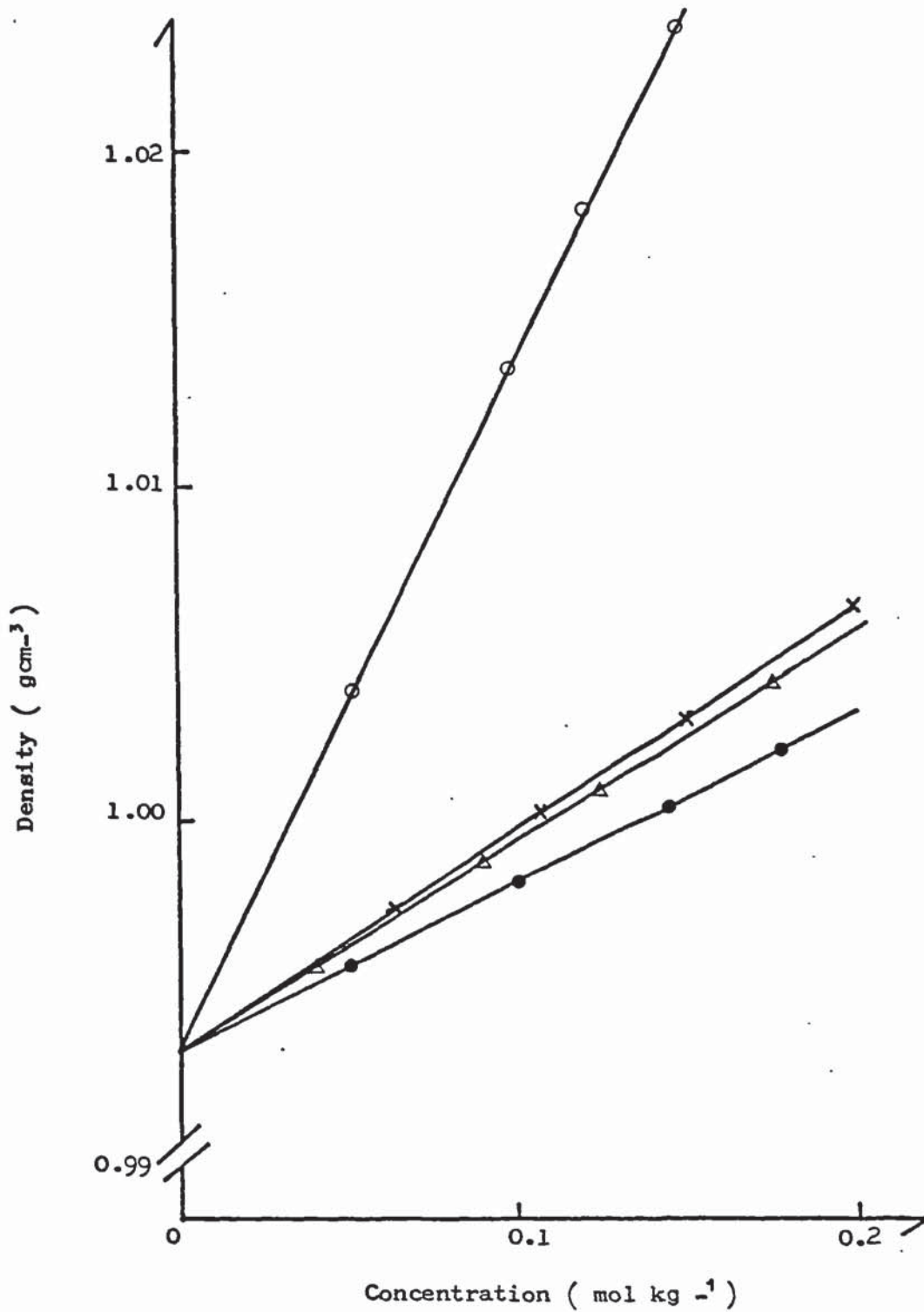


Figure 2.6 Calibration of surface tension apparatus, instrumental response versus surface tension. The mean of three determinations is illustrated, individual readings were with ± 1 instrumental response unit of the mean.

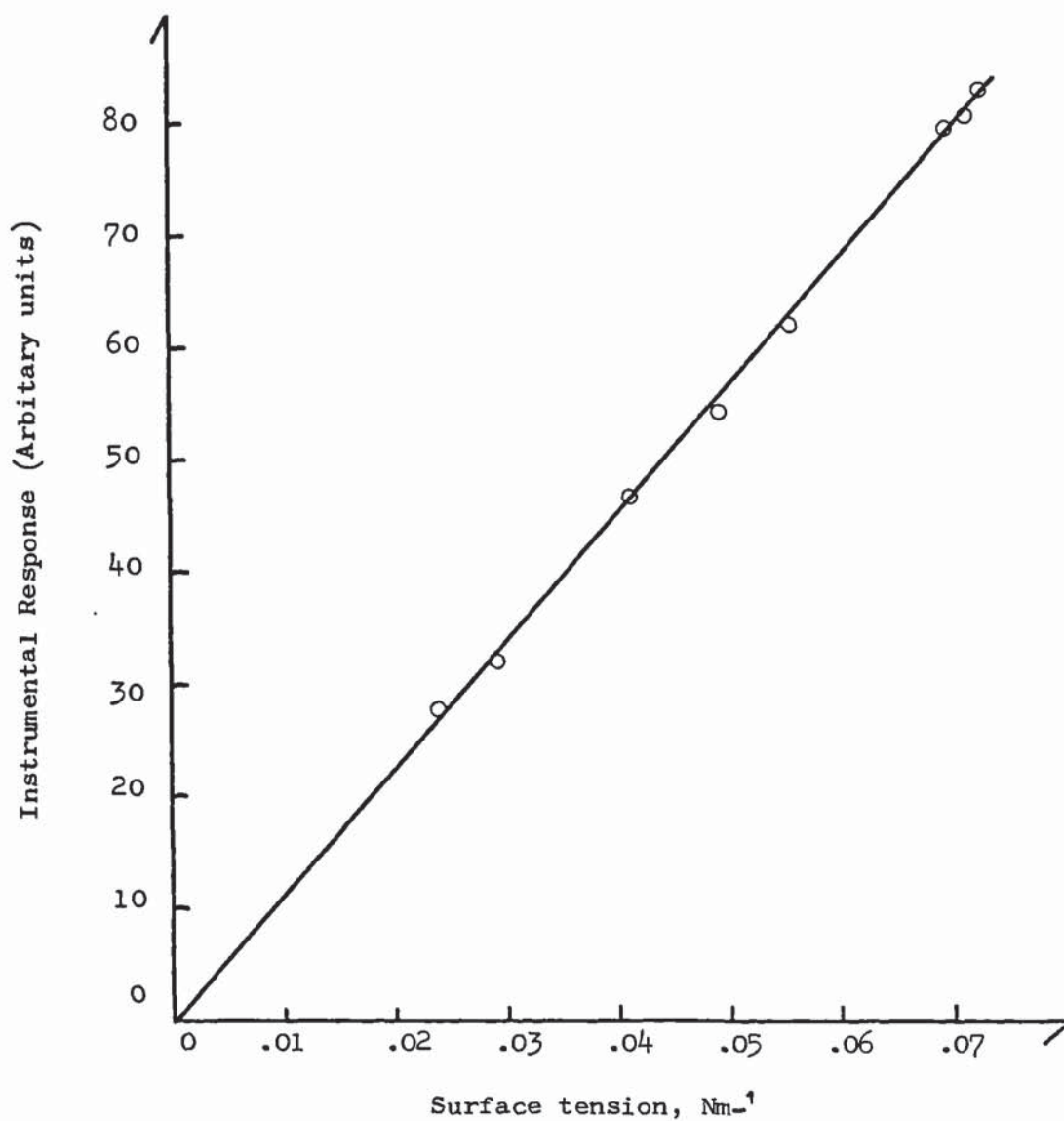


Figure 2.7 Surface tension against tension molality at 37° C for aqueous solutions of disodium cromoglycate (●), isoprenaline hydrochloride (▲), isoprenaline sulphate (△) and salbutamol sulphate (○). The solid lines indicate the linear approximations used to compute the equilibrium diameters with inclusion of the Kelvin effect.

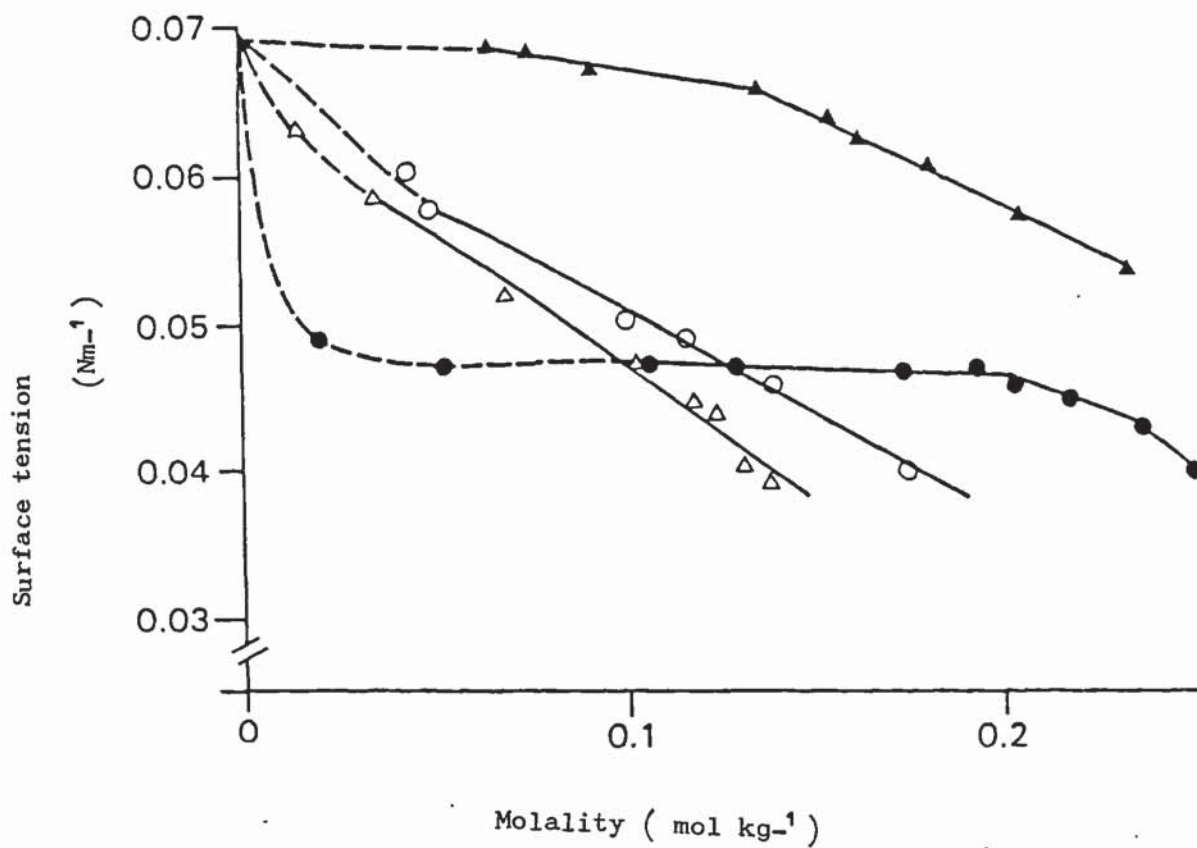
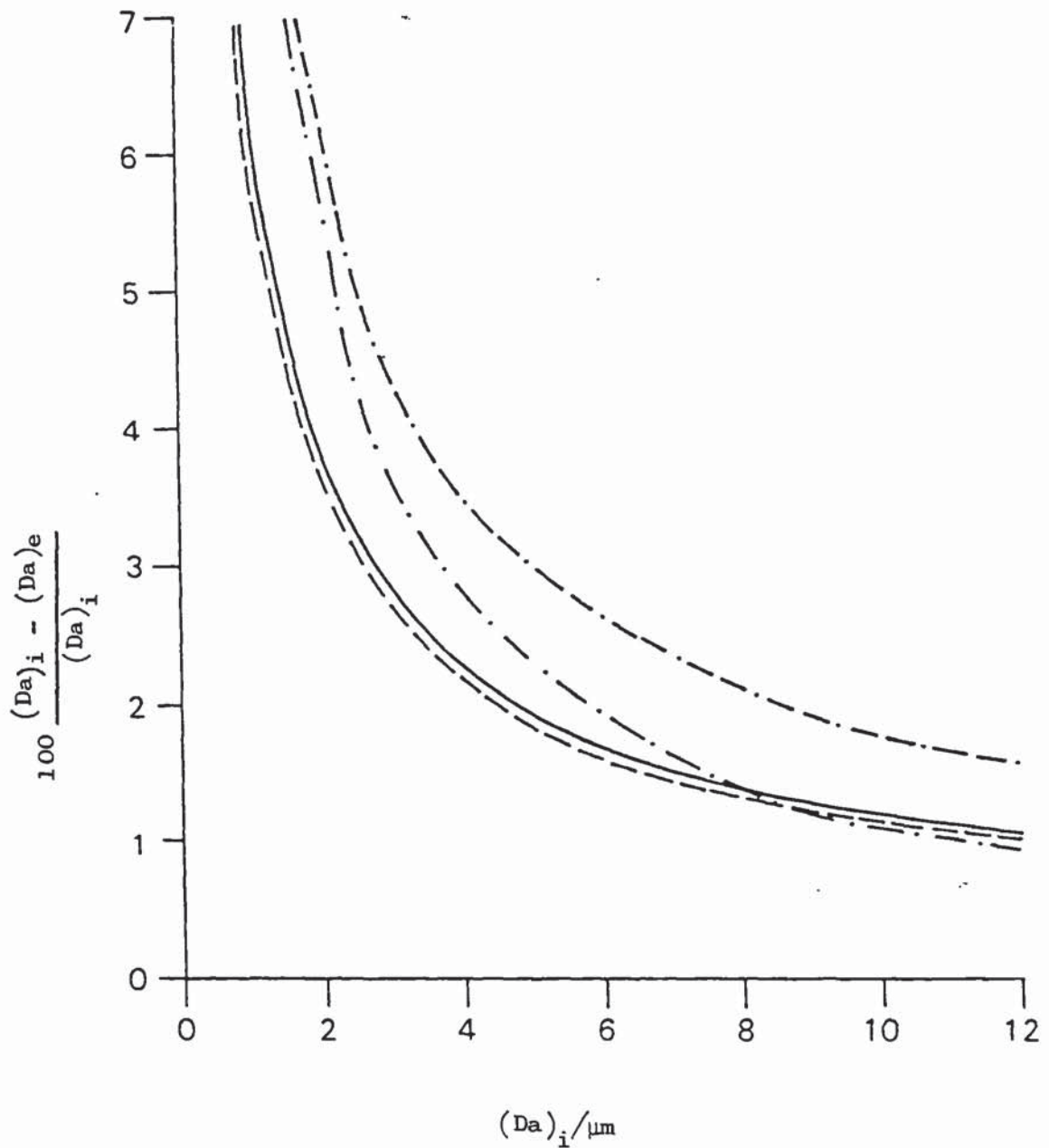


Figure 2.8 Percentage error caused by neglecting the Kelvin effect in calculation of equilibrium droplet size: $(D_a)_e$ & $(D_a)_i$ - aerodynamic diameters calculated with and without the Kelvin correction, respectively. Results for isoprenaline sulphate (—), isoprenaline hydrochloride (-.-.-.), salbutamol sulphate (---) and disodium cromoglycate (-.-), all at 37° C



Chapter 3 PREDICTED DEPOSITION OF INHALATION AEROSOLS IN THE RESPIRATORY TRACT

3.1 INTRODUCTION

It has been shown that the drugs examined are likely to more than double in aerodynamic diameter when exposed to the high humidity of the respiratory tract. As the site and extent of deposition is a function of aerodynamic diameter this increase in diameter is likely to affect the available dose of drug administered. Large particles may deposit higher in the respiratory tree and be subject to ciliary clearance with subsequent swallowing. However smaller particles which would initially be expected to be exhaled may be deposited in the respiratory tract because of the increase in aerodynamic diameter. It is useful therefore to quantify the changes in deposition that may arise from condensation growth.

Deposition in the respiratory tract is known to be determined by both physiological parameters and aerosol particle characteristics. The experimental determination of aerosol deposition is by no means easy, indeed large discrepancies in reported results have been attributed to uncontrolled experimental variables and poor experimental technique (Davies, 1974). Lippmann (1977) has reviewed the available experimental data and found that elimination of data collected using doubtful techniques reduced scatter, but in trials involving more than one subject there was considerable individual variation between subjects which may be attributed to differences in the morphology of the lungs.

Experimental determinations have revealed differences in tracheo-bronchial deposition between healthy smokers and non-smokers (Lippmann, 1977; Stahlhofen et al, 1980) and deposition patterns in patients with respiratory diseases would be expected to differ from deposition in the healthy, normal population.

Predictive models of deposition have mainly been developed to estimate the impact of environmental pollutant aerosols. The TASK model (1966) and its successor (ICRP, 1979) have been developed to determine lung dosimetry after exposure to radioactive aerosols. As the usual mode of breathing is through the nose these models use data for nose deposition in healthy volunteers as their basis (Pattle, 1961). In inhalation therapy the drug aerosol is normally inhaled through the mouth, frequently a breath-holding manoeuvre is also employed. A more realistic model for determining trends in inhalation therapy deposition should take this into account. Davies (1980) has developed an empirical model for total deposition during mouth breathing for individuals, in which the model parameters are obtained from a large number of experiments on each individual. For particles below $3\mu\text{m}$ diameter, this model would indicate the dose deposited in the tracheobronchial and pulmonary regions of the respiratory tract (as defined by TASK, 1966). Above this diameter when head deposition becomes significant total deposition no longer reveals the tracheobronchial and pulmonary dose. This type of approach could however be useful when an individual patients respiratory characteristics can be found (for example with the hospital patient) to determine the dose of therapeutic aerosol likely to

deposit in the tracheobronchial and pulmonary regions.

Models applicable to the whole population or discrete populations (for example certain age groups or disease states) could be useful in designing aerosol formulations to optimise tracheobronchial and or pulmonary deposition.

The model used in this study (developed by Dr. I Gonda) is based on empirical descriptions of regional deposition in healthy volunteers breathing through the mouth. Currently this model does not include the breath-holding manoeuvre. The absolute numerical values obtained using this model are therefore unlikely to give true values for the deposition of a drug administered by the inhalation route. The model does however provide a means of testing the difference which very rapid hygroscopic growth could make to the regional deposition of an inhaled aerosol.

The cumulative weight distribution with regard to equivalent volume diameter for micronised disodium cromoglycate (DSCG) was obtained using a Coulter Counter (Model ZB, Coulter Electronics Ltd) with a 50 μ m orifice. The electrolyte system used was ammonium thiocyanate in isopropyl alcohol presaturated with DSCG and filtered through a 0.1 μ m pore cellulose filter (MF-Millipore, Millipore (UK) Ltd). As the number of counts per channel did not change with time, it was assumed that the electrolyte system had no effect on the original size distribution of the powder. The results obtained are shown in Figure 3.1.

Assuming the particles to be spherical, the equivalent volume diameters were converted to aerodynamic diameters by means of Equation 1.3 and the dry powder density determined by air comparison pycnometry (see section 2.3.3.1.). The size distribution of the droplets that would be formed in equilibrium with the humidity of the respiratory tract was determined using the physicochemical data described in Chapter 2 and the iterative programme described in that chapter (i.e. they include the Kelvin effect). The cumulative weight distribution versus aerodynamic diameter is shown in Figure 3.2 and may be adequately described by a lognormal distribution with a mass median aerodynamic (MMAD) of 5.45 μ m and geometric standard deviation (σ_g) of 3.11. The equilibrium droplet distribution could also be described by a lognormal distribution with MMAD of 11.26 μ m and σ_g of 3.18.

The cumulative weight distribution versus equivalent volume diameter of micronised isoprenaline sulphate determined using a Coulter Counter was supplied by Riker Laboratories. Isoprenaline hydrochloride was said to have a similar size distribution. The aerodynamic diameter size distributions for the dry particles and equilibrium droplets were calculated including the Kelvin effect using the physicochemical data described in Chapter 2. The aerodynamic dry particle size distributions for the two isoprenaline salts will differ as the two salts have different densities (see section 2.3.3.1). The distributions may be approximated by two normal distributions: for example, the cumulative weight distribution versus aerodynamic diameter of dry isoprenaline sulphate powder may be described by a normal distribution with a mass median aerodynamic diameter of $3.77\mu\text{m}$ and a standard deviation of $1.34\mu\text{m}$ for particles below $6.2\mu\text{m}$ and a normal distribution with MMAD of $56.32\mu\text{m}$ and standard deviation of $33.48\mu\text{m}$ for particles greater than $6.2\mu\text{m}$. These approximated distributions are shown as the solid lines in Figure 3.4 and 3.5.

3.3 DEPOSITION MODEL FOR MOUTH INHALATION

A model of deposition for mouth inhalation developed by Dr. Gonda based on published empirical data and the TASK model was used in this study.

Experimental data for aerosol deposition in the head during mouth breathing (Lippmann, 1977) when plotted against $Da^2 If$, where Da is the aerodynamic diameter and If the mean inspiratory flow rate, may be approximated by two intercepting rectilinear lines (Mercer, 1975). The mean inspiratory flow rate for any particular tidal volume, Iv and respiratory rate, r , may be calculated from

$$If = 2 \times Tv \times r \quad \text{Equation 3.1}$$

So, for example, at 15 respirations per minute and a tidal volume of 0.75 litres, the mean inspiratory flow rate will be

$$\begin{aligned} If &= 2 \times 0.75 \times 15 \quad 1 \text{ min}^{-1} \\ &= 22.5 \quad 1 \text{ min}^{-1} \quad \text{Equation 3.2} \end{aligned}$$

The intercept for the two rectilinear lines correspond to an aerodynamic diameter of $4.99\mu\text{m}$ for a tidal volume of 0.75 litres and 15 respirations per minute, resulting in a discontinuity in the curve for head deposition at that value (see Figure 3.6).

Lippmann (1977) has also shown that tracheobronchial deposition, when expressed as the fraction depositing of that entering the trachea, versus $\log Da^2$ may also be described by a rectilinear plot. The experimental data in Lippmann's study did not extend below approximately 10% deposition, corresponding to an aerodynamic diameter of $3\mu\text{m}$ at a tidal volume of 0.75 litres and 15 respirations per minute. The model therefore draws upon the TASK model (TASK group, 1966) for tracheobronchial deposition of particles below $3\mu\text{m}$. The data from the TASK model was corrected for nose inhalation by

$$TB = \frac{TB_n}{(1 - H_n)} \quad \text{Equation 3.3}$$

where TB is the fractional tracheobronchial deposition of the amount of aerosol entering the trachea and TB_n and H_n the depositing fractions in the tracheobronchial and head regions after nose inhalation respectively. The tracheobronchial deposition for mouth inhalation, TB_m was calculated from

$$TB_m = TB (1 - H_m) \quad \text{Equation 3.4}$$

where H_m is the deposition in the head region after mouth inhalation. The values for TB_m were fitted using NONLIN (Metzler, 1969) to an empirical equation of the form

$$TB_m = \frac{1 + a^1 Da + b^1 Da^2 + c^1 Da^3}{d^1 + e^1 Da + f^1 Da^2 + g^1 Da^3} \quad \text{Equation 3.5}$$

where a^1 , b^1 , c^1 , d^1 , e^1 , f^1 and g^1 are empirical constants
The deposition in the tracheobronchial region for particles
less than $0.01\mu\text{m}$ aerodynamic diameter is set at the deposition
value at $0.01\mu\text{m}$ in this model.

The values for pulmonary deposition used in this model
have similarly been determined from the TASK model. Mercer
(1975) has determined that the TASK model will tend to over-
estimate pulmonary deposition at the expense of tracheobronchial
deposition. When total deposition, that is head deposition
plus tracheobronchial and pulmonary deposition, exceeded 1,
the deposition in the pulmonary region, P_m , was described by

$$P_m = 1 - (TB_m + H_m) \quad \text{Equation 3.6}$$

The model at 1.45 litres and 2.15 litres tidal volumes and 15
respirations per minute are illustrated in Figures 3.7 and 3.8
respectively.

3.4

CALCULATED DEPOSITION OF INHALED AEROSOLS

The fraction of the dose, F, deposited in the head, tracheobronchial and pulmonary regions of the respiratory tract have been calculated from the probability of deposition, P(Da), of a particle with aerodynamic diameter, Da, and the mass size distribution function, f (Da), integrated with respect to aerodynamic diameter.

$$F = \int_0^{\infty} P(Da) \cdot f(Da) \cdot d Da \quad \text{Equation 3.7}$$

The integral was evaluated numerically.

In calculating the effects of condensation growth on the regional deposition of an inhalation aerosol, it has been assumed that equilibrium is instantaneously attained on the entry of the aerosol into the respiratory tract.

The calculated deposition values are summarised in Table 3.1.

Table 3.1: Calculated deposition fractions in the head tracheobronchial and pulmonary regions of dry powders and equilibrium droplets of DSCG, Isoprenaline hydrochloride and Isoprenaline Sulphate

Disodium cromoglycate

	Dry Powder			Equilibrium Droplets		
	750ml	1450ml	2150ml	750ml	1450ml	2150ml
Head	0.35	0.45	0.51	0.57	0.67	0.73
Tracheobronchial	0.20	0.16	0.16	0.18	0.13	0.12
Pulmonary	0.27	0.25	0.21	0.17	0.14	0.11
Total	0.82	0.86	0.88	0.92	0.94	0.96

Isoprenaline hydrochloride

	Dry Powder			Equilibrium Droplets		
	750ml	1450ml	2150ml	750ml	1450ml	2150ml
Head	0.09	0.18	0.27	0.55	0.74	0.83
Tracheobronchial	0.23	0.26	0.27	0.31	0.18	0.12
Pulmonary	0.49	0.44	0.37	0.10	0.07	0.04
Total	0.81	0.88	0.91	0.96	0.99	0.99

Isoprenaline Sulphate

	Dry Powder			Equilibrium Droplets		
	750ml	1450ml	2150ml	750ml	1450ml	2150ml
Head	0.09	0.19	0.28	0.45	0.65	0.76
Tracheobronchial	0.23	0.26	0.30	0.35	0.23	0.17
Pulmonary	0.48	0.43	0.36	0.16	0.10	0.06
Total	0.80	0.88	0.94	0.96	0.98	0.99

3.5 DISCUSSION

These calculations are an attempt to quantify the effect of condensation growth on regional deposition. It has been assumed that the size distribution from the commercial aerosol generators (for DSCG the spinhaler ^(R) and for the isoprenaline salts pressure pack generators) will be similar to those of the micronised dry powders used in the preparation of these dosage forms. This is probably an over optimistic view, Bell et al (1971) has shown that the output from the spinhaler will consist of drug particles adhering to the lactose particles included in Intal capsules to improve flow from the capsule, some aggregates of drug particles as well as primary drug particles.

It has also been assumed that equilibrium is attained instantaneously; however calculations for the deposition of soluble inorganic aerosols by Ferron (1977) indicate that considerations of growth rates may alter the calculated deposition pattern. In the absence of data on the rate of condensation growth of pharmaceutical aerosols, models for real time growth would be based on simple electrolyte systems, and thus result in further uncertainty on the absolute deposition values obtained. Because of these assumptions and the simplicity of the model employed the trends of deposition are of more significance than the absolute values obtained. The calculated deposition fractions illustrate that while total deposition increases with increasing tidal volume, this is mainly because of increased head deposition with correspondingly

less dose available for tracheobronchial and pulmonary regions. As would be expected, for small differences in the particle size distributions, as for the dry powders of the isoprenaline salts, the calculated deposition fractions are very similar. When hygroscopic growth is considered the potential differences between the two isoprenaline salts become more apparent. The calculations reveal that given the same initial particle size distribution of the generated aerosol, isoprenaline sulphate would be expected to deliver more drug to the tracheobronchial and pulmonary regions, than the hydrochloride salt.

The results also predict that less aerosol would be exhaled if the aerosols form equilibrium droplets compared with the aerosol remaining as a dry powder in the respiratory tract. The deposition model used here does not include the breath-holding manoeuvre which is commonly employed in inhalation therapy. With this manoeuvre small particles which are exhaled during normal breathing, can deposit in the lower part of the respiratory tract given sufficient time (Byron et al, 1977). Consequently the predicted difference in exhaled aerosol due to condensation growth is unlikely to be observed in reality.

It should also be noted that the deposited dose may not in fact reflect the systemically available dose. In the tracheobronchial region the deposited dose will be subject to competing ciliary clearance and absorption. In the pulmonary region the deposited dose will be subject to competing absorption and lymphatic clearance.

FIGURESFigure Captions

- Figure 3.1 Cumulative mass size distribution of Disodium Cromoglycate (DSCG). Percent weight undersize versus equivalent volume diameter of dry powder.
- Figure 3.2 Cumulative mass size distribution of DSCG. Percent weight undersize versus aerodynamic diameter of the dry powder (o) and droplets in equilibrium with 99.5% relative humidity (●).
- Figure 3.3 Cumulative mass size distribution of Isoprenaline Sulphate (courtesy of Riker Laboratories). Percent weight undersize versus equivalent volume diameter of dry powder.
- Figure 3.4 Cumulative weight versus aerodynamic diameter of Isoprenaline Sulphate of the dry powder (o) and droplets in equilibrium with 99.5% relative humidity (●).
- Figure 3.5 Cumulative weight versus aerodynamic diameter of Isoprenaline Hydrochloride of the dry powder (o) and droplets in equilibrium with 99.5% relative humidity (●).
- Figure 3.6 Model for deposition: Fraction deposited versus aerodynamic diameter, 750ml tidal volume, 15 respirations per minute for mouth breathing. Total deposition (____), head deposition (____), tracheobronchial deposition (---) and pulmonary deposition (.....).
- Figure 3.7 Model for deposition: Fraction deposition versus aerodynamic diameter, 1450ml tidal volume, 15 respirations per minute for mouth breathing. Total deposition (____), head deposition (____), tracheobronchial deposition (---) and pulmonary deposition (.....).
- Figure 3.8 Model for deposition: Fraction deposited versus aerodynamic diameter; 2150ml Tidal volume, 15 respirations per minute, mouth breathing. Total deposition (____), head deposition (____), tracheobronchial deposition (---) and pulmonary deposition (.....).

Figure 3.1 Cumulative mass size distribution of disodium cromoglycate. % weight undersize versus equivalent volume diameter of dry powder.

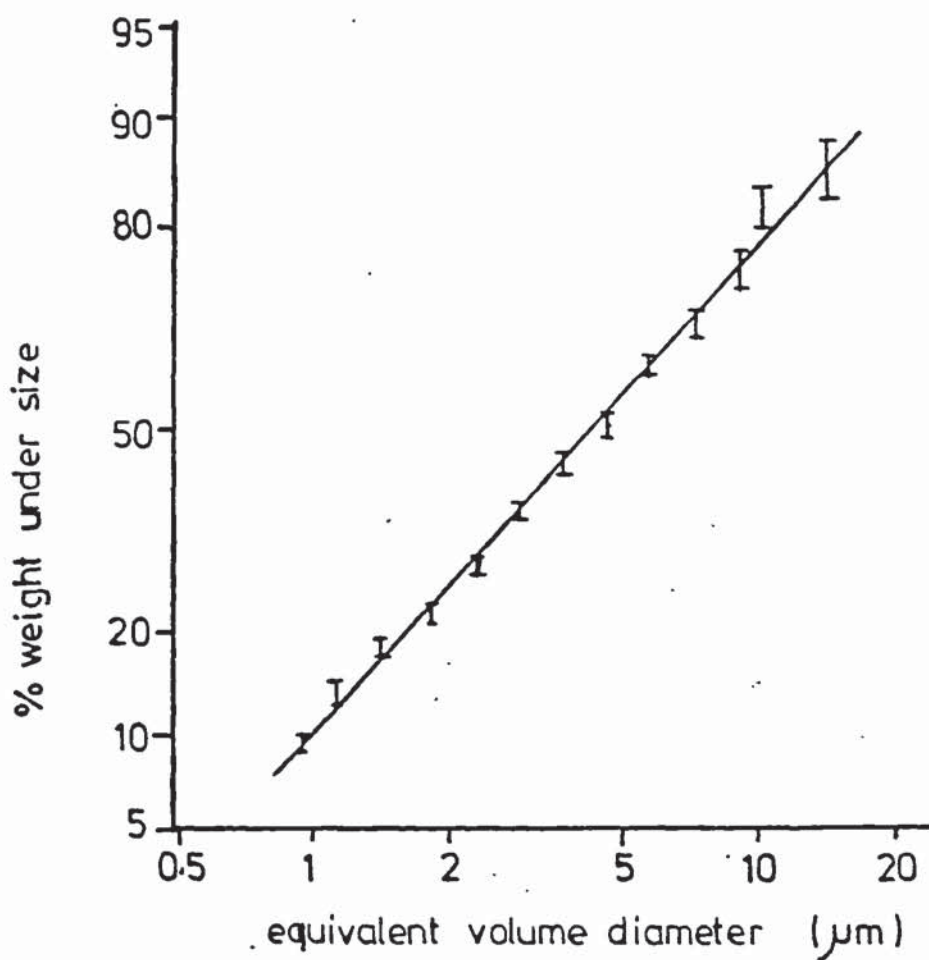


Figure 3.2 Cumulative mass size distribution of disodium cromoglycate % weight undersize versus aerodynamic diameter of the dry powder (o) and droplets in equilibrium with 99.5% relative humidity (●).

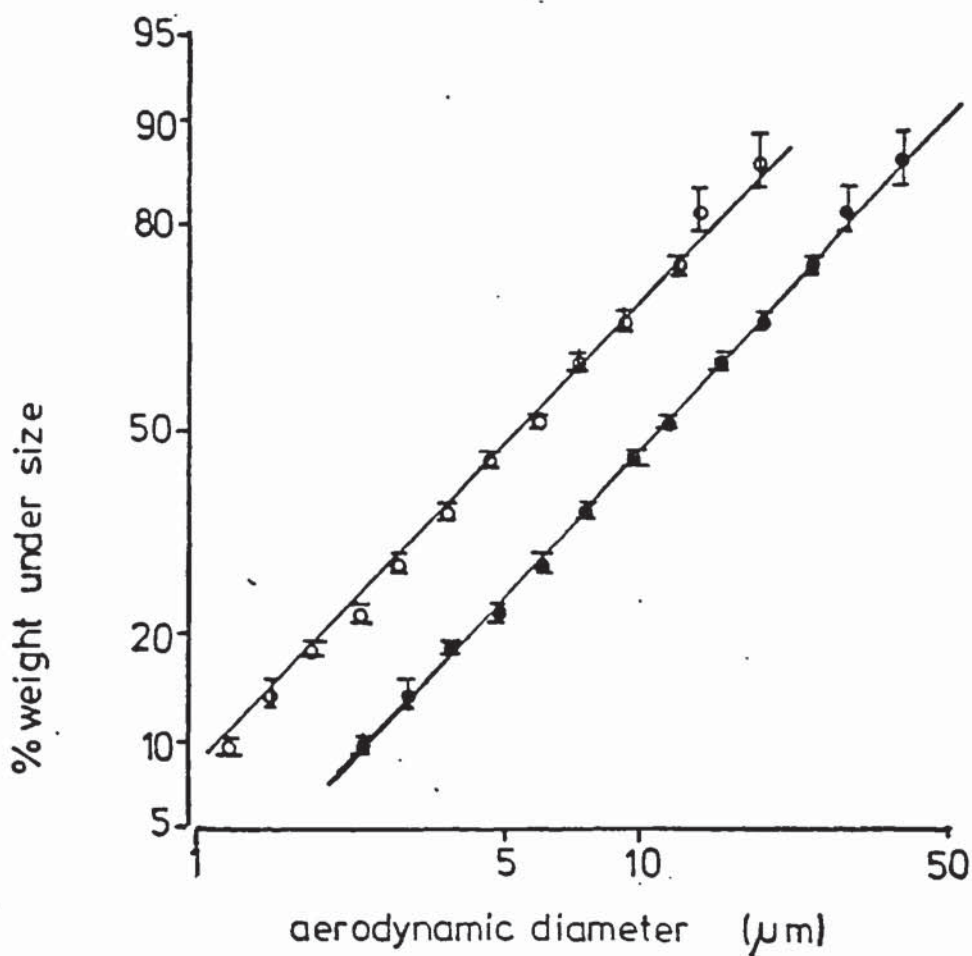


Figure 3.3 Cumulative mass size distribution of Isoprenaline sulphate (courtesy of Riker Laboratories) % weight undersize versus equivalent volume diameter.

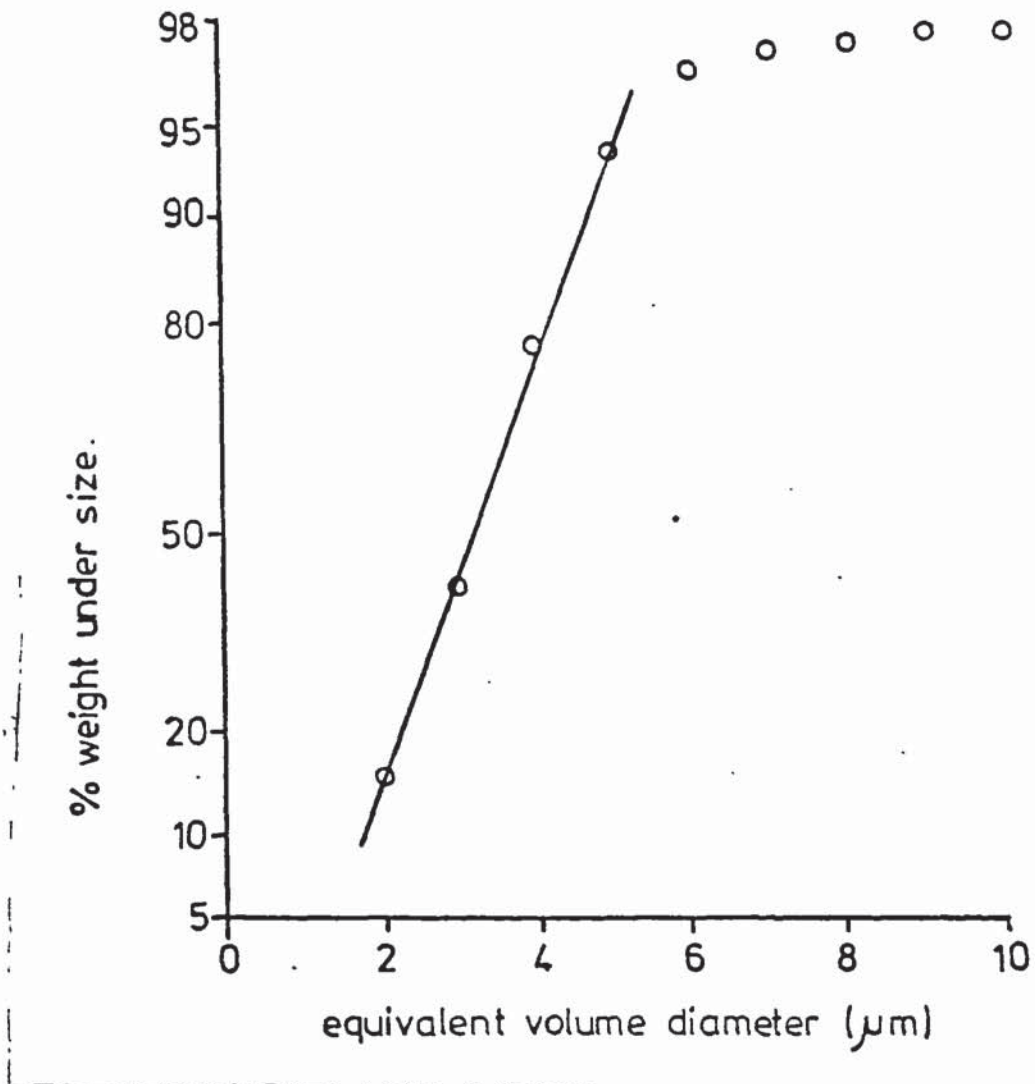


Figure 3.4 Cumulative weight versus aerodynamic diameter of Isoprenaline sulphate of the dry powder (o) and droplets in equilibrium with 99.5% relative humidity (●)

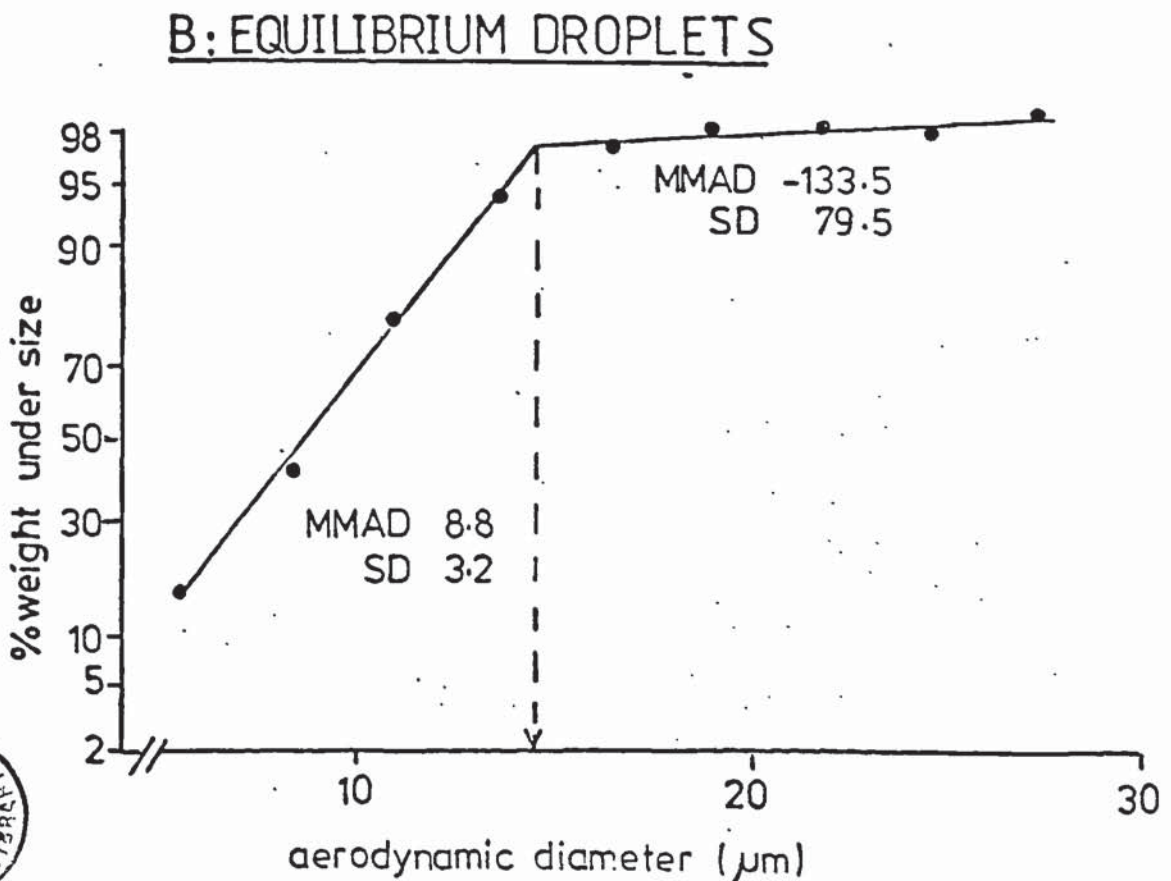
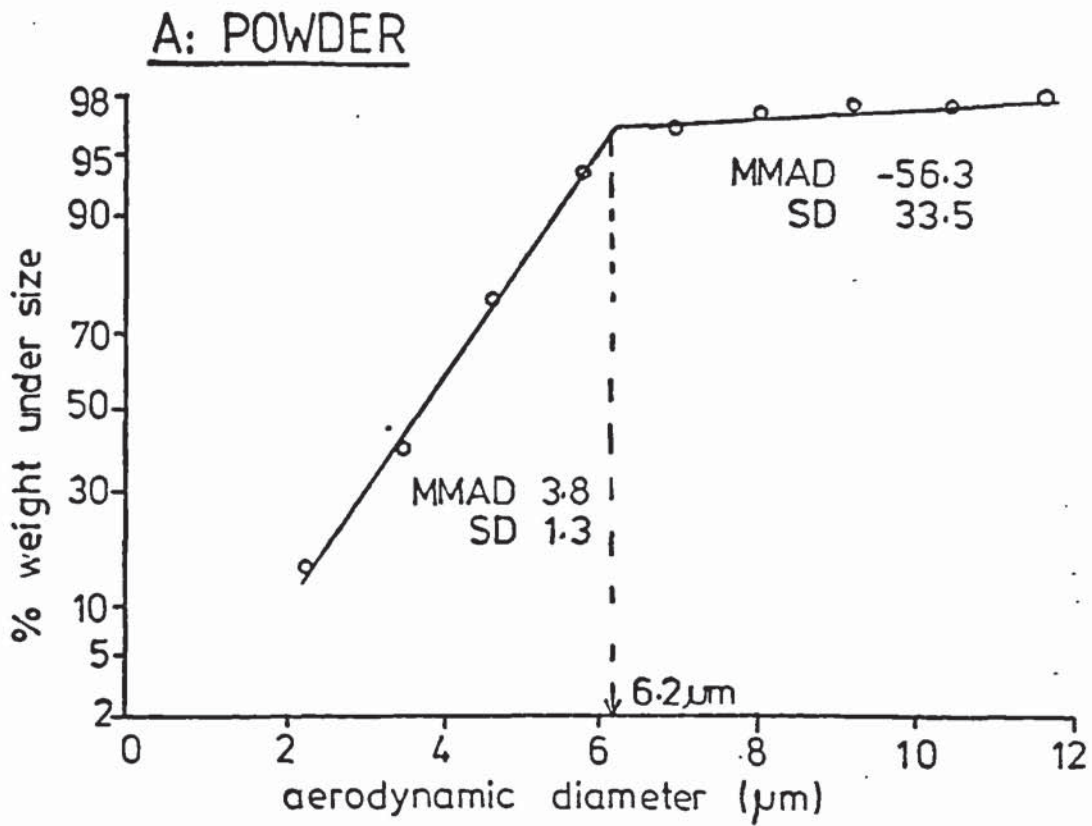


Figure 3.5 Cumulative weight versus aerodynamic diameter of Isoprenaline hydrochloride of the dry powder (o) and droplets in equilibrium with 99.5% relative humidity (●).

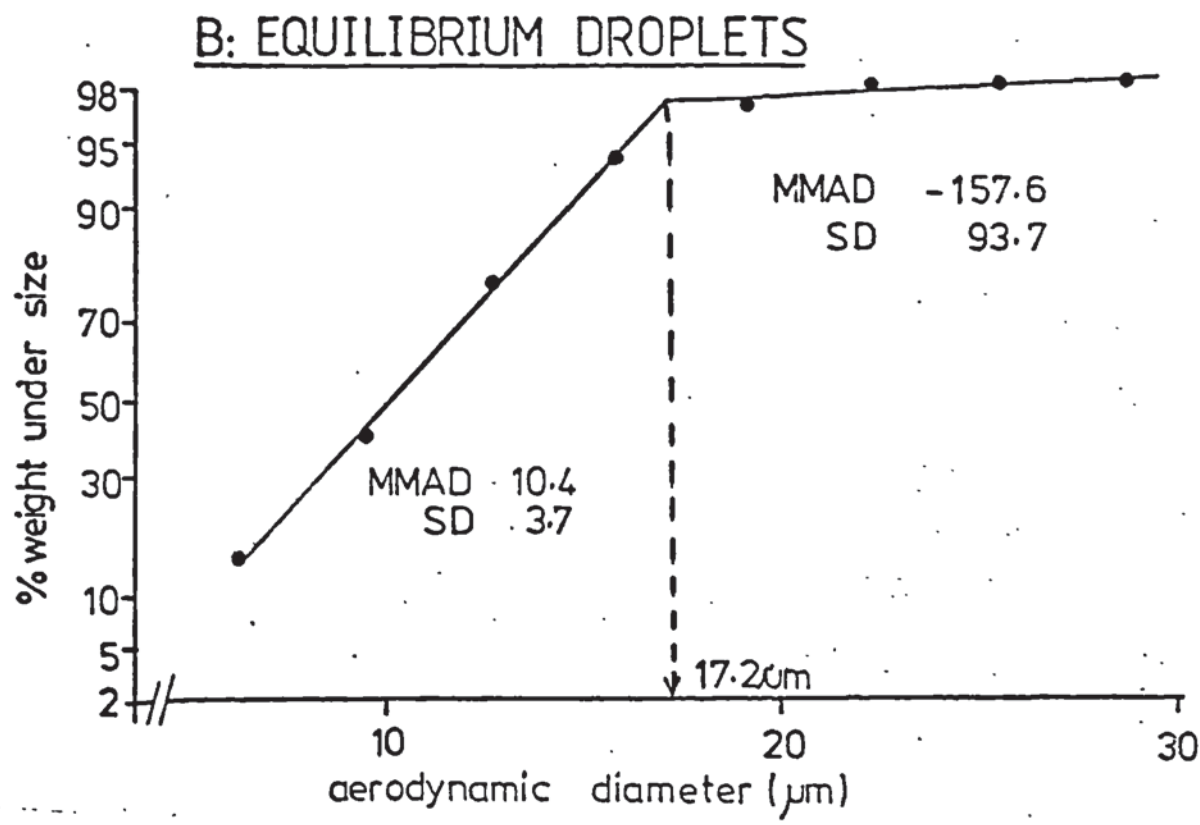
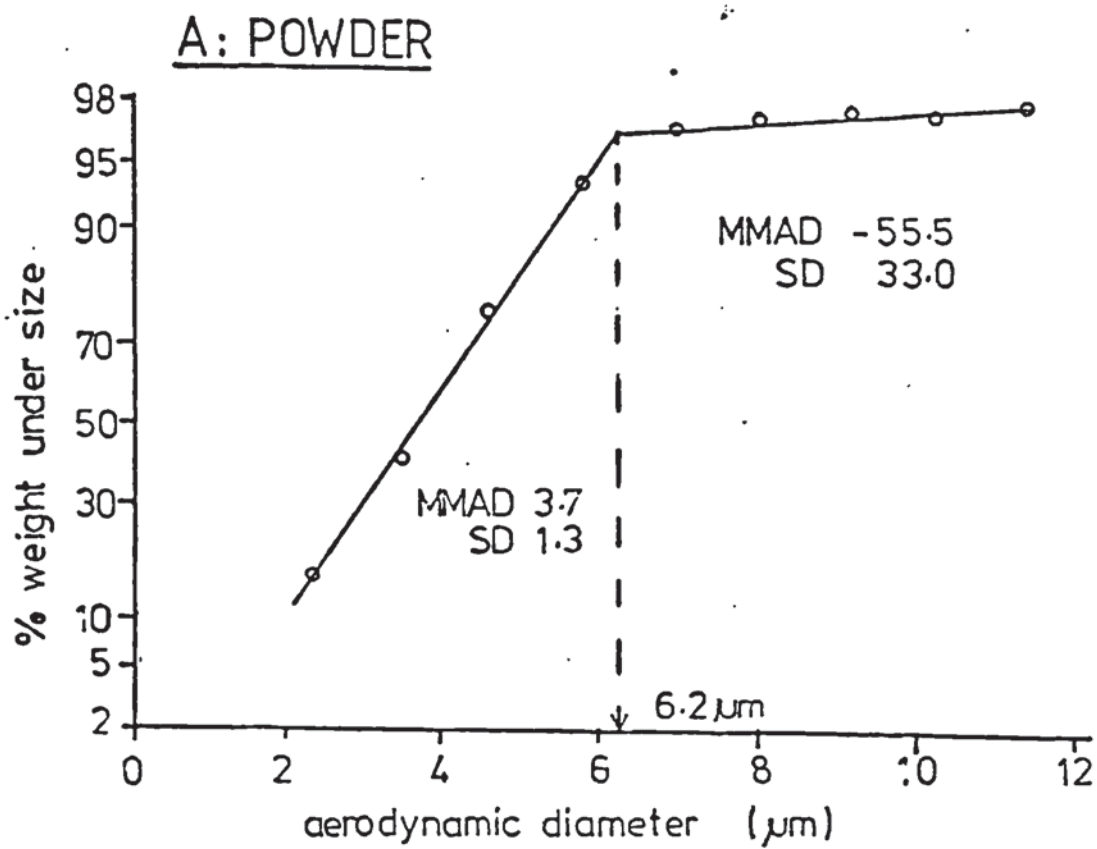


Figure 3.6 Model for deposition: Fraction deposited versus aerodynamic diameter, 750ml Tidal volume, 15 respiration min^{-1} for mouth breathing, Total deposition (—), head deposition (— · —) tracheobronchial deposition (---) and pulmonary deposition (.....).

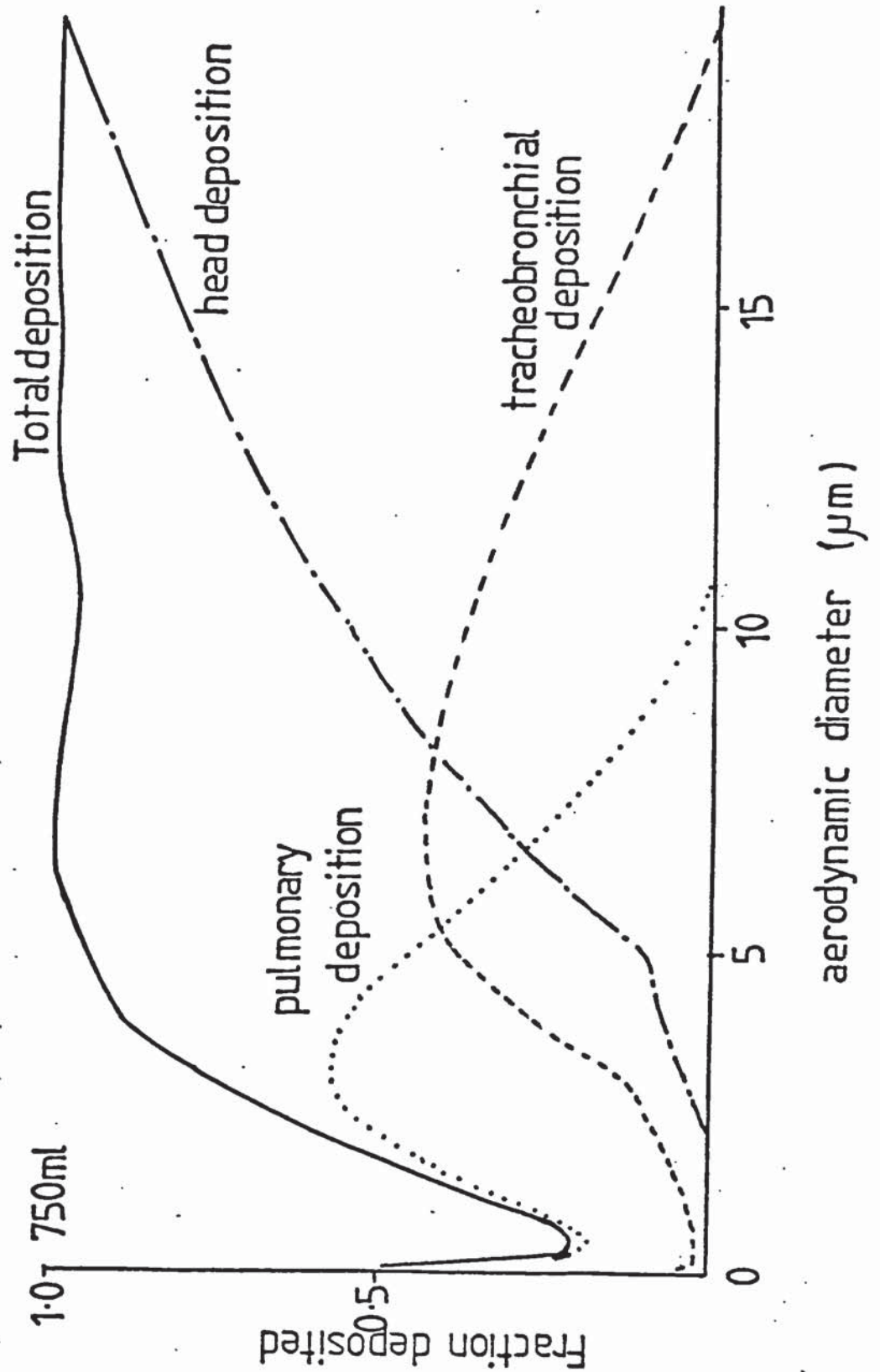


Figure 3.7 Model for deposition: Fraction deposited after mouth breathing, 1450ml tidal volume, 15 respirations per minute, mouth breathing. Total deposition (—) head deposition (—·—), tracheobronchial deposition (----) and pulmonary deposition (.....).

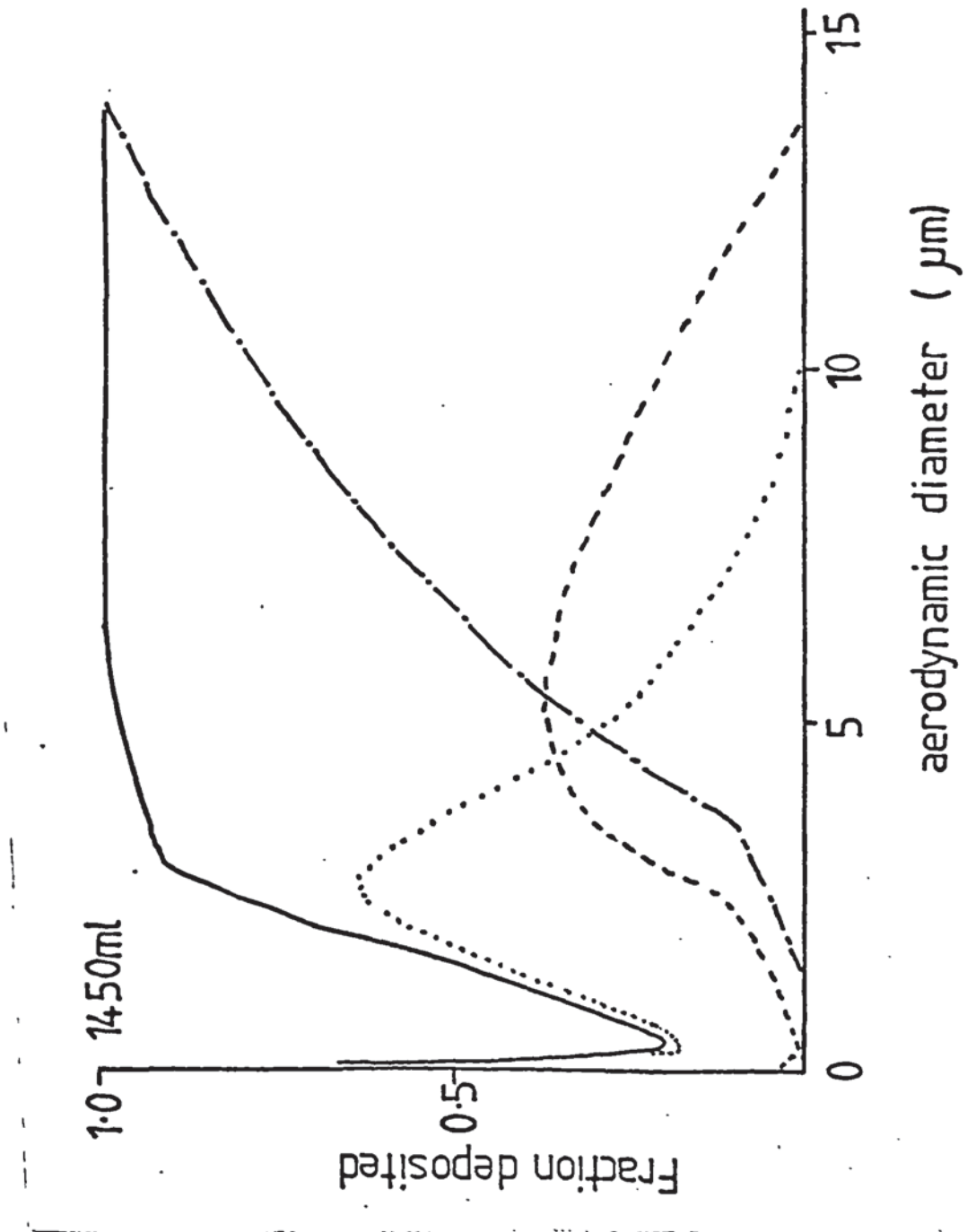
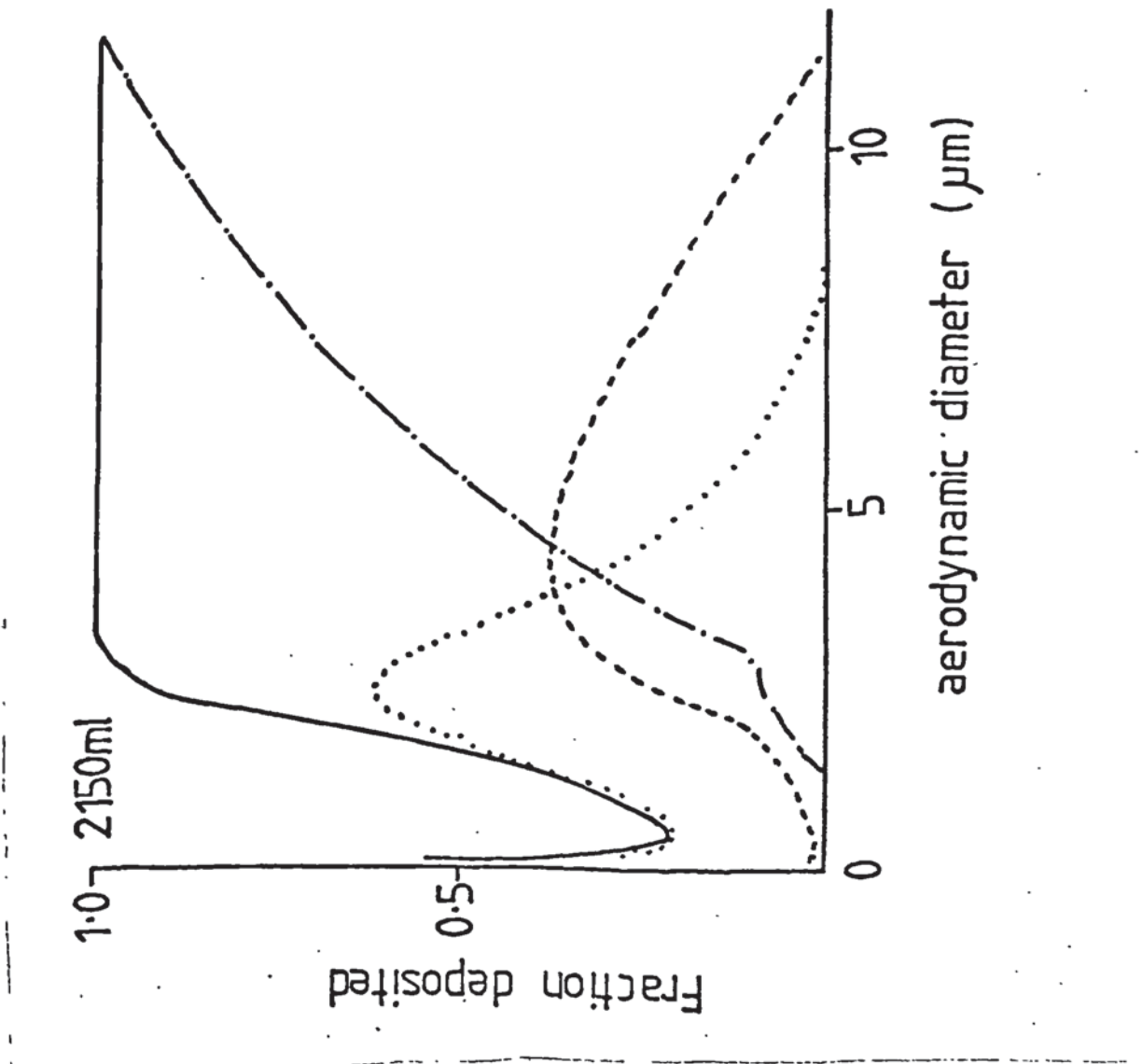


Figure 3.8 Model for deposition: Fraction deposited versus aerodynamic diameter; 2150ml Tidal volume, 15 respirations per minute, mouth breathing. Total deposition (—), head deposition (—•—), tracheobronchial deposition (---) and pulmonary deposition (.....).



4.1 INTRODUCTION

The major domicilliary aerosol generator used in inhalation therapy is the pressure pack. Aerosols generated from the pressure pack will be polyphasic and so it is not possible to predict the aerosol behaviour at high humidity on the basis of the physicochemical measurements described in chapter 2 for pure medicament alone. In these instances direct measurement of changes in the aerosol size distribution at high humidity are desirable. From a therapeutic viewpoint it is the behaviour of aerosol particles which contain the drug which are of interest. For this reason the use of a sizing device capable of distinguishing between drug containing aerosol particles and those void of medicament is desirable. Impaction techniques allow the collection of aerosols in various aerodynamic size fractions. Chemical or radioactive analysis of the deposits provides a means of distinguishing the aerodynamic size distribution of the drug.

The cascade impactor was the first instrument specifically developed for the separation of an heterogeneous aerosol cloud into several fractions each containing only particles between certain size limits (May, 1945). A schematic diagram of the instrument is shown in Figure 4.1a. It consists of a series of jets, each followed by an impaction slide, and is based on the principle that particles in a moving airstream will impact on a slide placed in the path of the airstream if their

momentum is sufficient to overcome the drag exerted by the airstream as it moves around the slide. Each jet is smaller than the preceding one, so the velocity of the airstream and that of the aerosol particles is increased as the aerosol cloud advances through the impactor. Consequently smaller particles eventually acquire enough momentum to impact on a slide. The final jet stage is followed by a filter to capture 'all' particles escaping impaction on the slides (Laskin, 1949).

When gravitational and electrical effects are small compared to inertial effects, the impaction process can be characterised by a single impaction parameter, Ψ , as derived by Ranz and Wong (1952).

$$\Psi = \frac{d_p \cdot V \cdot D_p^2}{18 \cdot g \cdot D_j} \quad \text{Equation 4.1}$$

where D_j is the diameter of the impaction jet, D_p the diameter of the aerosol particle; V , the velocity of the jet; d_p , the density of the aerosol particle and g the gas viscosity.

The relationship between the impaction parameter, Ψ and the impaction efficiency, E , will depend on the ratio of the jet to slide distance J , to Jet diameter (Mercer and Stafford, 1969) and Reynolds number, Re (Marple, 1979).

$$E = \Psi \left(\frac{J}{D_j}, Re \right) \quad \text{Equation 4.2}$$

The Battelle cascade impactors used in these studies (DCI5 and

DCI6, Delron Research Company, Powell, Ohio,) have been designed so that the ratio of jet to slide distance to jet diameter is constant (Mitchell and Pilcher 1959). These impactors, in common with many others, have been calibrated by determining impaction efficiency versus impaction parameter for one stage, then using Equation 4.1 to obtain calibration curves for all other stages (Mitchell and Pilcher, 1959). However, the Reynolds number of each jet is not constant throughout the impactor (see Table 4.1). Recent studies with other cascade impactors have revealed the inadequacies of this calibration technique (Cushing, 1979; Rao and Whitby, 1978b; Gonda et al. 1981). It was therefore felt necessary to calibrate the cascade impactor used in this study at the operating flow rates.

It has been shown that rebound can be a serious problem if the collection surfaces are not coated with a soft layer to cushion the impact of the particle (Mercer and Stafford, 1969). The performance of several types of coating have been assessed in various models of cascade impactors (Rao and Whitby, 1978a; Rao and Whitby, 1978b; Cushing, 1979; Groom and Gonda, 1980). Other sources of operating error may arise from disaggregation of loose particle aggregates which would be aerodynamically equivalent to a large single particle. If the sampling duration is too short (less than 10 seconds) systematic errors will occur mainly because of the effect of build up and decay of flow rates on impaction efficiencies (Blyth and Picknett, 1966). Particles not in direct contact with the collection surface may be re-entrained by the passing airstream (Corn and Stein, 1965). Wall losses or interstage losses, are caused by particles

depositing on surfaces other than the collection surface.

Mitchell and Pilcher (1957) have shown that this can be reduced to less than 4% by proper design of cascade impactors. These non-ideal collection characteristics of cascade impactors are illustrated schematically in Figure 4.1b.

4.2 EXPERIMENTAL PROCEDURES

4.2.1 Generation of monodisperse aerosols

Aerosols used for calibrating the cascade impactors were generated using a vibrating orifice monodisperse aerosol generator (Model 3050, Thermosystems Inc., St Paul Minnesota) with a Harvard syringe pump (compact infusion pump, Model 975, Harvard Apparatus Millis, Mass) and frequency generator (B and K Precision solid state Model E - 310B Sine/Square wave generator, Dynascan Corp, West Belle Alaine, Chicago, Illinois). This generator is based on the instability and break up of a cylindrical liquid jet (Rayleigh, 1878 and 1879). By applying a mechanical disturbance at constant frequency with sufficient amplitude, the jet will break up into equal sized droplets. To form a monodisperse aerosol these uniform droplets must be dispersed and diluted before coagulation occurs. Since one droplet is produced per cycle of disturbance, the droplet volume is given by the ratio of the liquid flow rate Q and the disturbance frequency f , so that the droplet diameter, D_d , is given by

$$D_d = \left(\frac{6Q}{\pi f} \right)^{1/3} \quad \text{Equation 4.3}$$

If a solution containing a non-volatile solute is sprayed through the orifice and the solvent allowed to evaporate, non-volatile particles of the solute are obtained. The particle diameter, D_p is given by

$$D_p = C^{1/3} \cdot D_d \quad \text{Equation 4.4}$$

where C is the volumetric concentration of the solute in the solution.

Any non-volatile impurities present in the solvent will cause an error in the calculated aerosol particle diameter, which may be corrected by

$$D_p^1 = \left(1 + \frac{N}{C}\right)^{1/3} D_p \quad \text{Equation 4.5}$$

where D_p^1 is the corrected particle diameter and N the volumetric concentration of the non-volatile impurity in the solvent (Berglund and Lui, 1973).

The aerosol particles used for calibration of the cascade impactors were solid fluorescein disodium particles and dioctyl phthalate, DOP, droplets containing less than 1% fluorescein disodium by weight, as a fluorescent tracer for quantitative analysis of deposited particles. The fluorescein disodium aerosols were prepared by dissolving the solute in analytical grade methanol. DOP aerosols were prepared by dissolving DOP in analytical grade isopropyl alcohol and adding fluorescein disodium to give a final ratio of fluorescein disodium to DOP of 1:1000 by weight. Following evaporation of solvent the desired fluorescein disodium tagged DOP aerosols were obtained. The size and solid nature of the fluorescein disodium aerosols were examined by light microscopy (Olympus model BHB, Olympus

Optical Company Ltd, Tokyo) and scanning electron microscopy (Cambridge 150a, Pye Unicam). For light microscopy samples were collected on coated round glass slides by impaction. Samples for scanning electron microscopy were collected on adhesive coated aluminium stubs. The stubs were coated with gold by the sputter coating technique. The sample stub was placed under a gold plate electrode at a distance of about 5cm. After evacuation of the chamber, argon gas was introduced around the sample to act as an ion carrier. Ionisation of the gold was produced by applying a high voltage across the gold plate electrode and sample stub causing gold ions to be deposited over the sample.

4.2.2 Quantitative determination of Fluorescein

4.2.2.1 Effect of pH on the absorbance of Fluorescein

A series of standard concentration (7.96 μm) fluorescein solutions were prepared with pH 2.8 to 12.0 Sorensen's glycine buffer (Sorensen, 1909). The absorbance of each solution was determined at 492nm, using 1cm path length, matched spectrophotometric cells in a Pye Unicam SP 500 Series 2 ultraviolet and visible spectrophotometer.

4.2.2.2 Determination of emission wavelength maximum

The percentage transmission of a 5.5ng per ml solution of fluorescein in pH 12.0 glycine buffer was measured at

emission wavelengths between 486nm and 525nm, with an excitation wavelength of 484nm in an Amino Bowman Spectrofluorimeter (Type 4-8202, American Instrument Company Inc) using 10mm spectrophotofluorimeter cells (transmission matched) with lids (Type 6010, code colour green, Helma (England) Ltd).

4.2.2.3 Determination of excitation wavelength maximum

The percentage transmission of a 5.5ng per ml solution of fluorescein in pH 12.0 glycine buffer was measured at an emission wavelength of 516nm, while changing the excitation wavelength between 460nm and 520nm.

4.2.2.4 Quantitative determination of Fluorescein

Calibration curves of relative fluorescent intensity (with reference to a standard of known concentration) versus concentration were constructed for concentrations of anhydrous fluorescein² ranging from 1 to 55ng per ml in pH 12.0 Sorensen's glycine buffer. Excitation and emission wavelengths of 486nm and 516nm respectively were employed. The standard reference solution contained a known concentration of fluorescein² of approximately 6ng per ml. Relative intensity (RI), with reference to the standard solution was calculated according to the following equation

$$RI = \frac{Z}{Z_s} \quad \text{Equation 4.6}$$

where Z_s is the % transmission of the standard solution and Z_t the % transmission of the test solution.

4.2.2.5 Fluorescein recovery from the collection surfaces

Clean glass slides (Quartz Grinding Company) porous stainless steel slides (Delron Research Company Powell, Ohio) and glass fibre filters (Type AF, Gelman) were spiked with 50 μ l of an aqueous fluorescein solution containing 100ng of anhydrous fluorescein⁻ per ml. After drying, fluorescein was recovered by ultrasonic extraction with 5cm³ of pH 12.0 glycine buffer for 10 minutes . The extract from the glass fibre filter was filtered through a 0.22 μ m pore size millipore filter to remove any suspended glass fibre fragments.

With the petroleum jelly (Silkolene 783/L, Dalton and Co) and silicone fluid (Dow-Corning 200/60 000) coated slides a double extraction technique was employed (Hering, 1978). The fluorescein disodium and coating material were ultrasonically extracted with 5cm³ of benzene (analytical grade) for 10 minutes. Five cm³ of pH 12.0 glycine buffer was added and the test tube shaken to mix the two solvents. The fluorescein-dissolved in the buffer layer which could be removed for fluorimetric analysis (see section 4.2.2.4) once the two immiscible solvents had separated. In this manner potential fluorescent quenching by the collection substrate could be prevented.

4.2.3 Preparation of collection surfaces

Clean glass discs were prepared by washing round glass slides (Quartz Grinding Company Ltd) in chromic acid/sulphuric acid, followed by several rinses with double distilled water. The slides were then polished with a lens cloth which had been previously soaked in alcohol. The clean glass discs were then allowed to dry.

Porous stainless steel discs (Delron Research Co) were cleaned in an ultrasonic bath with several changes of distilled water, then placed in an drying oven.

Silicone fluid (Dow Corning 200/60000) and white petroleum jelly (Silkolene 783/L, Dalton & Co) coated discs were prepared by spreading 400 μ l of 10% w/v solutions of silicone fluid and petroleum jelly in benzene (analytical grade) onto clean glass slides. Evaporation of the benzene leaves a thin smooth coat of silicone fluid or petroleum jelly on the glass slide.

4.2.4 Determination of collection efficiencies

Figure 4.2 is a schematic diagram of the experimental set up used to determine collection efficiencies. The monodisperse aerosol generator was set up to generate particles in the range 0.3 μ m to 26 μ m. For each size the generator was vented for five minutes, after shifting the syringe pump gear to the final position to ensure steady liquid flow.

Flow rates through the DCI5 and DCI6 cascade impactors are controlled by critical orifices. In the DCI6 impactor this is beyond the filter stage and will give a flow rate of 12.5 litres min⁻¹ if a vacuum of greater than 17 inches of mercury is applied. In the DCI5 cascade impactor the fifth stage acts as the critical orifice when a vacuum of greater than 17 inches of mercury is applied, giving a flow rate of 1.1 litres min⁻¹.

Collection efficiencies were determined by comparison of the mass of fluorescein on the collection surface to the total mass on the collection surface and glass fibre filter.

4.3 RESULTS

4.3.1 Monodisperse aerosol generation

Figure 4.3 is a scanning electromicrograph of a fluorescein disodium particle generated using the vibrating orifice generator. Solutions containing more than 1% w/v fluorescein disodium in methanol were found to block the 20 μ m orifice, thus setting an upper limit of 9 μ m to the aerosol particles of fluorescein disodium which could be prepared. Large particles could be generated using dioctyl phthalate. Table 4.2 gives the operating conditions for the Berglund-Lui vibrating orifice monodisperse aerosol generator and the range of droplet sizes that can be prepared using this instrument.

4.3.2 Quantitative determination of Fluorescein

4.3.3.1 The effect of pH on the absorbance of Fluorescein

Figure 4.4 shows the effect of pH on the absorbance (at 492nm) of a 7.96 μ m solution of fluorescein. The apparent spectrophotometric pKa (bearing in mind that fluorescein is dibasic) is 5.7. Consideration of the Hendersen-Hasselbalch equation reveals that at pH 7.7 and above fluorescein is more than 99% ionised. Solutions for quantitative determination of fluorescein were subsequently prepared in pH 12.0 glycine buffer.

4.3.2.2 Determination of Emission Maximum

The percentage transmission of the 5.5ng per ml solution of fluorescein⁻ in pH 12.0 glycine buffer at a fixed excitation wavelength varied with emission wavelength. The results of a single determination are shown in Figure 4.5 and clearly show an emission wavelength maximum at 516nm.

4.3.2.3 Determination of Excitation Maximum

At a fixed emission wavelength the percentage transmission of a 5.5ng per ml fluorescein⁻ solution determined using an Aminco Bowman spectrofluorimeter varied with excitation wavelength. Figure 4.6 shows the percentage transmission versus excitation wavelength; an excitation wavelength maximum occurs at 486nm.

4.3.2.4 Quantitative determination of fluorescein

Calibration curves of relative intensity versus concentration of fluorescein disodium, such as that shown in Figure 4.7, were rectilinear for concentrations up to 63ng per ml. The solid line in Figure 6.2 is the best fit by linear regression to the data for RI versus concentration of fluorescein disodium in buffer. Repetitions of the experiment enabled $\geq 5\%$ errors to be ascribed to concentrations ≤ 2.0 ng per ml of fluorescein disodium. This limit was determined by the method of accuracy of coefficients of the line of regression (Topping, 1962) using data from an experiment performed in quintuplicate. More than 5% errors are incurred in concentrations determined for relative intensities

≤ 0.3 (Equation 4.6).

4.3.2.5 Fluorescein recovery from collection surfaces

It was found that extracts from petroleum jelly coated slides, in the absence of fluorescein disodium registered a reading on the fluorimeter versus a buffer blank. It was necessary to establish a calibration curve for fluorescein disodium in the presence of water soluble extracts from 40mg of petroleum jelly. Calibration curves of relative intensity versus concentration of fluorescein disodium in the presence of the water soluble extracts from 40mg of petroleum jelly could not be distinguished from calibration curves obtained in buffer alone provided the fluorimeter was first zeroed with an appropriate reference solution and that the standard solution included these water soluble extracts.

Table 4.3 shows the recovery of fluorescein disodium from the collection surfaces. Except for the slight modification required to assay fluorescein disodium recovered from petroleum jelly coated slides, satisfactory recovery and the absence of any quenching phenomena has been shown.

4.3.3 Collection Efficiency of Different Collection Surfaces

Figure 4.8 shows the collection efficiency of the first stage of the DCI5 impactor with various types of collection surfaces of solid fluorescein disodium particles of various aerodynamic diameters. The solid line indicates the manufacturers

calibration curve (Mitchell and Pilcher, 1958). The mean and standard deviation of three determinations are indicated.

On clean glass slides the collection efficiency did not exceed 70% and there is some evidence of a decrease in collection efficiency for particles of higher aerodynamic diameters.

At low aerodynamic diameter the collection efficiency onto porous stainless steel slides is greater than for any of the other surfaces examined. However for this type of slide the maximum collection efficiency observed was only 60%. This type of broad collection efficiency curve has been reported by researchers using glass fibre discs (Hering, 1978). One possible explanation of the higher collection efficiency at low aerodynamic diameters is the penetration of the air stream into the porous matrix of the plate and subsequent retention of aerosol particles within the porous matrix (Rao and Whitby, 1978b).

The maximum collection efficiency observed on white petroleum jelly coated plates was 80% and approached 100% for silicone fluid coated slides. Consequently, the slides treated with the latter material were used in subsequent experiments.

4.3.4 Calibration of DCI 6 impactor

Figure 4.9 to 4.14 show the collection efficiencies versus aerodynamic diameter for stages 1 to 6 of the DCI-6 cascade impactor using silicone fluid coated glass slides. The mean and standard deviation of three determinations is shown .

The collection efficiencies could be empirically described by curves of the form

$$E = A^1 \tanh\left(\frac{Da - B^1}{2C^1}\right) + D^1 \quad \text{Equation 4.7}$$

The best estimates for the empirical constants A^1 , B^1 , C^1 and D^1 were determined by non-linear least mean square fitting (Metzler, 1969). The best fits to the experimental data is indicated as the solid lines in Figures 4.9 to 4.14. Best fits to the upper and lower limits (mean \pm standard deviation) are indicated on the figures by the dashed lines.

The traditional method of interpreting cascade impactor data is to assume that the collection efficiency of each stage can be approximated to a step function passing through the 50% collection efficiency (D_{50}) of the stage. Examination of the observed collection efficiencies (Figures 4.9 to 4.14) reveals that the efficiency curves deviate significantly from a step function and even with the best collection surfaces some rebound or re-entrainment occurs. Consequently traditional data treatment may lead to biased estimates of size distribution. The problems with this bias and limitations of previous methods of correction, were discussed by Cooper and Spielman (1976), Cushing et al (1978) and Gonda and Groom (1981).

If we consider an aerosol of mass size distribution $f(x)$ with respect to aerodynamic size, x , entering a cascade impactor, neglecting wall losses the mass of aerosol, M_1 , collected on the first stage will be

$$M_1 = \int_0^{\infty} f(x) \cdot E_1(x) dx \quad \text{Equation 4.8}$$

where $E_1(x)$ is the collection efficiency of the first stage with respect to aerodynamic diameter, x . The mass size distribution of the aerosol passing onto the second stage will be

$$\begin{aligned} & f(x) - f(x) \cdot E_1(x) \\ = & f(x) [1 - E_1(x)] \quad \text{Equation 4.9} \end{aligned}$$

To simplify notation the variable x will be neglected for the efficiency term. If E_2 is the collection efficiency of the second stage with respect to x , the amount of aerosol collected on the second stage will be

$$M_2 = \int_0^{\infty} f(x) \cdot E_2 [1 - E_1] dx \quad \text{Equation 4.10}$$

At the n th stage the mass collected will be

$$M_n = \int_0^{\infty} f(x) E_n [1 - E_{(n-1)}] \dots \dots [1 - E_1] dx \quad \text{Equation 4.11}$$

Empirical descriptions of the collection efficiency curves for each stage of the DCI-6 cascade impactor were obtained as previously described. The final filter stage was assumed to have a collection efficiency of 100%. These equations can be used to calculate the theoretical percentages of aerosol deposited on the six stages and the final filter for any assumed particle size distribution (Fuchs, 1978 ; Gonda and Groom, 1981).

The calculation of the theoretical amounts landing on each stage is aided by the following interactive computer programme: The user decides upon a particular type of distribution function which may be characterised by two parameters, for example the log-normal distribution. A range of parameter values is selected of 10 mass median diameters and 10 geometric standard deviations for a log-normal distribution. The sum of the squares of the differences between the theoretical and experimental deposition results using average efficiencies for each stage are computed. The programme gives a two dimensional error map for the range of

parameters from which a narrower range of parameters may be selected, potentially ambiguously assigned distributions arising from multiple local minima are thus avoided (Huang et al, 1970; Gonda and Groom 1981). The programme is then rerun with a narrower range of parameters. For the best fit the residue values are shown to ascertain the random nature of errors. A systematic trend in errors indicates that a different type of size distribution should be attempted.

Gas flowing through the cascade impactor will gain velocity at jet inlets and lose velocity at the exit. As the gas loses velocity it will correspondingly experience a temperature change. It is necessary to determine whether the increase in humidity arising from the temperature change is likely to affect the size distribution of the aerosol passing through the impactor.

Linear velocities in the impactor may be calculated from the volume flow rate, F' (which for the DCI-6 cascade impactor is 12.5 litres per minute) and the cross-sectional area. Thus for a jet of diameter D_j , the linear velocity, V will be

$$V = \frac{4 F'}{\pi D_j^2} \quad \text{Equation 4.12}$$

The linear velocity at each of the stages of the DCI-6 impactor is given in Table 4.1. The maximum diameter of the DCI-6 impactor is 7.6×10^{-2} m. The linear velocity at the maximum cross-section will therefore be 4.57×10^{-2} m sec⁻¹. Assuming that the change in linear velocity is totally absorbed by a temperature change of the gas (adiabatic isentropic process) the temperature change may be calculated from (Hering et al, 1978)

$$C_p' .dT = - V dV.$$

$$C_p' (T_2 - T_1) = - \frac{(V_2^2 - V_1^2)}{2} \quad \text{Equation 4.13}$$

where C_p' is the specific heat, T_1 and V_1 the temperature and linear velocity at the maximum cross-sectional area respectively; and T_2 and V_2 , the temperature and linear velocity at the jet.

The specific heat may be approximated from (Coulson and Richardson, 1977)

$$C_p' = 1.00 + 1.9 H \quad \text{kJ kg}^{-1} \text{ K}^{-1} \quad \text{Equation 4.14}$$

where H is the fractional relative humidity. At high humidity therefore

$$C_p' \approx 2.9 \text{ K J kg}^{-1} \text{ K}^{-1} \quad \text{Equation 4.15}$$

At all stages $V_2 \gg V_1$ and so V_1 may be neglected from Equation 4.13. The temperature change at each stage may therefore be calculated from

$$\Delta T = \frac{V_2^2}{2 \times C_p'} \quad \text{Equation 4.16}$$

It is apparent therefore that the temperature change at each jet will be less for humid air than for dry air. The temperature change at each jet for humid air, ΔT_H and for dry air, ΔT_D , is given in Table 4.4.

It can be seen that the largest perturbation occurs at the final stage.

In order to assess the effect these temperature changes are likely to have upon the aerosol cloud it is necessary to determine the 'transit time', that is the time the aerosol is

likely to experience an increased humidity arising from the temperature drop. The DCI-6 cascade impactor is designed so that the jet-to-slide distance at all stages is $\frac{3}{8} D_j$. A minimum 'transit time' t_{\min} , may therefore be regarded as the time to traverse this distance. The maximum 'transit time' t_{\max} may be calculated from the maximum length of the jet which is approximately $2 \times 10^{-2}m$ for all stages. The maximum and minimum transit times are given in Table 4.4.

Significant changes in the aerosol size is unlikely to occur in a time scale of less than 1 msec. From Table 4.4 it is obvious that when t_{\max} is greater than 1msec the maximum temperature change ΔT_D is less than 0.05K.

These calculations therefore indicate that the cascade impactor is a suitable instrument for investigating the effect of humidity on the particle size distribution of hygroscopic aerosols. Hochrainer and Zebel (1981) have reached the same conclusion after examining this problem both theoretically and experimentally.

These experiments have confirmed the observations of other researchers (Rao and Whitby 1977a, 1977b; Cushing et al 1979) that a suitable coating on the collection surface is necessary in order to obtain collection efficiency curves that approach 100% collection efficiency. Silicone fluid (200/60000) was shown to be the best coating of those examined here. However, even with this type of coating there was some evidence that the collection efficiency declined after reaching a maximum value approaching 100%, presumably through rebound and re-entrainment of the larger particles. In the light of these observations it would be wise to avoid overburdening the stages and only collect amounts of aerosols on any one stage in the order of the loading limits suggested by Mercer (1966). These loading limits represent the amount of aerosol of average size of the range likely to reach the stage which could be collected as a single layer in the area of the jet.

The D_{50} values obtained experimentally were found to vary from the manufacturer's calibration and are shown for each stage in Table 4.4 with the manufacturer's values for comparison. The DCI-6 cascade impactor, in common with many others, has been calibrated by determining impaction efficiency versus impaction parameter for one stage, then using Equation 4.1 to obtain calibration curves for all other stages (Mitchell and Pilcher, 1959). However, when the collection efficiencies obtained experimentally are plotted against the square root of the impaction parameter, $\sqrt{\Psi}$, (Figure 4.15) a shift in the relation-

ship is seen from stage to stage. The value of $\sqrt{\Psi}$ corresponding to the D_{50} value used in the manufacturers calibration was 0.29 (Mitchell and Pilcher, 1959). While this is consistent with the experimental values obtained here for stages 4, 5 and 6, it does not adequately describe the results obtained for the first three stages. These observations indicate the necessity of calibration at the operating flow rates. Adiabatic expansion of air in the jets of the impactor will lead to temperature changes and corresponding changes in relative humidity. Theoretical consideration of this potential problem reveals that particle size changes are unlikely to occur because of the short time spent by particles in the jets. The cascade impactor is therefore a suitable instrument for size analysis of hygroscopic aerosol particles.

TABLE LEGENDS

Table 4.1 Characteristics of Battelle Cascade Impactors, DCI-5 and DCI-6 cascade impactor; jet diameter, D_j ; Reynolds number, Re ; and linear velocity, V , for each stage (Hering et al, 1978)

Table 4.2 Operating conditions for the Berglund Lui, model 3050, vibrating orifice monodisperse aerosol generator.

Table 4.3 Manufacturer's calibration and experimentally obtained D_{p0} values for each stage of the DCI-6 cascade impactor.

Table 4.4 Adiabatic perturbations in the DCI-6 cascade impactor
Transit times: t_{\min} , the time taken to traverse the jet to slide distance; t_{\max} , the time taken to traverse the jet length.
Temperature changes: ΔT_H , the temperature change for high humidity air; ΔT_D , the temperature change for dry air.

Table 4.1 Characteristics of Battelle Cascade Impactors, DCI5 and DCI6.

DCI-5 flow rate 1.05Lmin ⁻¹			
Stage Number	Dj (cm)	Re	V (m/s)
1	0.249	560	3.5
2	0.140	990	11
3	0.099	1400	22
4	0.064	2170	54
5	0.036	3500	164

DCI-6 flow rate 12.45Lmin ⁻¹			
Stage Number	Dj (cm)	Re	V (m/s)
1	1.364	1160	1.4
2	0.859	1850	3.6
3	0.541	2930	9
4	0.341	4650	23
5	0.216	7340	57
6	0.141	11250	133

Table 4.2 Operating conditions for the model 3050 vibrating orifice monodisperse aerosol generator.

Orifice diameter	Syringe capacity	Gear position	Liquid feed rate ($\text{cm}^3\text{min}^{-1}$)	Frequency range (KHz)	Droplet diameter range (μm)
20	50	18	0.139	40-80	38-48
10	20	18	0.071	130-260	21-26
5	10	18	0.0406	300-600	12-16

Table 4.3 Manufacturers' calibration and experimentally obtained D_5 values for the stages of the DCI-6 cascade impactor.

Stage Number	D_{50} value (μm)	
	Manufacturers value	Value obtained by least mean square analysis of experimental data
1	16	11.2 ± 0.7
2	8.0	5.5 ± 0.5
3	4.0	3.3 ± 0.3
4	2.0	1.95 ± 0.1
5	1.0	0.94 ± 0.05
6	0.5	0.51 ± 0.03

Table 4.4 Adiabatic perturbations in the DCI-6 cascade impactor. Transit times: t_{\min} , the time taken to traverse the jet to slide distance; t_{\max} , the time taken to travel the jet length and temperature changes, ΔT_H , the temperature change for high humidity air, and ΔT_D , the temperature change for dry air, at each of the stages.

Stage Number	$10^3 t_{\min}$ (sec)	$10^3 t_{\max}$ (sec)	ΔT_H (K)	ΔT_D (K)
1	3.60	14.1	0.0003	0.001
2	0.90	5.6	0.002	0.006
3	0.22	2.2	0.014	0.041
4	0.056	0.88	0.089	0.26
5	0.014	0.35	0.55	1.60
6	0.004	0.15	3.04	8.83

FIGURESFIGURE LEGENDS

Figure 4.1 Schematic diagram of aerosol collection by cascade impactor a) Ideal collection efficiencies and b) non-ideal collection efficiencies.

Figure 4.2 Schematic diagram of the apparatus for determination of collection efficiencies.

Figure 4.3 Scanning electromicrograph of a fluorescein disodium particle generated using the vibrating orifice generator.

Figure 4.4 Effect of pH on absorbance of 7.6 μ M solution of fluorescein disodium at 492nm.

Figure 4.5 Percentage transmission of 5.5ng per ml solution of fluorescein versus emission wavelength (excitation wavelength, 486nm).

Figure 4.6 Percentage transmission of 5.5ng per ml solution of fluorescein⁼ versus excitation wavelength (emission wavelength 516nm).

Figure 4.7 Relative intensity (Equation 4.6) versus concentration of fluorescein⁼ in buffer (pH 12).

Figure 4.8 Collection efficiency versus aerodynamic diameter for stage 1 of DCI5 cascade impactor

Figure 4.9 Percentage collection efficiency (100 xE) versus aerodynamic diameter (Da) for stage 1 of DCI6 cascade impactor manufacturer's calibration (-.-), mean efficiency (—) and maximum and minimum contours (— —) obtained by least mean squares fitting of the experimental data to Equation 4.7. The mean and standard deviation (n=3) of the experimental values are indicated

Figure 4.10 Percentage collection efficiency ($100 \times E$) versus aerodynamic diameter (D_a) for Stage 2 of DCI6 cascade impactor: Manufacturer's calibration (-.-), mean efficiency ($\bar{\quad}$) and maximum and minimum contours (---) obtained by least mean squares fitting of experimental data to Equation 4.7. The mean and standard deviation ($n=3$) of the experimental values are indicated

Figure 4.11 Percentage collection efficiency ($100 \times E$) versus aerodynamic diameter (D_a) for Stage 3 of DCI6 cascade impactor: Manufacturer's calibration (-.-), mean efficiency ($\bar{\quad}$) and maximum and minimum contours (---) obtained by least mean squares fitting of the experimental data to Equation 4.7. The mean and standard deviation ($n=3$) of the experimental values are indicated

Figure 4.12 Percentage collection efficiency ($100 \times E$) versus aerodynamic diameter (D_a) for Stage 4 of DCI6 cascade impactor: Manufacturer's calibration (-.-), mean efficiency ($\bar{\quad}$) and maximum and minimum contours (---) obtained by least mean square fitting of the experimental data to Equation 4.7. The mean and standard deviation ($n=3$) of the experimental values are indicated

Figure 4.13 Percentage collection efficiency ($100 \times E$) versus aerodynamic diameter (D_a) for Stage 5 of DCI6 cascade impactor: Manufacturer's calibration (-.-), mean efficiency ($\bar{\quad}$) and maximum and minimum contours (---) obtained by least mean square fitting of the experimental data. The mean and standard deviation ($n=3$) of the experimental values are indicated

Figure 4.14 Percentage collection efficiency ($100 \times E$) versus aerodynamic diameter (D_a) for Stage 6 of DCI6 cascade impactor: Manufacturer's calibration (-.-), mean efficiency ($\bar{\quad}$) and maximum and minimum contours (---) obtained by least mean square fitting of the experimental data to Equation 4.7. The mean and standard deviation ($n=3$) of the experimental values are indicated

Figure 4.15 Mean experimental collection efficiency versus square root of impaction parameter (Ranz and Wong, 1952) for the DCI-6 cascade impactor.

Figure 4.1 Schematic diagram of aerosol collection by cascade impactor
 a) Ideal collection efficiencies and b) non-ideal collection efficiencies.

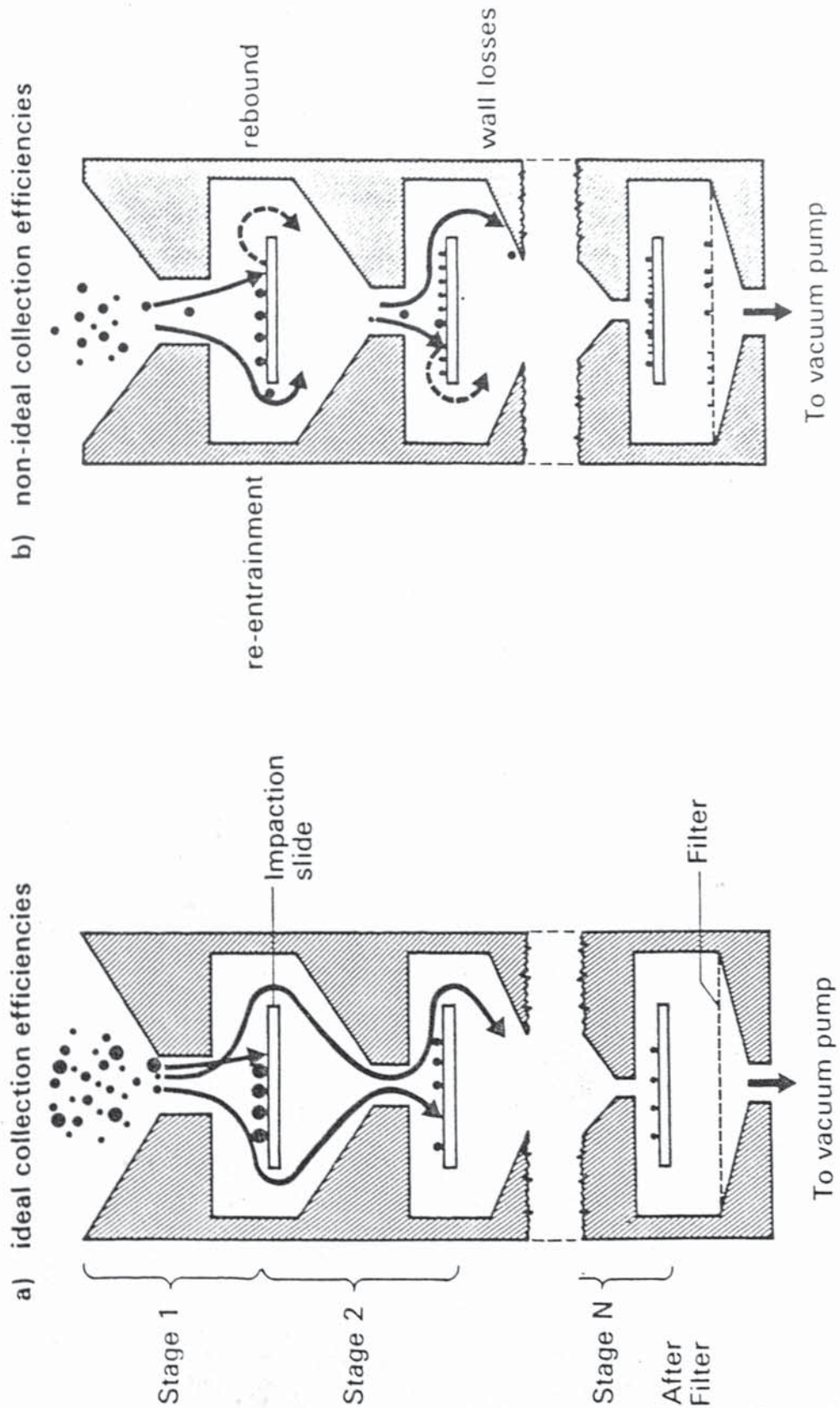


Figure 4.2 Schematic diagram of the apparatus for determination of collection efficiencies.

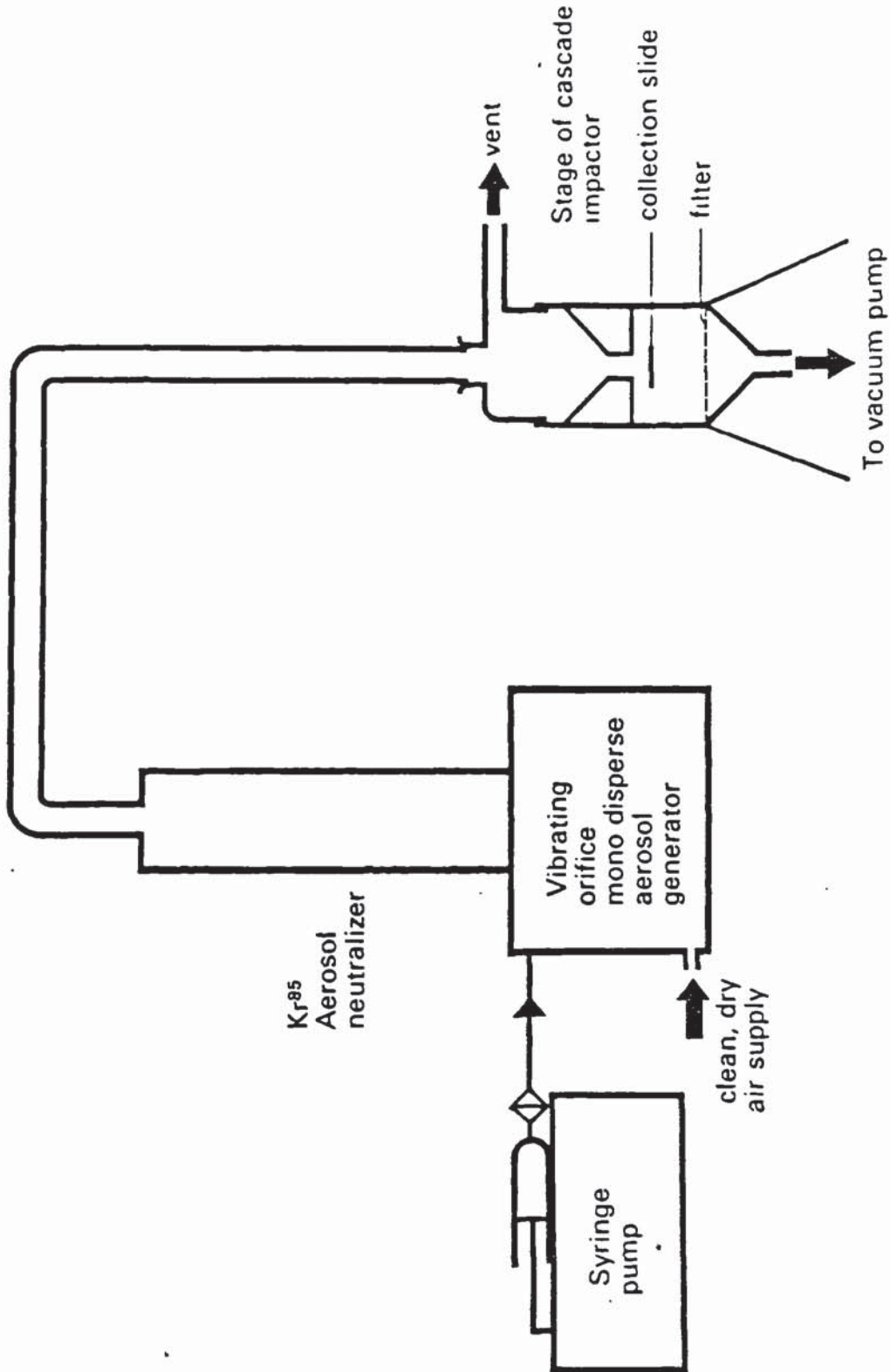


Figure 4.3 Scanning electromicrograph of fluorescein disodium particle generated using the vibrating orifice generator.

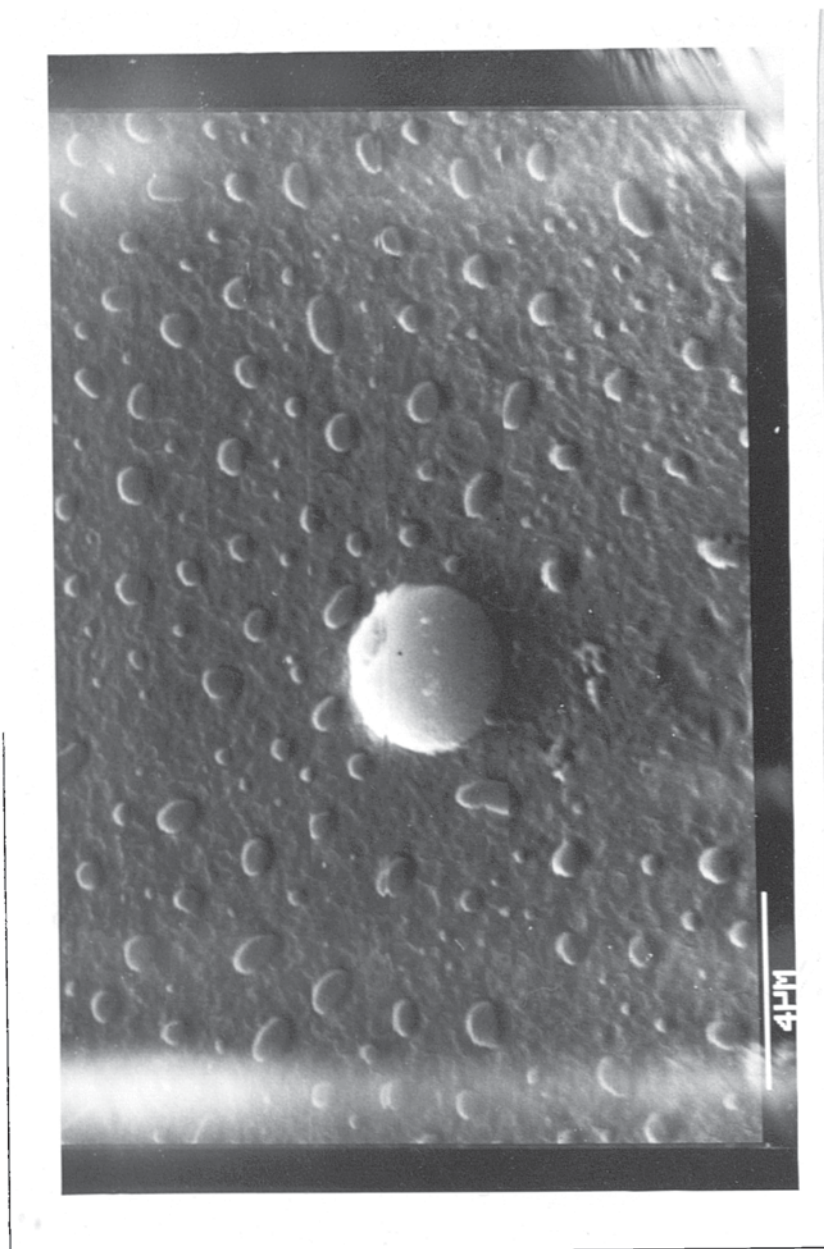


Figure 4.4 Effect of pH on absorbance of Fluorescein disodium at 492nm.

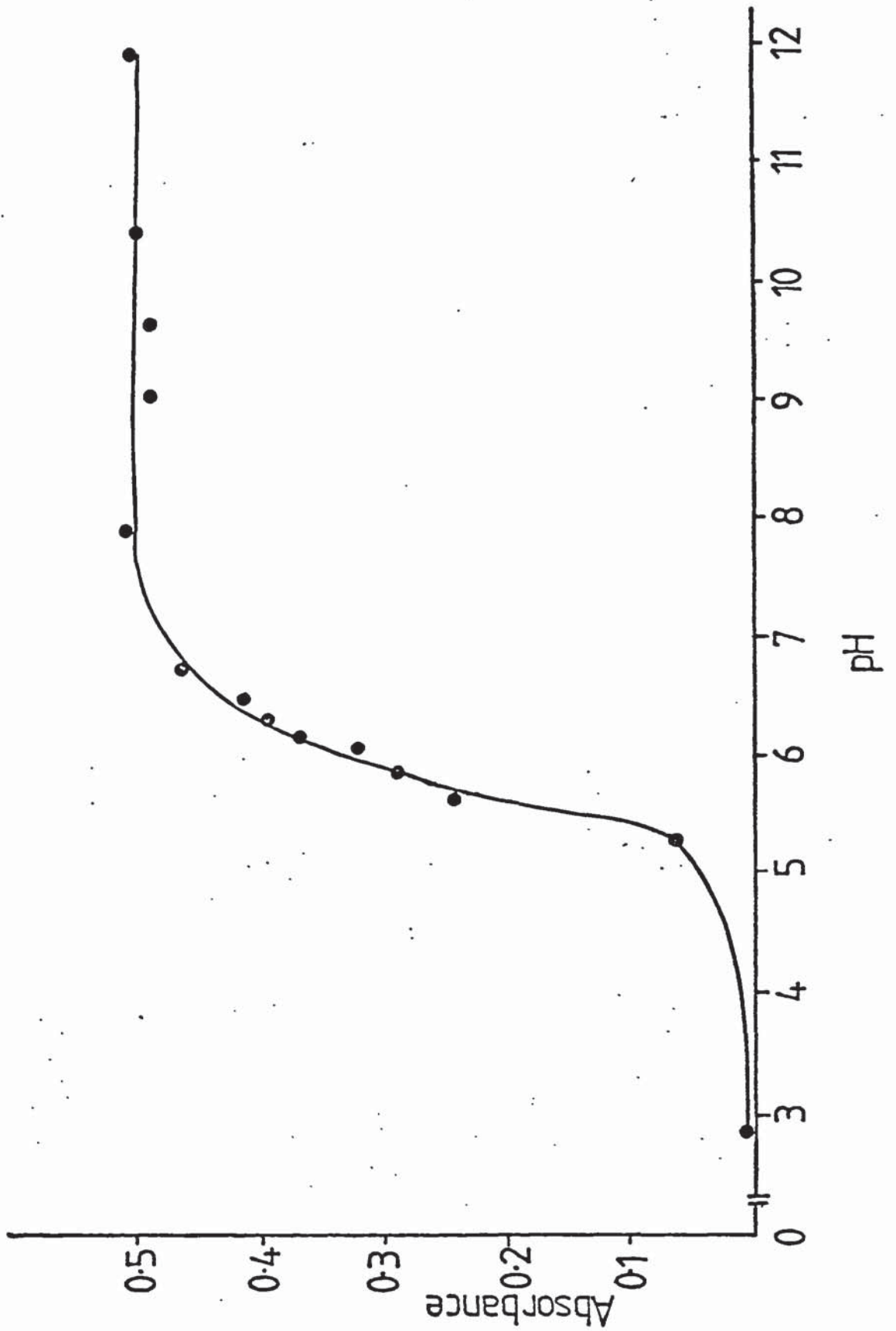


Figure 4.5 % Transmission of 5.5ng per ml solution of fluorescein⁻ versus emission wavelength (excitation wavelength, 486nm).

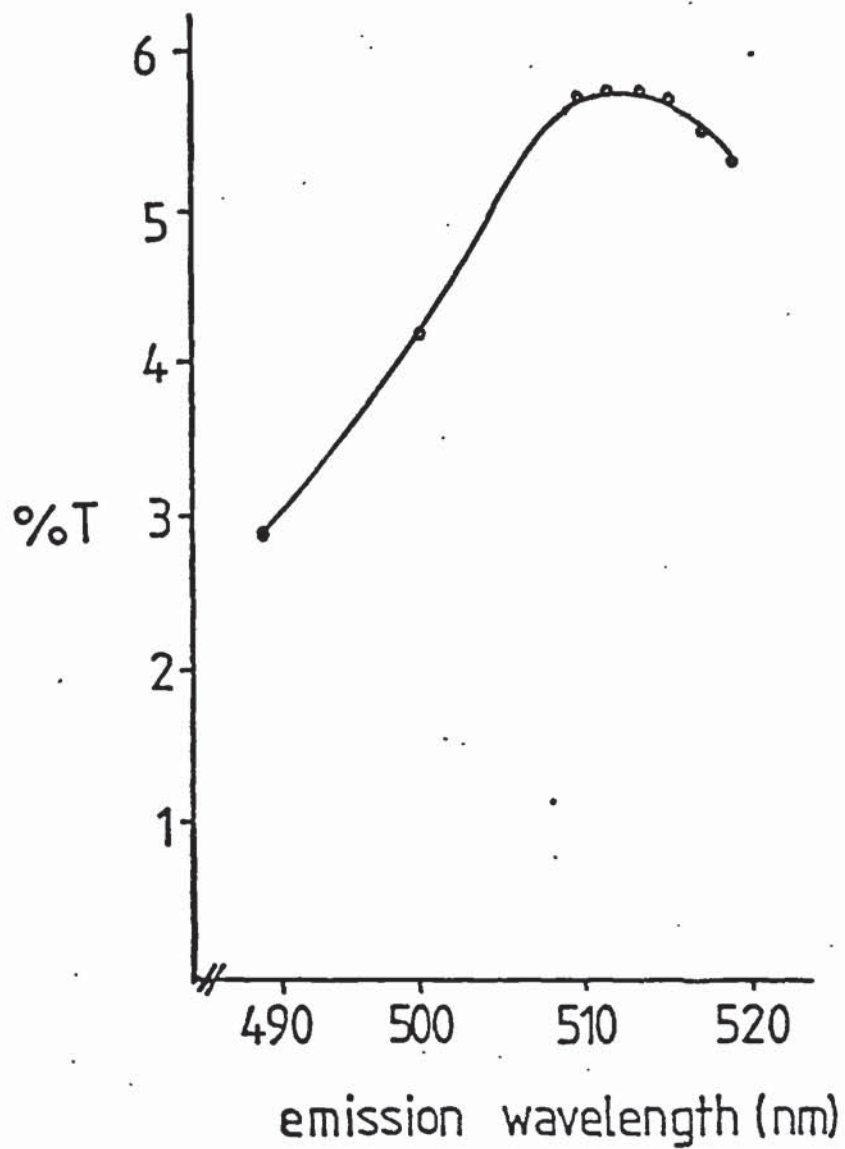


Figure 4.6 % Transmission versus excitation wavelength of 5.5ng per ml solution of fluorescein⁻ (emission wavelength 516nm).

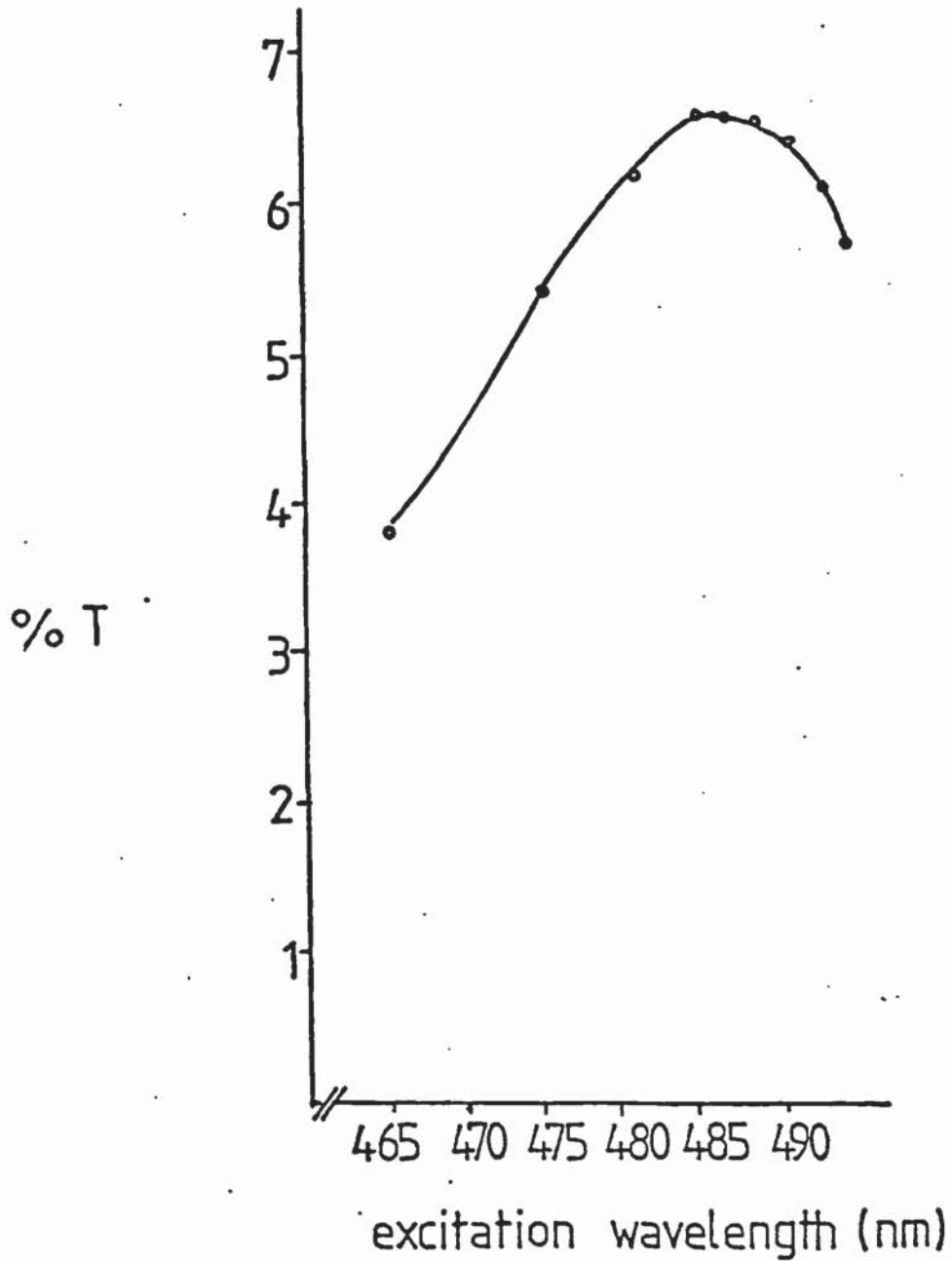


Figure 4.7 Relative Intensity (Equation 4.6) versus concentration of fluorescein⁻ in buffer (pH 12). The solid line is the 'best fit' by linear regression. Each relative intensity was determined in quintuplicate.

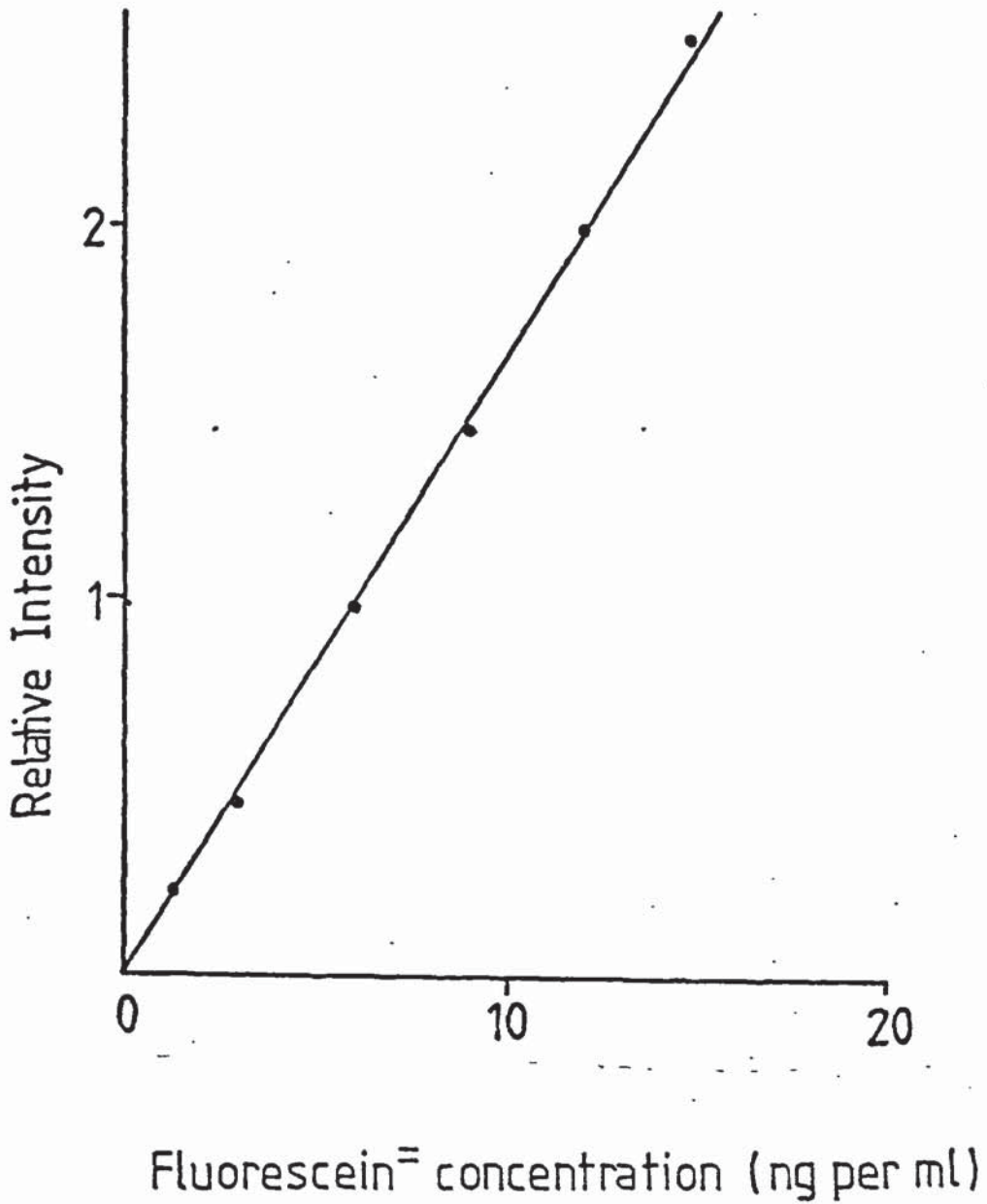


Figure 4.8 Collection efficiency versus aerodynamic diameter for stage 1 of DCI5 cascade impactor.

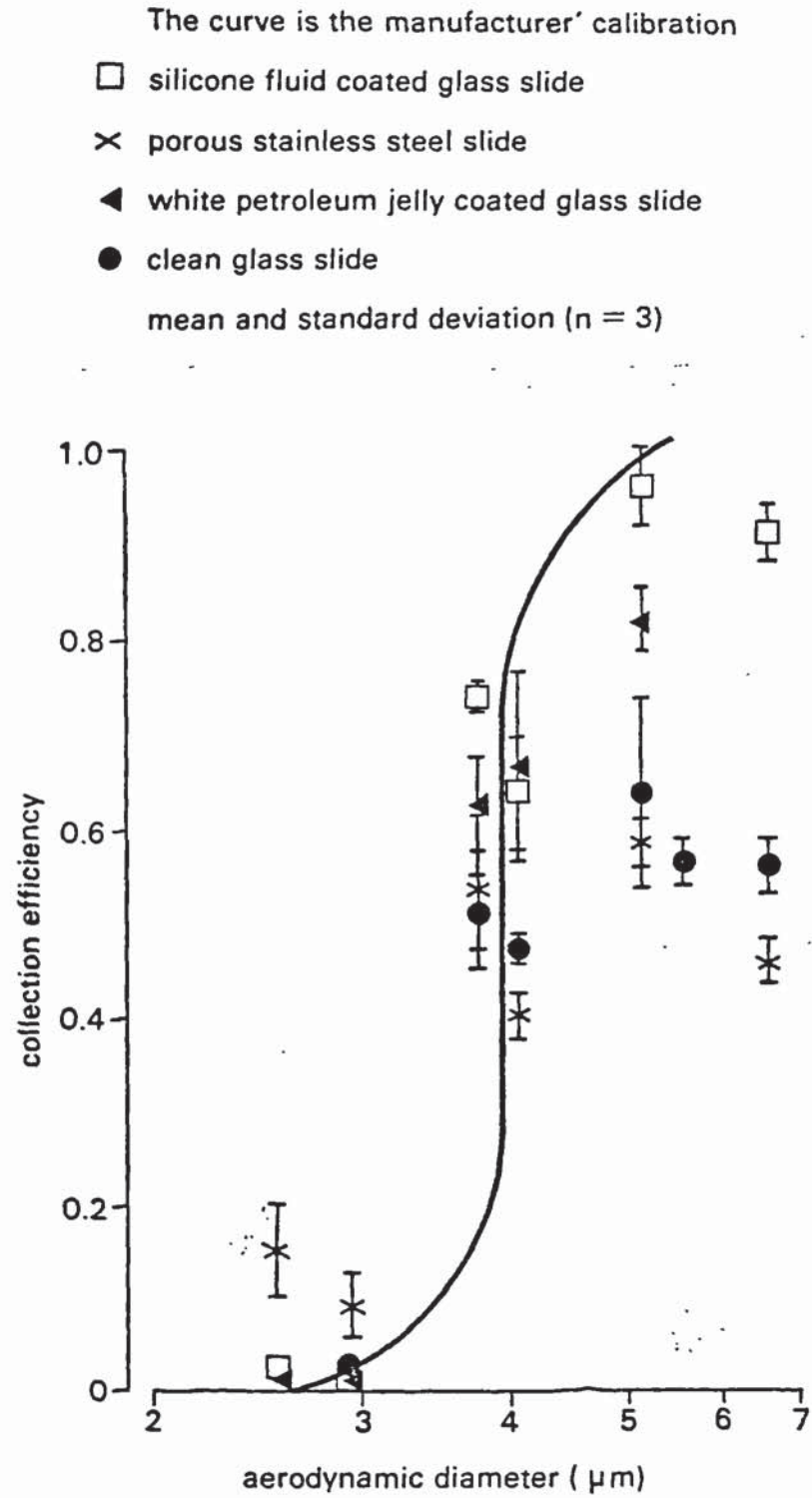


Figure 4.9 Percentage collection efficiency ($100 \times E$) versus aerodynamic diameter (Da) for stage 1 of DCI6 cascade impactor manufacturer's calibration (---), mean efficiency (—) and maximum and minimum contours (---) obtained by least mean squares fitting of the experimental data to Equation 4.7. The mean and standard deviation ($n=3$) of the experimental values are indicated

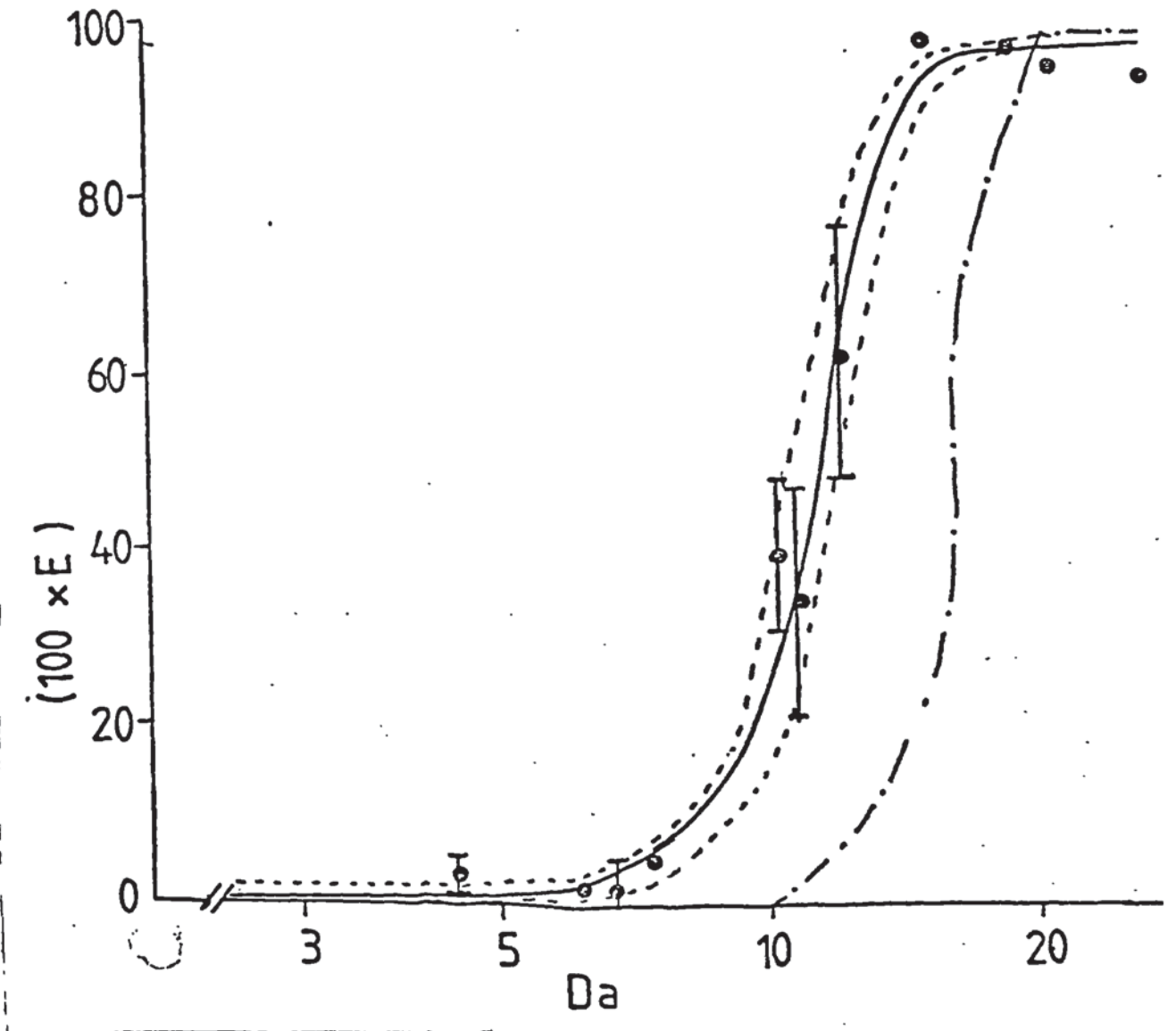


Figure 4.10 Percentage collection efficiency ($100 \times E$) versus aerodynamic diameter (Da) for stage 2 of DCI6 cascade impactor: Manufacturer's calibration (---), mean efficiency (—) and maximum and minimum contours (---) obtained by least mean squares fitting of experimental data to Equation 4.7. The mean and standard deviation ($n=3$) of the experimental values are indicated

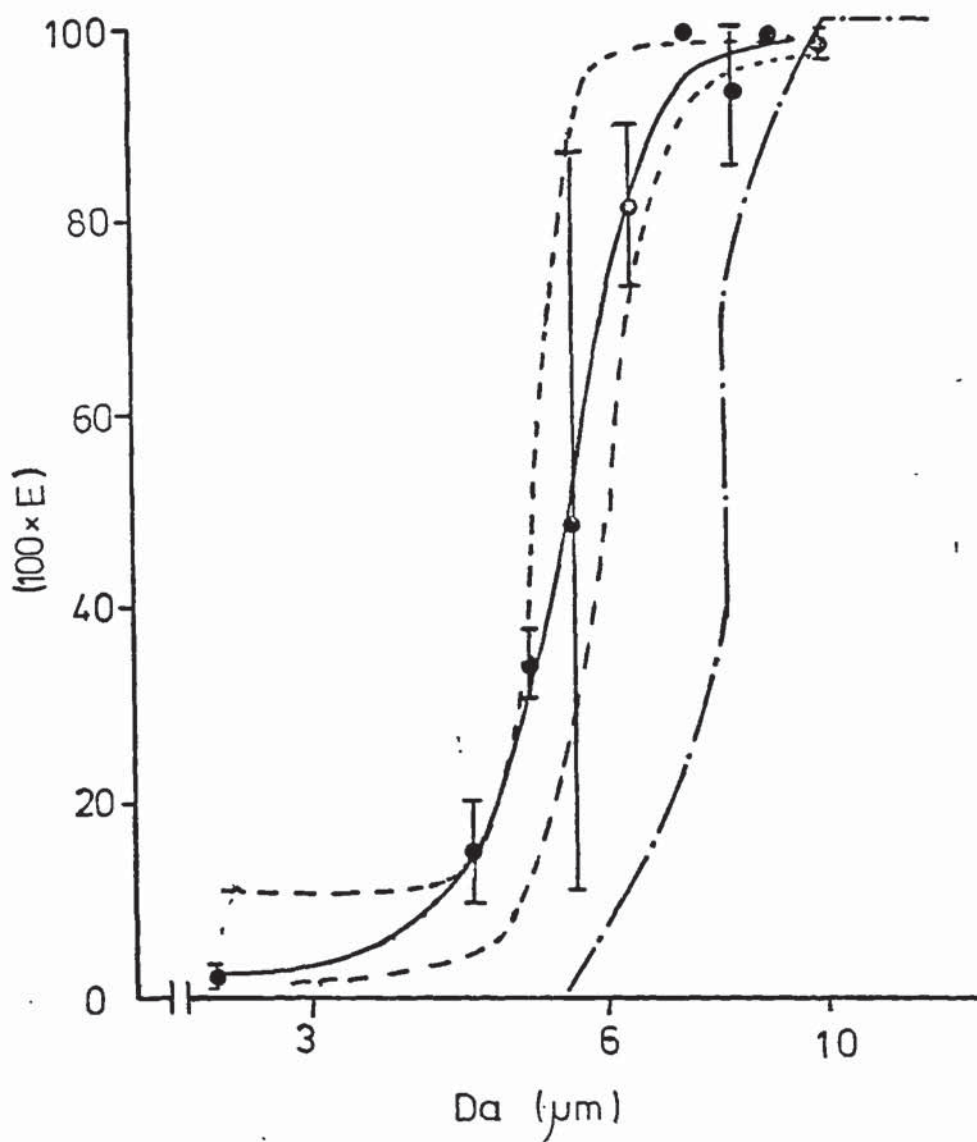


Figure 4.11 Percentage collection efficiency ($100 \times E$) versus aerodynamic diameter (Da) for Stage 3 of DCI6 cascade impactor: Manufacturer's calibration (---), mean efficiency (—) and maximum and minimum contours (---) obtained by least mean squares fitting of the experimental data to Equation 4.7. The mean and standard deviation ($n=3$) of the experimental values are indicated

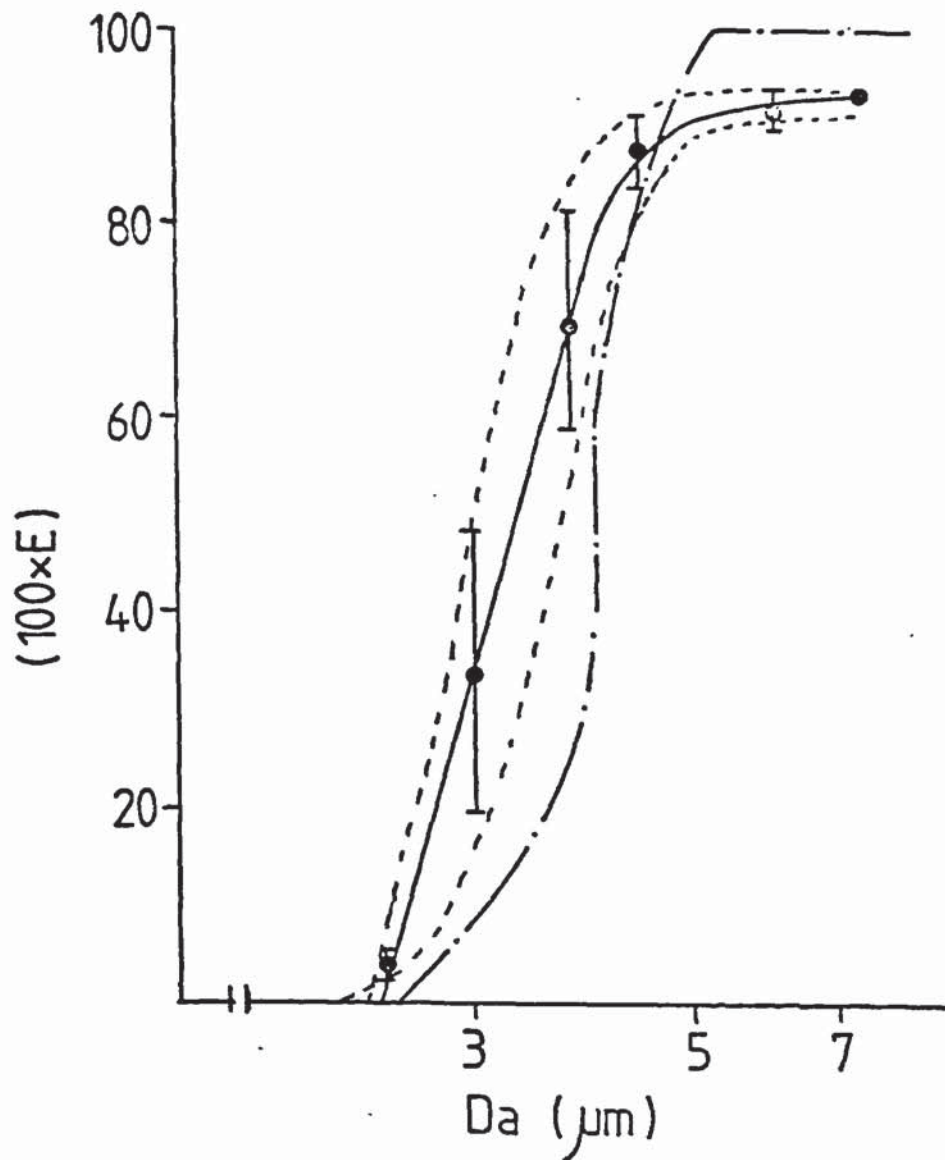


Figure 4.12 Percentage collection efficiency ($100 \times E$) versus aerodynamic diameter (Da) for Stage 4 of DCI6 cascade impactor: Manufacturer's calibration (---), mean efficiency (—) and maximum and minimum contours (---) obtained by least mean square fitting of the experimental data to Equation 4.7. The mean and standard deviation ($n=3$) of the experimental values are indicated

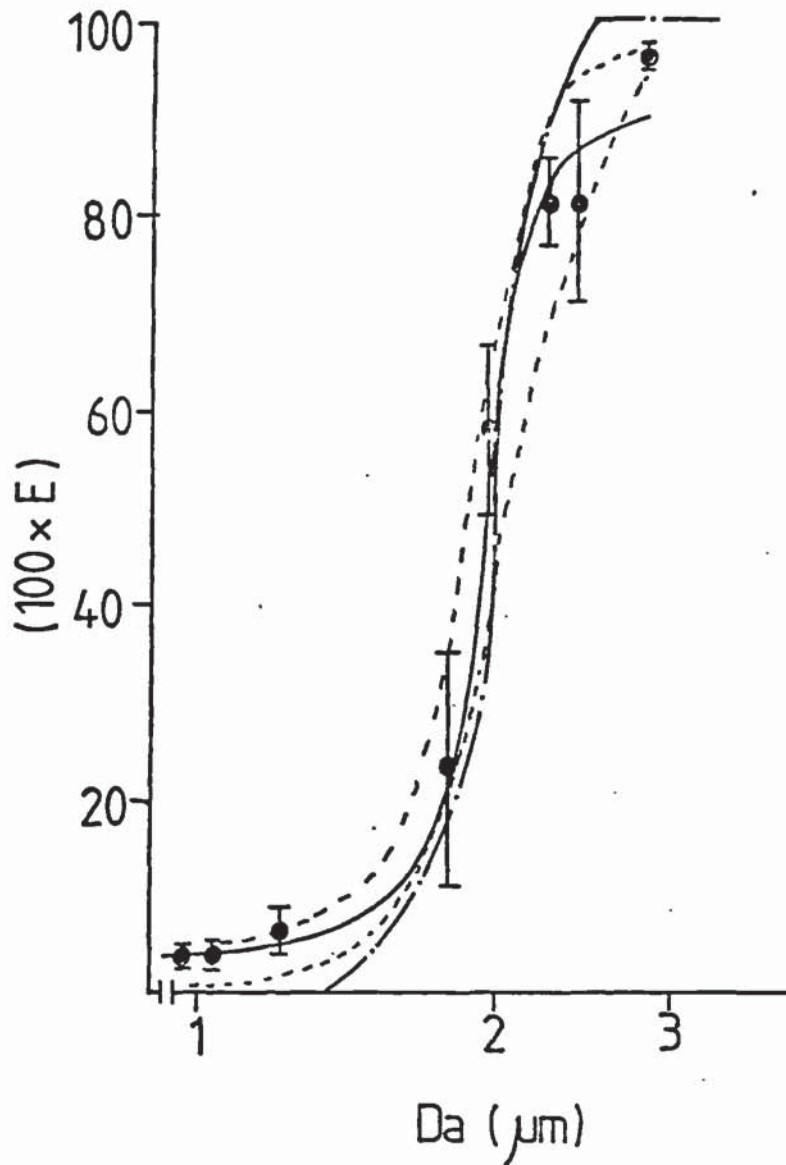


Figure 4.13 Percentage collection efficiency ($100 \times E$) versus aerodynamic diameter (Da) for Stage 5 of DCI6 cascade impactor: Manufacturer's calibration (---), mean efficiency (—) and maximum and minimum contours (---) obtained by least mean square fitting of the experimental data. The mean and standard deviation ($n=3$) of the experimental values are indicated

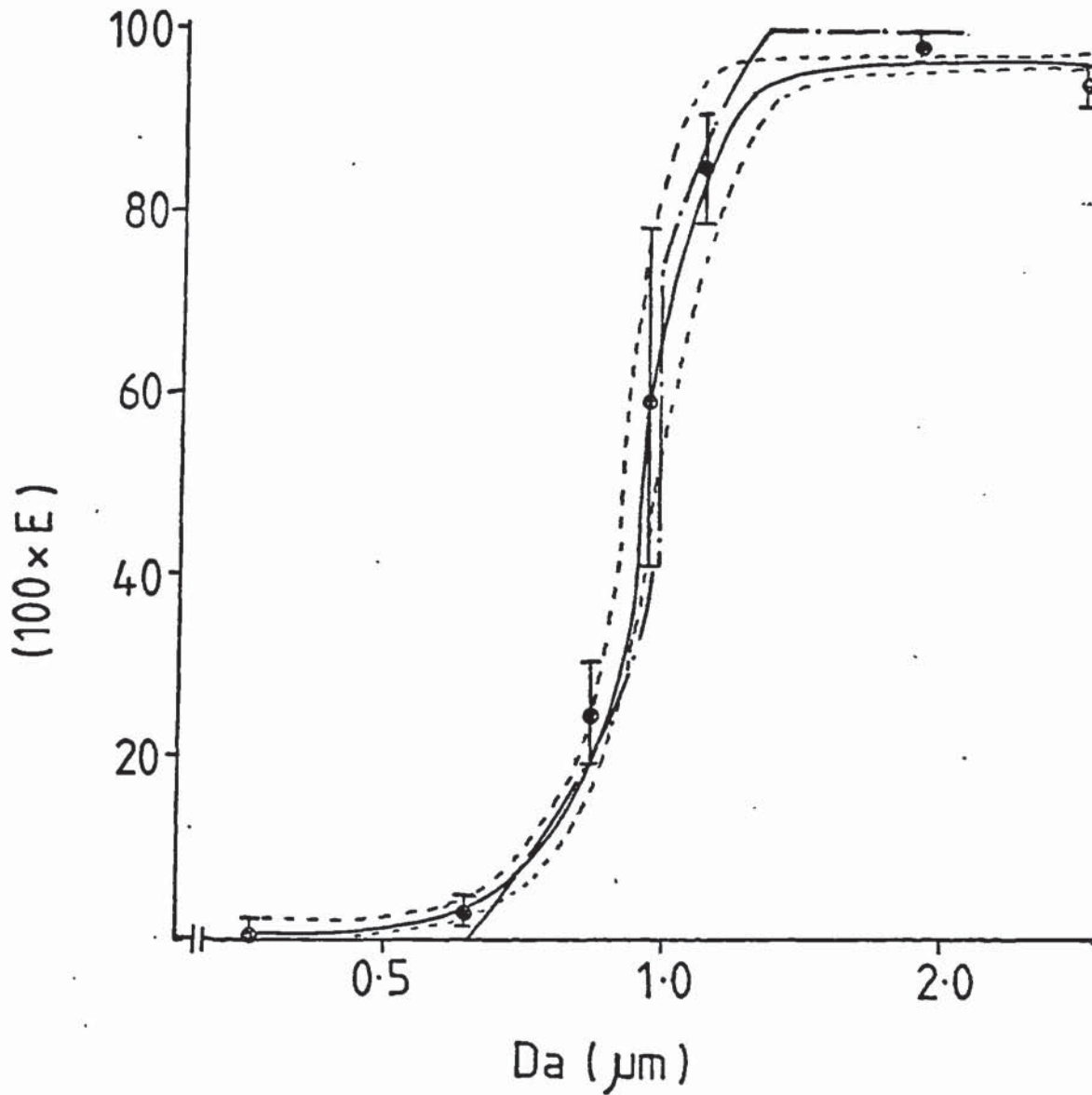


Figure 4.14 Percentage collection efficiency ($100 \times E$) versus aerodynamic diameter (Da) for Stage 6 of DCI6 cascade impactor: Manufacturer's calibration (---), mean efficiency (—) and maximum and minimum contours (---) obtained by least mean square fitting of the experimental data to Equation 4.7. The mean and standard deviation ($n=3$) of the experimental values are indicated

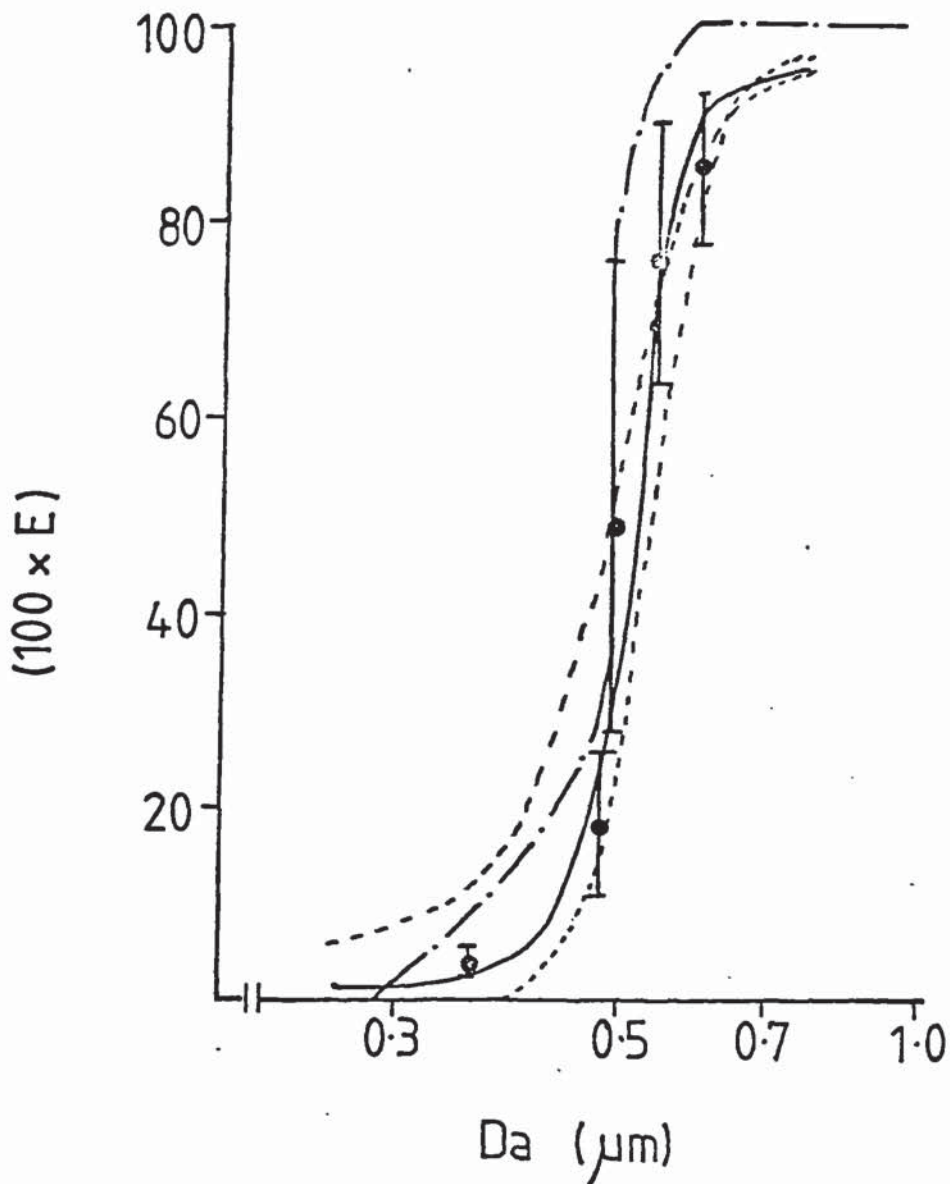
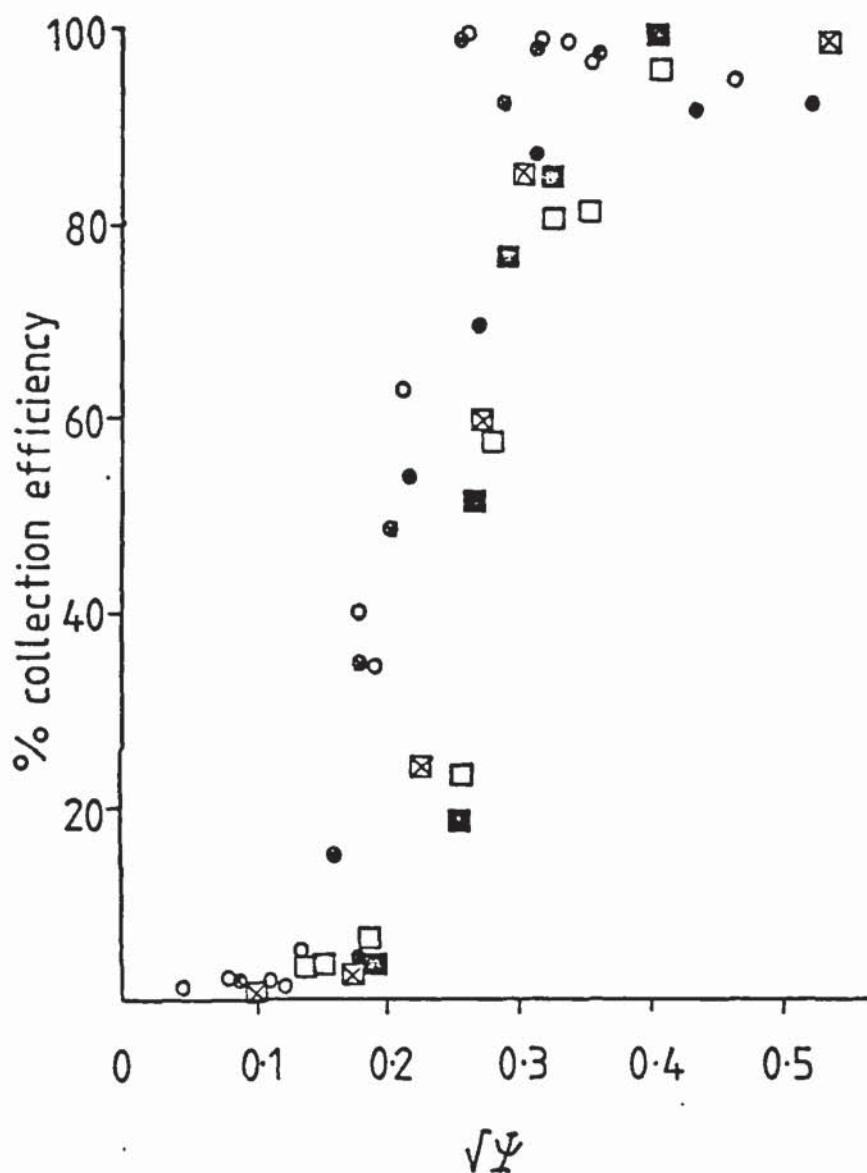


Figure 4.15 Mean experimental collection efficiency versus square root of impactation parameter (Ranz and Wong, 1952) for the DCI-6 cascade impactor.

- stage 1
- stage 4
- ⊠ stage 2
- ⊠ stage 5
- stage 3
- stage 6



Chapter 5 THE EFFECT OF RELATIVE HUMIDITY ON THE PARTICLE SIZE OF INHALATION AEROSOLS

5.1 INTRODUCTION

In Chapter 2 a technique for predicting the behaviour of single water-soluble compounds in the high humidity of the respiratory tract has been described. This technique is however only applicable to aerosols generated as dry powders (for example from powder insufflators) or as nebuliser solutions of drug and water alone. However, nebuliser solutions may contain other solvents such as alcohols or glycols and other formulating agents such as buffer salts, antioxidants and preservatives. For example Davis has examined water-propylene glycol (Davis, 1978a) and water-propylene glycol-ethanol (Davis et al, 1978b) systems as potential vehicles for nebuliser solutions of a test steroidal compound of limited water solubility. The most widely used aerosol generator in inhalation therapy is the 'pressurised pack'. The drug may be dissolved in the liquified propellant, usually with the addition of cosolvents or may be suspended as micronised powder in the liquid propellant system. Surfactants are frequently added to prevent drug agglomeration. Lubricants may be included to improve powder flow through the valve. Desiccants may be added to minimise moisture content. For complex nebuliser solution systems and aerosols generated from pressurised packs it is not possible to determine the behaviour of the aerosol under high humidity conditions from the physicochemical characteristics of the drug alone. In these instances direct

measurement of the change in the size distribution of the aerosol at high humidity is desirable.

In practise it is difficult to achieve the degree of temperature control required to maintain the relative humidity experienced within the respiratory tract. For example, in order to obtain the growth ratio of a single water-soluble compound with an accuracy of 5% at 99.5% relative humidity would require temperature control within $\pm 0.015^{\circ}\text{C}$ at 37°C (Gonda et al, 1981). Correspondingly, studies on the effect of relative humidity on the particle size of aerosols are performed at sub-physiological humidities.

The behaviour of aerosols with varying humidity is pertinent to both the behaviour of aerosols in the respiratory tract and in cloud formation. A number of controlled humidity experiments are described in the literature. In his studies with atmospheric aerosols, Winkler (1974) controlled the humidity by lining a tube mounted prior to a cascade impactor with a filter paper wetted with a saturated salt solution. The equilibrium humidity above a saturated salt solution is constant (Kaye and Laby, 1973), however for the incoming aerosol to be exposed to a constant humidity, it is necessary for the flow rate to be sufficiently slow for diffusion of water vapour from the filter paper into the body of the aerosol cloud to occur. The filter paper reservoir should also contain sufficient water to accommodate this diffusion without drying the filter paper.

A number of commercial humidity cabinets are available, these are basically of two designs. In one the required humidity is

produced by a tray of saturated salt solution. Again sufficient water must be available to humidify the cabinet without exhausting the reservoir. Fans may be incorporated to induce good mixing within the cabinet. This type of cabinet however, usually takes some time to re-equilibrate if perturbed. In the second type of cabinet the humidity is monitored by wet and dry bulb thermometers. When the humidity falls below the desired level, water is sprayed over the cabinet heaters to supply additional water vapour. Because of the lag time before the wet-bulb thermometer re-equilibrates, the humidity within this type of cabinet will tend to fluctuate around the required humidity. The periodicity of these fluctuations will tend to be longer than the time required for the aerosol droplets to equilibrate.

In their studies on the behaviour of inorganic salt aerosols Tang et al (1977a, 1977b, 1977c) used a controlled humidity system whereby air saturated with water is mixed with dry air to produce the required humidity. In their continuous flow system only the humidity of the air which will be mixed with the aerosol is controlled rather than that of the whole cabinet as in commercial designs.

Dry aerosol particles of a single water-soluble compound exposed to increasing humidity, will at a distinct humidity, the deliquescence point, undergo an abrupt increase in size as a saturated droplet is formed. If the droplet formed is then exposed to a reduced humidity, a continuous reduction in size takes place as a result of the droplet forming a supersaturated solution. This hysteresis phenomenon is well documented for

inorganic salt aerosols (Orr, 1954; Tang, 1977b). It is important therefore to consider the direction of the humidity change below the deliquescence point of a single water-soluble compound. At high humidity the aerosol will undergo large change in size for small changes in humidity. This makes prediction of growth ratios at 99.5% relative humidity difficult from direct measurement of size changes at lower humidities.

Atmospheric aerosols, which generally consist of mixtures of inorganic water-soluble materials and insoluble materials by comparison, a continuous growth character by gradual deliquescence of water-soluble material (Winkler 1974). These aerosols still however display large size changes for small humidity changes at high humidity.

This chapter describes the development of a controlled temperature and humidity apparatus and its use in characterising the behaviour of a model inhalation aerosol, fluorescein disodium with varying humidity. For comparison the predicted growth ratio of fluorescein disodium with varying relative humidity could be calculated from physicochemical data using the techniques described in Chapter Two.

5.2 CONTROLLED TEMPERATURE AND HUMIDITY APPARATUS

5.2.1 Design considerations

The relative humidity over saturated salt solutions is constant and relatively insensitive to temperature (Robinson and Stokes, 1959a). The passage of air through saturated salt solutions at the same temperature therefore provides a relatively simple method of generating an airstream of known moisture content. The limits to the temperature control in order to reduce errors in the growth ratio D_d/D_o to less than 5% were calculated as follows:

Consider the passage of air through a bubble humidifier containing saturated potassium sulphate solution at $(37.00 \pm 0.05)^\circ\text{C}$ into an equilibrium chamber maintained at $(37.00 \pm 0.05)^\circ\text{C}$. The maximum lower deviation in relative humidity from 96% (the equilibrium humidity over saturated potassium sulphate) solutions will correspond to the humidifier maintained at the lower limit of the temperature range, that is 36.95°C and the equilibrium chamber at the upper limit of the temperature range, 37.05°C . The saturated water vapour at 36.95°C is 46.96 Torr (Handbook of Chemistry and Physics, 1978), correspondingly the water vapour pressure of air after its passage through the bubble humidifier will be 45.96 Torr. At 37.05°C the saturated water vapour pressure is 47.20 Torr. The relative humidity in the equilibrium chamber will therefore be $((45.96/47.20) \times 100) \% = 95.5\%$. The upper limit to relative humidity will correspond to the opposite temperature limits resulting in a humidity of 96.5%.

Assuming ideal solution behaviour and negligible surface tension effects the growth ratio D_d/D_o may be calculated from Equation 1.12. For a solute of molecular weight of 400 Daltons forming 3 ions in solution and with the density of the dry particle equal to that of the equilibrium droplet, the growth ratio, D_d/D_o at 96% relative humidity will be 1.619, at 95.5% relative humidity the growth ratio will be 1.569 and at 96.5% relative humidity the growth ratio will be 1.677. Thus with temperature control of $\pm 0.05^\circ \text{C}$ at 37.00°C the growth ratio can theoretically be determined with less than $\pm 3\%$ error at 96% relative humidity.

The humidity bottles were placed in a water bath whose temperature was controlled by a proportional temperature controller (YSI Model 72, Cole Palmer Instruments) using a 1 Kilowatt immersion heater and a pyrex tubular glass thermistor probe (YSI Model 404, Cole Palmer Instruments). The equilibrium chamber was heated by pumping water from a reservoir, through a water jacket. The temperature of the reservoir was maintained using a second proportional temperature controller (YSI Model 72, Cole Palmer Instruments) with a stainless steel thermistor probe (YSI 410, Cole Palmer Instruments). The required temperature is controlled on these instruments by setting dials. The temperature difference required to give 100% power to the heater is controlled by a bandwidth setting. This must be turned to take into account the lag time of the system being controlled. If the bandwidth is too narrow the controller will switch fully on when the detected temperature is below the required temperature then switch fully off when the detected temperature is equal

to the required temperature. However, because of the lag time of the system the water temperature would not have finished rising. In this instance regular large cyclic fluctuations in temperature may occur. Figure 5.1 shows the temperature fluctuations observed in the growth chamber reservoir when a bandwidth of 0.5°C was set on the temperature controller. By trial and error the bandwidth giving minimal temperature fluctuations was found to be 1.5°C . The temperature control dials of the proportional temperature controllers were marked in degrees centigrade and the markings were within 0.5°C of the controlled temperature. For the controller used for the humidifier water bath the dial setting corresponding to 37°C was found to be 37.27°C and for the controller used for the growth chamber reservoir it was found to be 37.31°C .

The water bath, reservoir and growth chamber were placed in a box whose walls were insulated with $\frac{1}{4}$ " thick expanded polystyrene sheeting. Using a proportional controller built by Mr. D. Briggs of the Pharmacy Department of the University of Aston in Birmingham (see Appendix 3) connected to a 375 watt fan heater (Calor, model 92-01) and a bead thermistor, the temperature of the outer box was maintained at $(36.5 \pm 0.1)^{\circ}\text{C}$. Circulation within the box was assisted by the use of a second fan (Pifco, Spinair) in the upper part of the box.

The humidifier water bath and growth chamber reservoir were insulated using expanded polystyrene sheeting. All connecting air pipes and water pipes were insulated to minimise heat loss. Using the above experimental conditions the water bath and reservoir temperature could be controlled at $(37.00 \pm$

0.05)⁰C. Initially air was bubbled directly from the inlet line through the bubble humidifiers but measurement of the air temperature at the outlet revealed that using this procedure the air temperature was still some 0.5⁰C below that of the water bath. This problem was overcome by passing the air through a glass coil situated in the humidifier water bath before its passage through the bubble humidifiers. This procedure brought the air temperature to within 0.1⁰C of the water bath temperature before its passage through the bubble humidifiers. The measured air temperature at the outlet was found to be $(37.00 \pm 0.05)^{\circ}\text{C}$ using the improved procedure.

5.2.2 Final Design

A schematic diagram of the controlled temperature and humidity apparatus is shown in Figure 5.2. The equilibrium chamber with an internal volume of approximately 3 litres was constructed from glass. At a flow rate of 12.5 litres per minute this provided a residence time of 15 seconds. The aerosol inlet into the equilibrium chamber was arranged tangentially to encourage mixing of the aerosol and humidified air. Both the equilibrium chamber and aerosol inlet were surrounded by water jackets and insulated with polystyrene sheeting. Water from the temperature controlled reservoir was passed through the water jackets of the equilibrium chamber and aerosol inlet using a water pump (Charles Austin, model CP25P).

Filtered compressed air was preheated by passing it through a glass coil in a water bath maintained at $(37.00 \pm 0.05)^{\circ}\text{C}$.

The preheated air was then passed through bubble humidifiers containing saturated salt solutions. The humidified air was passed through a glass sinter filter to remove any particulate matter or droplets before its passage into the equilibrium chamber.

5.3 EXPERIMENTAL

The behaviour of aerosol of single-water soluble compounds in the high humidity of the respiratory tract can be predicted from the physicochemical properties of solutions of the compound using the methods described in Chapter 2. In order to validate the use of the controlled temperature and humidity apparatus for more complex aerosols the behaviour of a single water-soluble model inhalation aerosol was investigated and compared to calculations based on its measured physicochemical properties.

5.3.1 Prediction of equilibrium growth of fluorescein disodium aerosols from bulk solution data

The water activity of aqueous fluorescein disodium solutions of concentrations approaching that of the saturated solution at 37° C, were determined using the vapour pressure osmometer as described in section 2.2.1.

Density measurements at 37° C were also made on these solutions using the techniques described in Chapter 2.

The density of dry fluorescein disodium powder was determined by air comparison pycnometry.

The relative humidity over a saturated fluorescein disodium solution at 37° C was determined using a dew-point hygrometer (E, G and G, model 911) at the output from bubble humidifiers containing the saturated solution.

5.3.2 Nebuliser characteristics

A compressed air nebuliser (Bird, Mark 7, BOC Medical Supplies) was used to generate the experimental aerosols in this study. The mass flow rate of air through compressed air nebulisers is a function of the air pressure before the orifice (Mercer, 1968). A schematic diagram of the experimental set-up used to determine flow-rate versus gauge pressure of the inlet line is shown in Figure 5.3. The gauge pressure of the inlet line was controlled by a needle valve (G A Planton Ltd) and measured using a mercury manometer. The flow rate was measured using a flow meter (G A P meter, G A Planton). Control of the operating pressure is important as there is some evidence that the size distribution of the aerosol produced by compressed air nebulisers is a function of operating pressure (Postendorfer, 1977). The total output from the nebuliser was determined by measuring the weight loss of the nebuliser filled with a 0.032 molal aqueous fluorescein disodium solution. The total output of the nebuliser will comprise of aerosol droplets escaping from the nebuliser and solvent vapour evaporating from the bulk solution which includes previously impacted droplets that spread as a thin layer of solution over the inner surface of the nebuliser as they drain back into the reservoir. A loss of water vapour would produce an increase in concentration of the solution in the nebuliser. If an increase in concentration occurs it is possible to determine aerosol output and solvent vapour output by mass balance (Davis, 1978a). Correspondingly the concentration of the remaining solution was determined after

each experiment.

In order to determine the original droplet size distribution from the nebuliser, a 0.191 Molal aqueous fluorescein disodium solution was nebulised at an inlet gauge pressure of 300mm of mercury. The aerosol was mixed with dry, filtered air to facilitate solvent evaporation and the size of the residual fluorescein disodium particles determined using a DCI-6 cascade impactor. The amount of fluorescein landing on each silicone fluid coated slide was determined by fluorimetry of the aqueous extract (see section 4.2.2.5). The cascade impactor is calibrated in terms of aerodynamic diameter, Da. Assuming that the residual dry particles are spherical, this is related to the geometric diameter of the residual dry particle, Dp by (TASK 1966)

$$C(Da) \cdot d_o \cdot Da^2 = C(Dp) \cdot d_p \cdot Dp^2 \quad \text{Equation 5.1}$$

where C(D) is the Cunningham slip factor for a particle with diameter, D, and dp the density of the dry particle. The mass of the dry particle in terms of particle diameter and density, assuming the particle to be spherical will be

$$m_p = \frac{4}{3} \pi \left(\frac{Dp}{2}\right)^3 \cdot d_p \quad \text{Equation 5.2}$$

The concentration of fluorescein disodium in the nebuliser solution was equivalent to 1 gram of fluorescein disodium for each 14.9 grams of solution. The mass of the droplet, md, from

which the residual dry particle originated will therefore be

$$m_d = \frac{4}{3} \pi \left(\frac{D_p}{2} \right)^3 \rho_p \cdot 14.9 \text{ (grams)} \quad \text{Equation 5.3}$$

and may also be described in terms of the droplet diameter D_d , and density, ρ_d , by

$$m_d = \frac{4}{3} \pi \left(\frac{D_d}{2} \right)^3 \rho_d \quad \text{Equation 5.4}$$

Equating Equations 5.3 and 5.4, the ratio of the diameters of the original droplet and residual dry particle may be described by

$$\frac{D_d}{D_p} = 3 \sqrt{\frac{\rho_p \cdot 14.9}{\rho_d}} \quad \text{Equation 5.5}$$

The size distribution of the original droplet output may therefore be calculated from the size distribution of the residual dry particles.

5.3.3 Fluorescein disodium aerosol size distributions with varying Relative Humidity

The controlled temperature and humidity apparatus described in section 5.2 was set to a temperature of $(37.00 \pm 0.05)^\circ \text{C}$. The temperatures in the growth chamber and water baths were monitored using precision thermistors (YSI 44031, Sasco). The thermistor used to measure the water bath temperature was

embedded in a protective araldite coat. When the chamber was at the required temperature filtered air was passed at 12.5 litres per minute through the bubble-humidifiers containing the required saturated salt solution. The humidity within the growth chamber was monitored using a dew-point hygrometer (E, G and G, model 911). When the humidity had established itself at the required level the pump to the cascade impactor was switched on to fill the impactor with humidified air. Before passing the aerosol into the chamber, the pump drawing air into the dew-point hygrometer was switched off to prevent any aerosol particles passing into the sensing chamber, which could result in erroneous readings.

There is some evidence that the size distribution of the aerosol produced by compressed air nebulisers is a function of operating pressure (Postendorfer, 1977). The nebuliser output was vented initially to prevent sampling of atypically sized aerosols arising from pressure surges. A nebuliser solution containing 0.032 molal fluorescein disodium was employed. The flow rate through the bubble humidifiers was reduced to 8 litres per minute and sample of the nebuliser output passed into the equilibrium chamber for ten seconds. The flow rate to the bubble humidifiers was then returned to 12.5 litres per minute. After two minutes collection to ensure capture of the aerosol, the pump to the cascade impactor was switched off. The quantity of fluorescein disodium landing on each slide was determined by fluorimetry of the aqueous extract (see section 4.2.2.5). After suitable dilution, the fluorescence of the residual nebuliser

solution was measured. For each humidity level the experiment was repeated three times. The saturated salt solutions used and the relative humidity over them at equilibrium are given in Table 5.1.

5.3.3.1 Humidity levels during aerosol sizing experiments

The introduction of the aerosol in its carrier gas into the equilibrium chamber will necessarily perturb the established humidity system. The aerosol is only introduced into the equilibrium chamber in a short burst (10 seconds) to avoid overloading of the cascade impactor. This is insufficient time for the dew-point hygrometer to detect and register the humidity.

In order to determine the exposure humidity the following series of experiments were performed. The nebuliser output at 4.5 litres per minute was mixed in the equilibrium chamber with humidified air from the bubble-humidifiers at a flow rate of 8 litres per minute, for 15 minutes. The resulting humidity was measured using a dew-point hygrometer (E, G and G, model 911). In order to prevent aerosol particles entering the sensing chamber the end of the inlet tubing to the dew-point hygrometer was plugged with glass fibre wool. The experiment was repeated with each of the saturated solutions used in section 5.3.3.

5.4 RESULTS AND CALCULATIONS

5.4.1 Predicted Growth Ratios for fluorescein disodium aerosols with varying relative humidity.

It has been shown in section 2.4 that the magnitude of the Kelvin effect relative to aerodynamic diameter is only significant for very small particles. In the calculation of growth ratios of fluorescein disodium aerosols with varying relative humidity the Kelvin effect has been neglected. The growth ratio at the required relative humidity may be calculated from

$$\frac{D_d}{D_o} = \sqrt[3]{\frac{d_o}{d_d} \left(1 + \frac{1000}{W_s M} \right)} \quad \text{Equation 5.6}$$

where M is the concentration of fluorescein disodium (in moles per kg of water) which has a water activity equal to the fractional humidity under consideration. The derivation of Equation 5.6 is analogous to Equation 1.15. As the data from the cascade impactor sizing studies are in terms of aerodynamic diameter, it is useful to express the growth ratio in terms of aerodynamic diameter. By neglecting the Kelvin effect, the growth ratios obtained refer to the limit of large spherical particles, it is reasonable therefore to neglect the Cunningham slip factor in the determination of aerodynamic diameters. The aerodynamic growth ratio, $\left(\frac{D_d}{D_o} \right)_a$, may be calculated from

$$\left(\frac{D_d}{D_o} \right)_a = \sqrt{\frac{d_d}{d_o}} \cdot \left(\frac{D_d}{D_o} \right) \quad \text{Equation 5.7}$$

Figure 5.4 illustrates the water activity of aqueous fluorescein disodium solutions as a function of concentration. The mean water activity of at least three determinations is given in the figure. The individual determinations were within 0.003 of the mean value on all points.

The humidity over saturated fluorescein disodium solutions at $(37.00 \pm 0.05)^{\circ}\text{C}$ was found to be $(53.7 \pm 0.2)\%$. If a particle of dry fluorescein disodium were exposed to an increasing humidity, a sudden increase in diameter would therefore be expected at $(53.7 \pm 0.2)\%$ relative humidity as the saturated solution was formed.

The density of aqueous fluorescein disodium solutions at 37°C is shown in Figure 5.5. Each determination was made in triplicate, individual determinations were within 0.0005g cm^{-3} of the mean value on all points. The density of dry fluorescein powder was found to be $(1.490 \pm 0.001)\text{g cm}^{-3}$ by air comparison pycnometry.

From these experimental data it was possible to calculate the growth ratios for fluorescein disodium aerosols with varying humidity using Equations 5.6 and 5.7. The calculated aerodynamic growth ratios versus increasing humidity are illustrated in Figure 5.6.

5.4.2 Nebuliser Characteristics

Figure 5.7 illustrates the air flow rate versus inlet gauge pressure and Figure 5.8 the total nebuliser output

versus inlet gauge pressure for the nebuliser (Bird, Mark 7, BOC Medical Supplies) used in these studies. At an inlet gauge pressure of 300 mm of mercury, the value used in the subsequent aerosol sizing experiments, the air flow rate was 4.5 litres per minute. Measurement of the concentration of the residual nebuliser solution after fifteen minutes continuous operation showed no detectable deviation from the initial concentration, indicating that the total output in this instance could be taken as aerosol output. However, it was observed that the nebuliser cooled during operation indicating that some evaporation was taking place, this was insufficient to be detected by the assay technique employed here.

The size distribution of the residual dry aerosol from a 0.191 Molal fluorescein disodium solution nebulised at 300mm of mercury gauge pressure was found by analysis of the fractional deposition pattern on the stages of the DCI-6 cascade impactor using the programme described in section 4.4. The size distribution could be satisfactorily described by a log-normal distribution with a mass median aerodynamic diameter of $(3.02 \pm 0.02) \mu\text{m}$ with a geometric standard deviation of (1.38 ± 0.06) . Correspondingly, the size distribution of the dry particles in terms of geometric diameter would be log-normal with a mass median diameter of $(2.48 \pm 0.02) \mu\text{m}$. The geometric mass median diameter of the original droplets calculated from Equation 5.5 was $(6.96 \pm 0.05) \mu\text{m}$ with a geometric standard deviation of (1.38 ± 0.06) .

5.4.3 Fluorescein disodium aerosol size distributions with varying relative humidity

In these experiments the concentration of fluorescein disodium used in the nebuliser was 0.0325 Molal. The ratio of the residual dry particle to original droplet size will therefore be

$$\frac{D_d}{D_p} = \sqrt[3]{\frac{1.49}{1} \cdot 82.877} = 4.98 \quad \text{Equation 5.8}$$

The original droplet particle size distribution for an aqueous 0.0325 molal nebuliser solution from the Bird (Mark 7) nebuliser operating at a gauge pressure of 300mm of mercury was assumed to be log-normally distributed with a mass median geometric diameter of $(6.96 \pm 0.05)\mu\text{m}$ with a geometric standard deviation of (1.38 ± 0.06) based on the results from a 0.191 molal nebuliser solution. The residual dry particle from a 0.0325 molal nebuliser solution will have a calculated mass median geometric diameter of $(1.40 \pm 0.01)\mu\text{m}$ with a corresponding mass median aerodynamic diameter of $(1.71 \pm 0.01)\mu\text{m}$.

The particle size distributions of the fluorescein disodium aerosols exposed to varying relative humidity were also found to be satisfactorily described by log-normal distributions by analysis of the fractional deposition on the stages of the DCI-6 cascade impactor using the programme described in section 4.4. The determined mass median aerodynamic diameters and geometric standard deviations are given in Table 5.2. Included in Table 5.2 are the aerodynamic growth

ratios with reference to the average mass median aerodynamic diameter of the residual dry particle of $1.71\mu\text{m}$.

The average measured resultant humidity level and the range from the mixing experiment (see section 5.3.3.1) are given in Table 5.3. These values give an indication of the exposure humidity within the main body of the aerosol cloud during the sizing experiments. The concentration of water from the nebuliser at an operating pressure of 300mm of mercury and a nebuliser solution of 0.0321 molal fluorescein disodium is 0.0286g per litre. This exceeds the concentration of water from the bubble humidifiers when they contain sodium hydroxide (0.00308g per litre) and potassium carbonate (0.01890g per litre) so the resultant humidity is higher than the equilibrium humidity over the saturated solution in the bubble humidifier. For the remaining saturated salt solution used, the concentration of water from the nebuliser humidifier will be less than the concentration of water in the airstream from the bubble humidifiers. The resultant humidity of the mixed airstream is therefore less than the equilibrium humidity over the saturated solutions in this instance. However, the aerosol cloud is preceded by and followed by air at the equilibrium humidity over the saturated salt solution in the bubble humidifier. The humidity at the periphery of the aerosol cloud will therefore tend to these values.

Figure 5.9 show the mean and standard deviation of the experimentally determined aerodynamic growth ratios for fluorescein disodium aerosols with varying humidity. The

growth ratios are plotted against the average humidity levels obtaining in the subsequent mixing experiments (see Table 5.3). The horizontal bars illustrate the range of humidity experienced by the aerosol cloud. For comparison the calculated aerodynamic growth ratios for fluorescein disodium aerosols based upon physicochemical characteristics of aqueous solutions is included as the solid line in Figure 5.9. Above the deliquescence point, $(53.7 \pm 0.2)\%$ relative humidity, there is good correlation between the calculated and experimentally determined aerodynamic growth ratios. The experimental aerosols were generated from a 0.0325 molal solution which had a water activity of approximately 0.998. The aerosols will therefore be decreasing in size at each of the experimental humidities. The results at humidities below the deliquescence point indicate that there is a hysteresis as a supersaturated solution is formed. This phenomenon has been previously described for inorganic electrolyte aerosols (Orr, 1954; Tang, 1977).

The design of a controlled temperature and humidity cabinet has been described. The major problem in the use of the apparatus arises from the addition of carrier gas bringing aerosol into the equilibrium chamber perturbing the previous established humidity. In the experiments described here the problem was further complicated by the need to limit the flow from the nebuliser to a 10 second burst to avoid overloading of the cascade impactor. The experimental aerosol cloud was therefore preceded and followed by air at the humidity above the saturated salt solutions used in the bubble humidifiers. The results have therefore been interpreted taking into account the extremes of humidity the aerosol cloud would have experienced. The results indicate good correlation between the predicted and observed growth ratios above the deliquescence point. Below the deliquescence point the results indicate a hysteresis with reducing relative humidity as a supersaturated solution is formed. This phenomenon has been previously described with inorganic aerosols (Orr, 1954; Tang, 1977).

A more constant humidity could be achieved by the use of a continuous mixing system. The problem of overloading the cascade impactor slides could be overcome by either reducing the output from the nebuliser or by introducing a by-pass device between the equilibrium chamber and the cascade impactor.

Reduction in nebuliser output could be achieved by decreasing the inlet gauge pressure. The inlet gauge pressure used in the experiment described in this chapter was 300mm of

mercury. This corresponded to a total output from the nebuliser of 0.029 grams per litre per minute, allowing only a ten second input into the equilibrium chamber if overloading of the cascade impactor was avoided. From examination of Figure 5.8 if the inlet gauge pressure were reduced to 50mm of mercury, the total output would only be reduced to 0.01 grams per litre per minute, allowing a maximum input time of only thirty seconds.

An alternative method of reducing the effective nebuliser output would be to allow only part of the total output to pass into the equilibrium chamber. This could be achieved by the use of a small bore sampling tube at the nebuliser outlet with the remainder of the aerosol passing to waste. The sample of aerosol passing into the equilibrium chamber need not necessarily be representative of the nebuliser output providing that the size fraction taken was constant between experiments. Problems could however occur in data interpretation, if the sampling device for example excluded particles above a certain size then it may be difficult to transform the fraction collected on each stage of the cascade impactor into a clearly defined size distribution as the original log-normal distribution, for example, would be truncated. Similarly, if a by-pass device was used between the equilibrium chamber and cascade impactor, data interpretation would be easier if the sample collected by the cascade impactor were representative of the whole size distribution.

The reduction in effective nebuliser output would have the advantage of enabling higher humidity levels within the equilibrium chamber to be achieved as the carrier gas input would also be reduced.

5.6 TABLES

5.6.1 Table Captions

Table 5.1 Humidifier solutions and the relative humidity above their saturated solutions at 37° C.

Table 5.2 Particle size distributions of fluorescein disodium aerosols exposed to varying humidity.

Table 5.3 Measured resultant humidity levels from mixing experiment (section 5.4.3.1)

Table 5.1 Humidifier solutions and the Relative Humidity above their saturated solutions at 37° C

Salt	Humidity over saturated solution (Robinson and Stokes, 1959)
NaOH	7.03
K ₂ CO ₃	42.76
K Br	80.71
K NO ₃	92.48
K ₂ Cr ₂ O ₇	98.0

Table 5.2 Particle size distributions of fluorescein disodium aerosols exposed to varying humidity

Humidity		Mass median aerodynamic diameter	Geometric standard deviation	Aerodynamic growth ratio
	Range			
15.5	7.03-15.9	1.85	1.80	1.08
		2.05	1.42	1.20
		1.975	1.52	1.15
49.7	42.76-50.0	1.95	1.58	1.14
		1.98	1.50	1.15
		1.96	1.48	1.16
72.3	71.8-80.71	2.22	1.37	1.30
		2.13	1.62	1.25
		1.95	1.76	1.14
81.7	81.0-92.48	2.08	1.62	1.22
		2.26	1.42	1.32
		2.18	1.62	1.27
92.3	91.3-98.0	2.58	1.34	1.51
		2.40	1.32	1.40
		2.17	1.37	1.27

Table 5.3 Measured resultant humidity levels from mixing experiment
(section 5.4.3.1)

Bubble-humidifier saturated solution	Measured humidity (% relative humidity)	
	<u>Average</u>	<u>Range</u>
NaOH	15.5	15.2-15.9
K ₂ CO ₃	49.7	49.5-50.0
K Br	72.3	71.8-72.8
KNO ₃	81.7	81.1-82.4
K ₂ Cr ₂ O ₇	92.3	91.4-93.3

5.7 FIGURES

5.7.1 Figure Captions

Figure 5.1 Temperature fluctuations in the equilibrium chamber reservoir using a bandwidth of 0.5°C on the proportional temperature controller.

Figure 5.2 Schematic diagram of the controlled temperature and humidity apparatus.

Figure 5.3 Determination of flow rate through the Bird nebuliser versus inlet gauge pressure: schematic diagram of apparatus.

Figure 5.4 Water activity of aqueous fluorescein disodium solution versus concentration.

Figure 5.5 Density of aqueous fluorescein disodium solutions at 37°C .

Figure 5.6 Calculated aerodynamic growth ratio versus relative humidity for fluorescein disodium.

Figure 5.7 Bird nebuliser operating characteristics: air flow rate versus inlet gauge pressure. Single determinations are shown.

Figure 5.8 Bird nebuliser operating characteristics: total output versus inlet gauge pressure.

Figure 5.9 Aerodynamic growth ratio versus relative humidity of fluorescein disodium aerosols.

Figure 5.1 Temperature fluctuations in the equilibrium chamber reservoir using a bandwidth of 0.5°C on the proportional temperature controller.

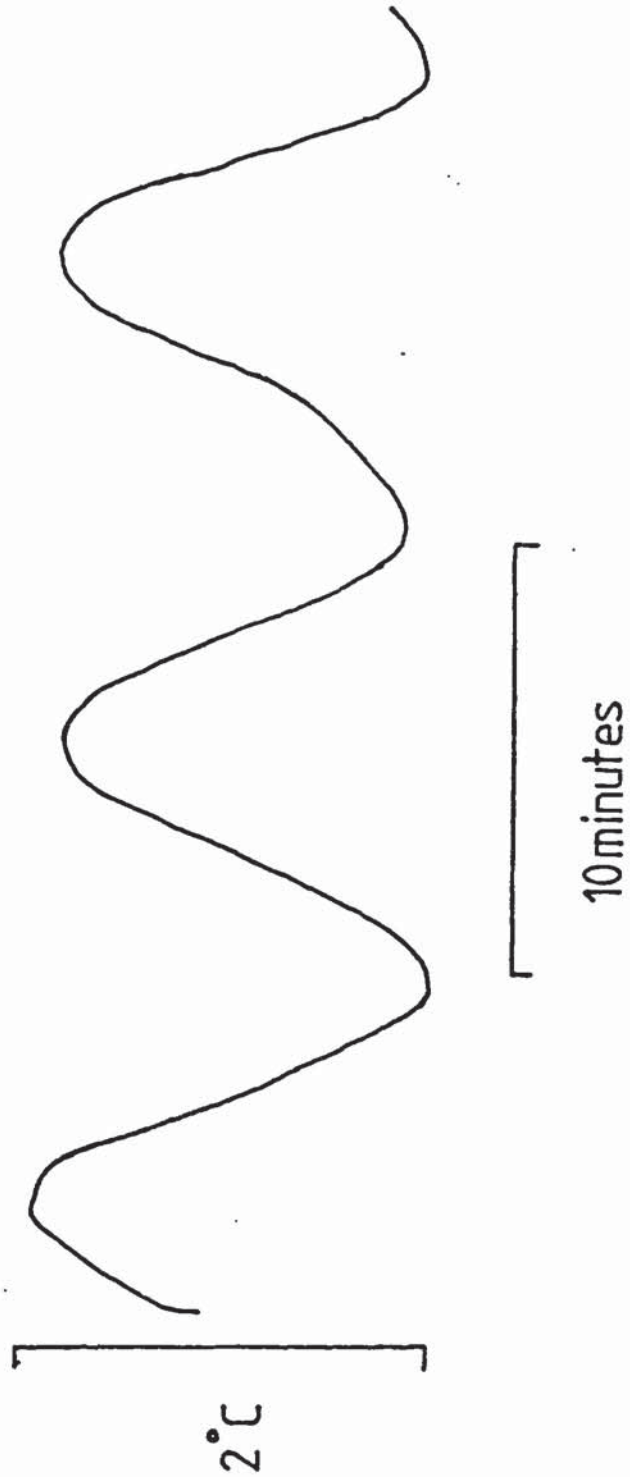


Figure 5.2 Schematic diagram of the controlled temperature and humidity apparatus.

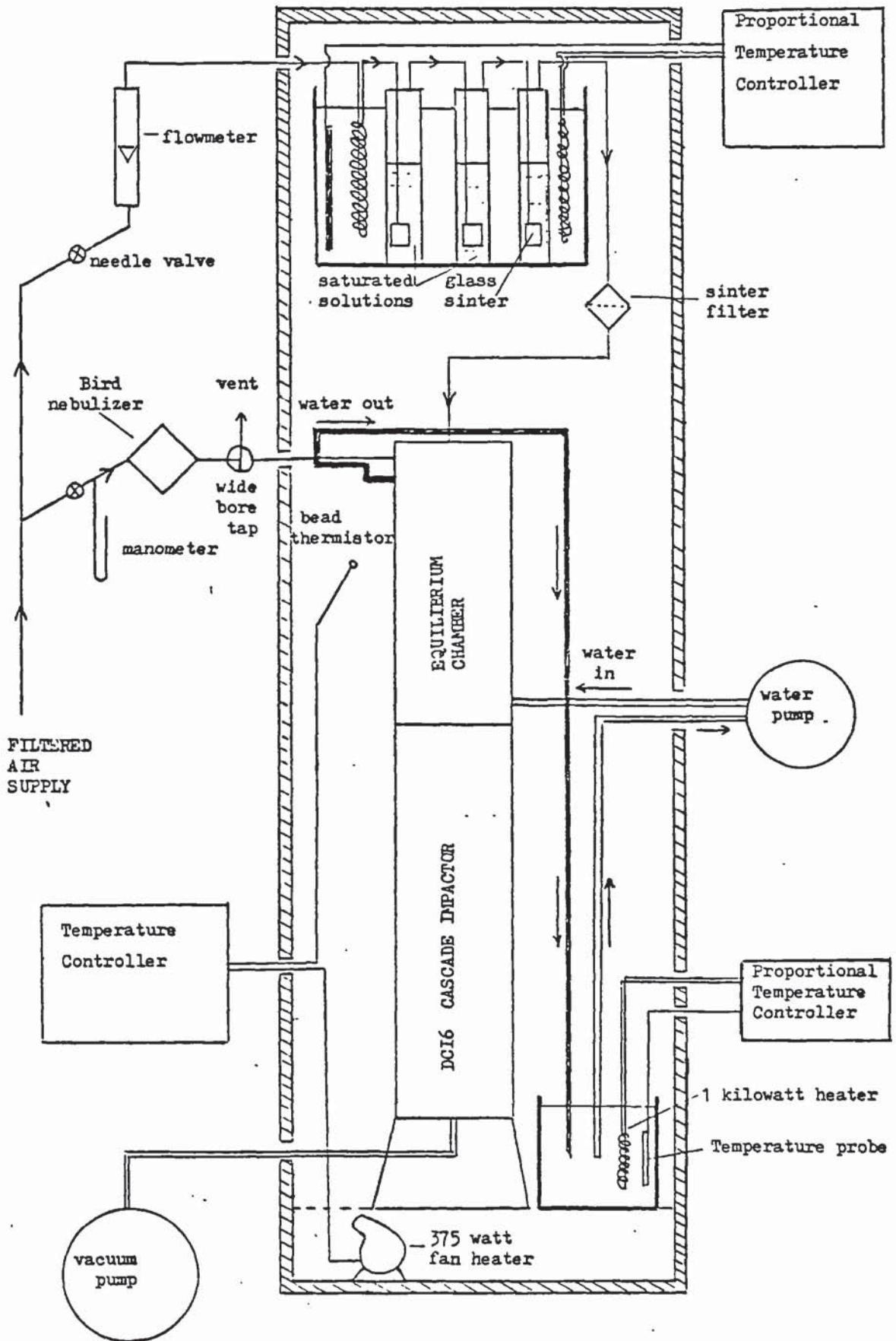


Figure 5.3 Determination of flow rate through the Bird nebuliser versus inlet gauge pressure: Schematic diagram of apparatus.

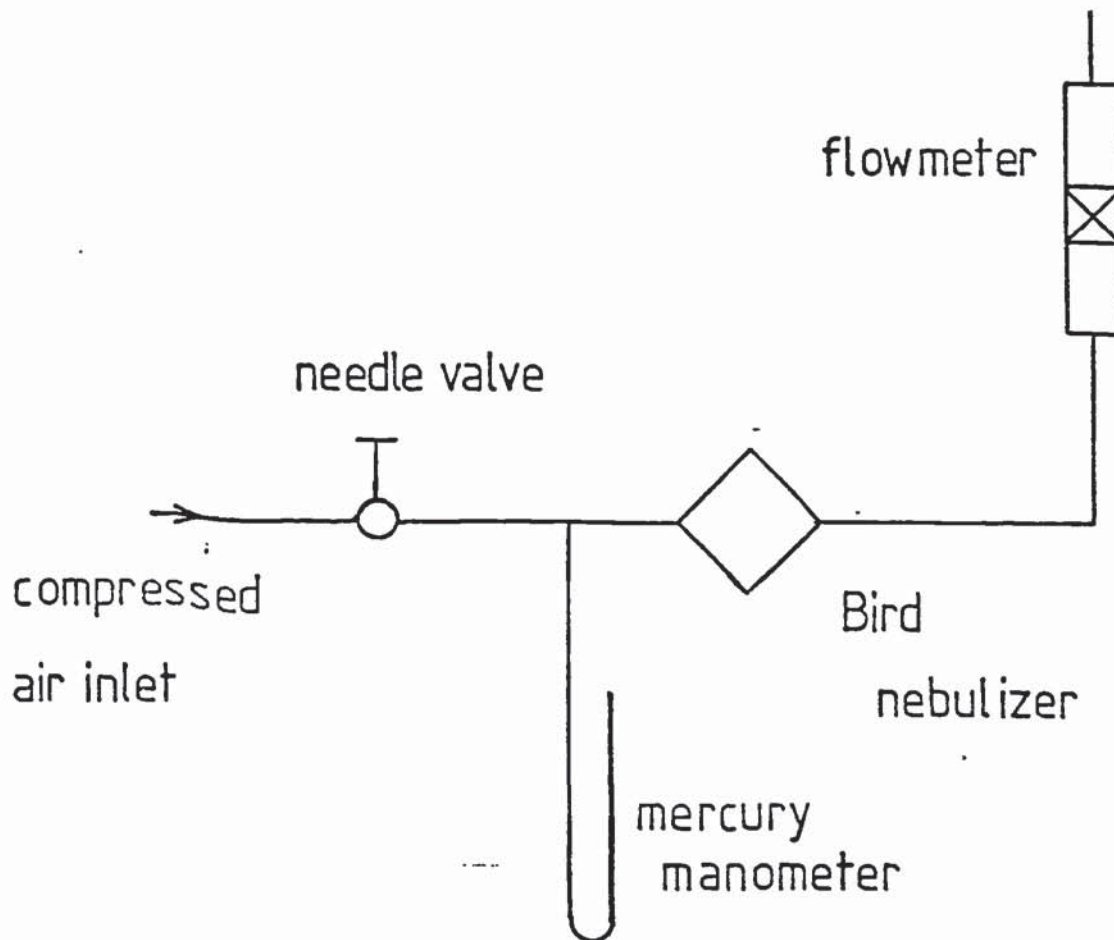


Figure 5.4 Water activity of aqueous fluorescein disodium solution versus concentration. The mean of at least three determinations is illustrated. Individual determinations were within 0.003 of the mean value on all points.

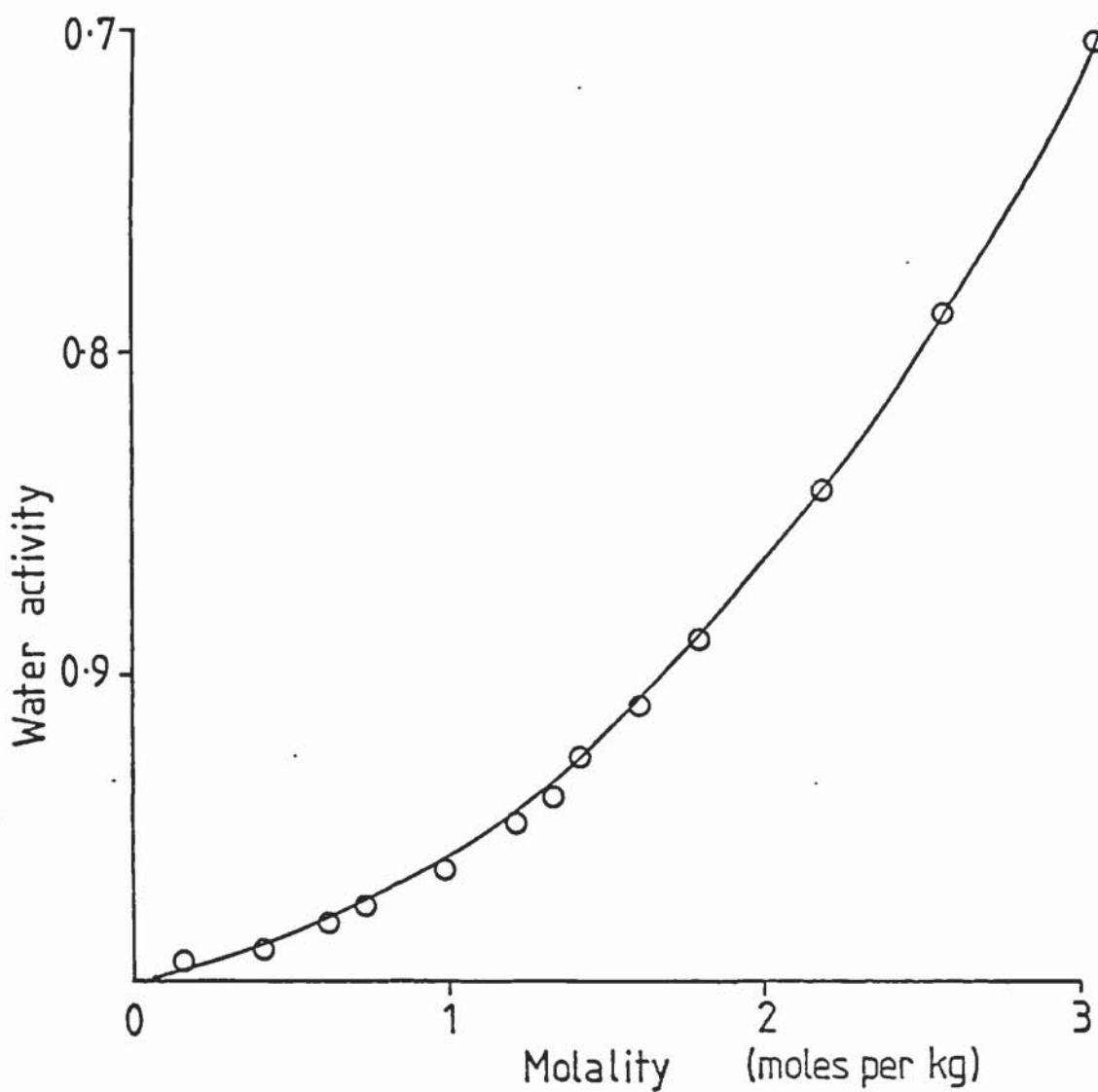


Figure 5.5 Density of aqueous fluorescein disodium solutions at 37° C
The mean value of three determinations is illustrated. Individual
determinations were within 0.0005g cm⁻³ on all points.

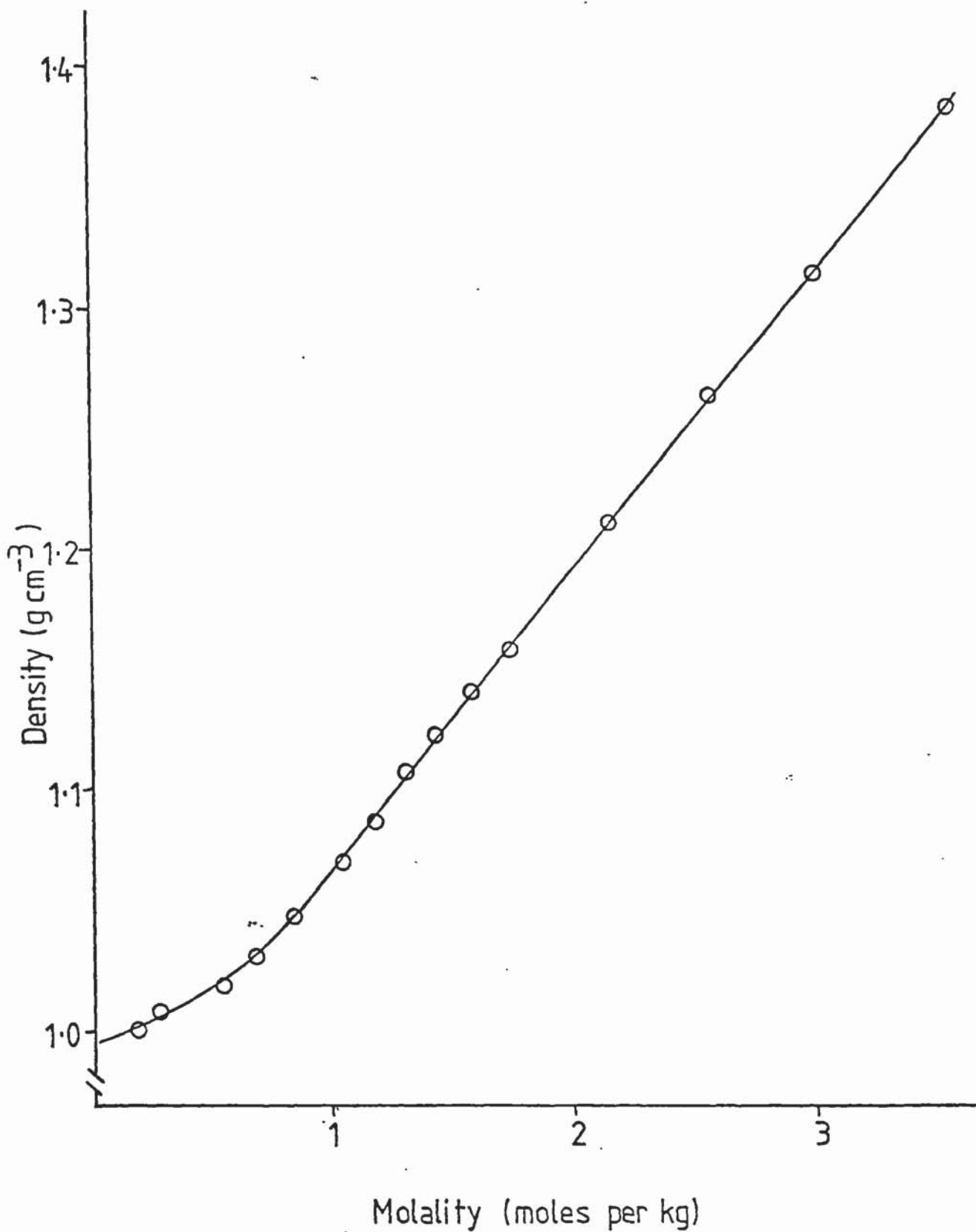


Figure 5.6 Calculated aerodynamic growth ratio versus relative humidity for fluorescein disodium.

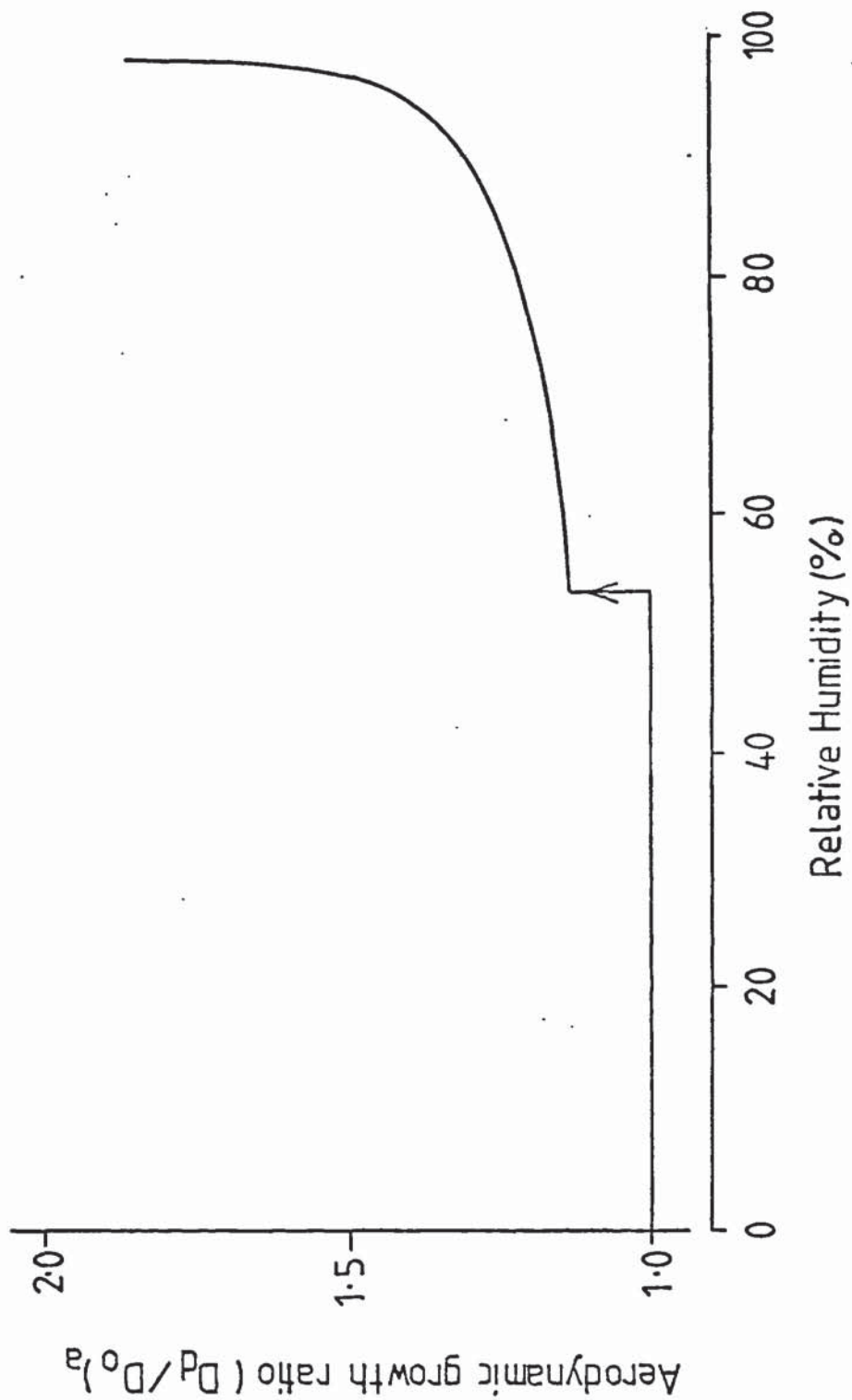


Figure 5.7 Bird nebuliser operating characteristics: air flow rate versus inlet gauge pressure. Single determinations are shown.

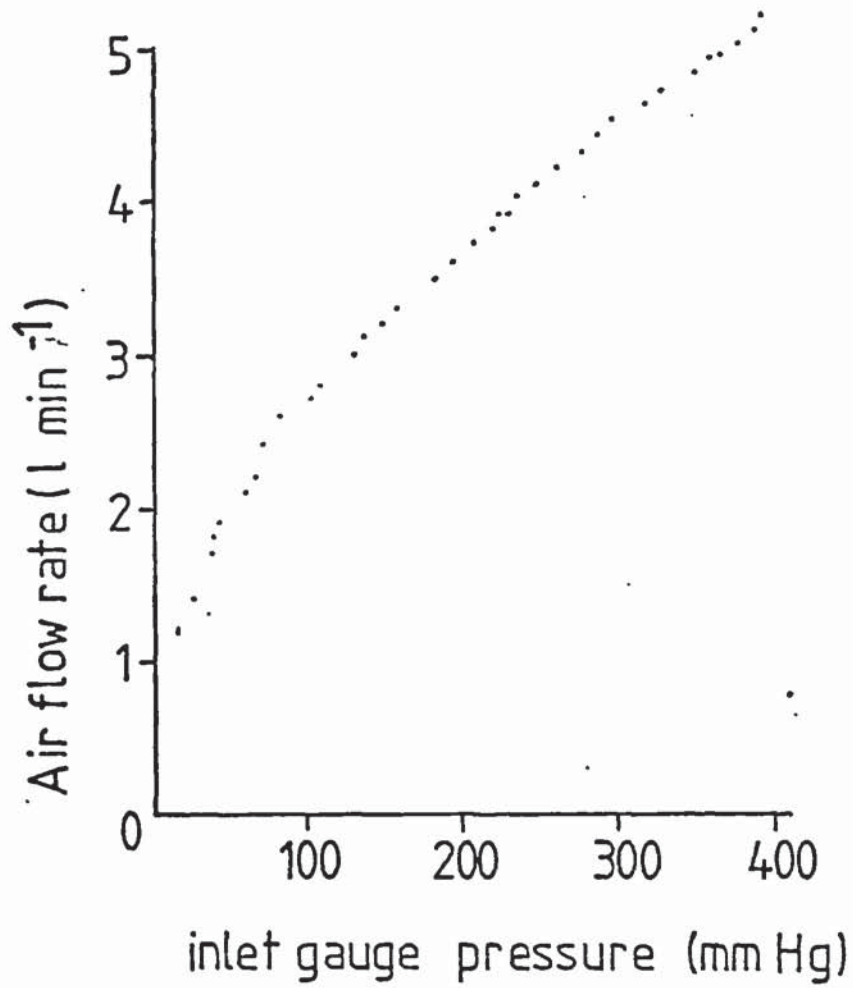


Figure 5.8 Bird nebuliser operating characteristics: total output versus inlet gauge pressure

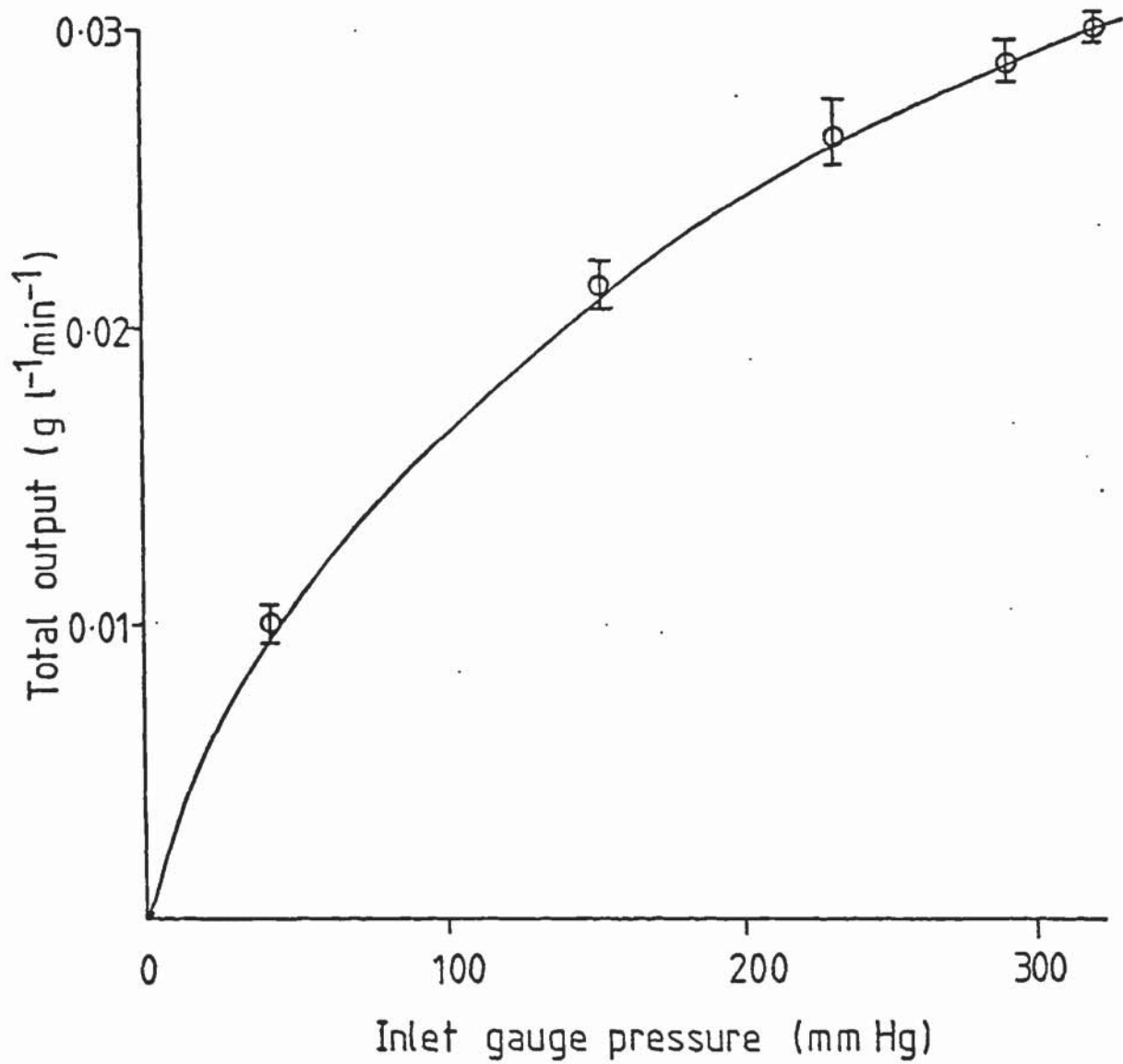
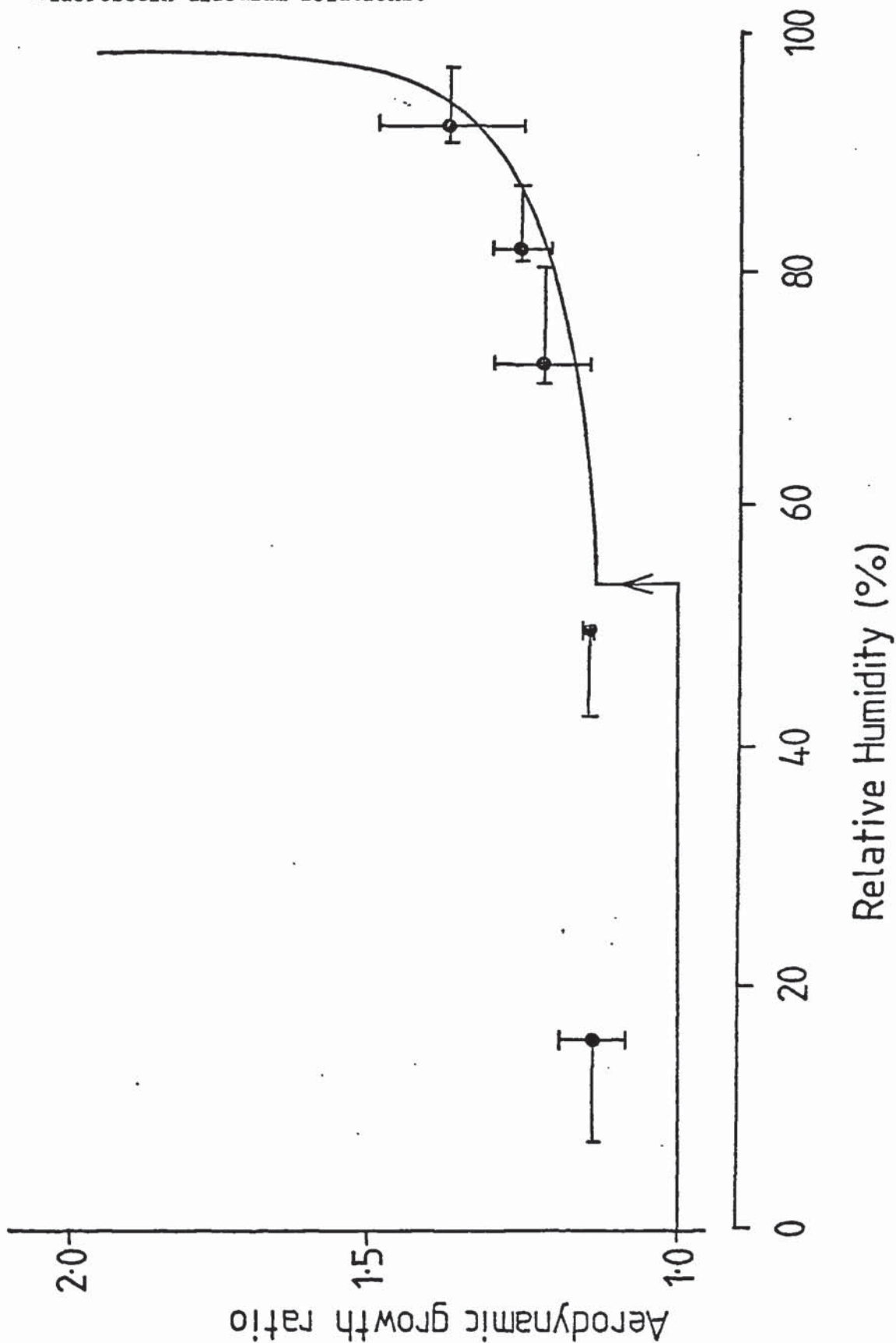


Figure 5.9 Aerodynamic growth ratio versus relative humidity for fluorescein disodium aerosols. The mean and standard deviation of three determinations plotted against average humidity is illustrated. The horizontal bars show the range of humidity at the extremes of the aerosol cloud. The solid line illustrates the calculated aerodynamic growth ratio based on the physicochemical characteristics of aqueous fluorescein disodium solutions.



Chapter 6 Development of an in vivo model for optimising systemic drug delivery by inhalation aerosol administration.

6.1 INTRODUCTION

The lungs offer many advantages as an absorption site for the systemic delivery of drugs. The surface area of the lungs is approximately 30m^2 (Hatch and Gross, 1964a), providing an absorptive area comparable with that of the gastrointestinal tract. Drugs administered by the inhalation route will not be subject to large pH changes (compared with the gastrointestinal tract) nor such a large number of degradative enzymes (Gonda and Byron, 1978). Sodium cromoglycate has been shown to be practically unabsorbed from the gastrointestinal tract but a competitive, saturable, carrier-type transport mechanism has been implicated in its absorption from the respiratory tract (Gardiner and Schanker, 1974). Moreover, large molecules, such as proteins, have been shown to pass through the alveolar wall intact (Schultz et al, 1964; Wigley et al, 1971). Despite these observations, most of the pharmaceutical inhalation aerosols currently in use are intended for local activity within the respiratory tract, a fact which probably reflects the difficulties associated with deposition of a known dose in the pulmonary and tracheobronchial regions (as defined by TASK, 1966). Moreover, aerosols designed for bronchodilator (local) activity may well require different particle size distributions for maximum deposition than those designed for maximum alveolar deposition with subsequent systemic absorption.

The inhalation route may be useful in attaining rapid delivery of drugs designed to act systemically. Indeed this route is already used to achieve rapid systemic onset of action of Ergotamine (Ergotamine Aerosol Inhalation, British Pharmaceutical Codex, 1979).

The purpose of the work to be described in this chapter was to develop a technique capable of providing information on the systemic availability of a compound administered in various inhalation aerosol formulations to an experimental animal. Such a technique should enable the effects of respiratory (e.g. tidal volume, inspiratory rate, expiratory time) and formulation variables (such as the particle size distribution, particulate shape) and the effects of hygroscopic growth to be investigated.

The fate of an inhalation aerosol depends on respiratory parameters and particulate characteristics. An aerosol particle may be deposited on the inspiratory or expiratory cycle or during a period of breath-holding (Gorman and Hall, 1973). Expiration of small particles is also a possibility. In the tracheobronchial region deposited drug will be subject to parallel competing mucociliary clearance (and subsequent swallowing) and absorption. The quantities cleared and absorbed will depend upon the relative rates of ciliary transport and absorption. Similarly drug particles deposited in the pulmonary region will be subject to systemic absorption and lymphatic clearance. For highly water soluble compounds however, it is anticipated that lymphatic clearance should be negligible (Hatch and Gross, 1964b).

Most of the work in the literature documents deposition of non-pharmaceutical aerosols in the lungs of humans and experimental animals respiring normally. Little work has been performed to delineate the deposition of pharmaceutical aerosol systems. Some work has been performed with the intention of investigating the effects of formulation (Sterling and Batten, 1969), methods of aerosol generation (Shenfield et al, 1974; Stauder and Hidingier, 1980) and modes of inhalation (Newhouse and Ruffin, 1978) upon pharmacological effects within the respiratory tract of drugs administered in inhalation aerosols. In the absence of precise dose-response relationships, however, it is impossible to learn a great deal about the available dose of such drugs in the respiratory tract.

Established pharmacokinetic techniques enable determination of systemic bioavailability and drug input functions (for example, Nyberg, 1977) given plasma concentration, C_p , versus time, t , profiles for compounds administered by any route. The only prerequisite is that the intrinsic pharmacokinetics (which reflect the behaviour of the compound once in the circulation) of the compound must be known in order to determine the amount absorbed versus time profile (Notari, 1980a). Bioavailability, which reflects both the amount absorbed and the speed of absorption, would be expected to change as a function of changes in drug deposition in the respiratory tract if a compound were administered by this route.

This chapter is devoted to the description and collection of a 'data base' which will enable the development of an in vivo model capable of estimating the bioavailability and input function of a marker compound administered in inhalation aerosols under standardised conditions to Beagle dogs. Subsequent to method development and evaluation, monodisperse aerosols may be administered via an endotracheal tube (eliminating the possibility of mouth deposition) to the respiratory tract. The bioavailability of the marker compound included in the aerosol formulation will be compared to the dose retained by the animal. This can be determined by measurement of the amount of inhaled aerosol and that exhaled and retained in the apparatus. It is hoped furthermore, that the speed of absorption will give some indication of the site of deposition (Schanker, 1978).

A marker compound was selected which had low toxicity, no pharmacological effect within the respiratory tract, insignificant metabolism and a chemical structure enabling the development of a highly sensitive assay procedure in biological fluids. Disodium fluorescein (I) fulfils all of these criteria. It has been used clinically in humans to determine circulation time (Lange and Boyd, 1942; Winsor et al, 1947; Neller and Schmidt, 1945). It has been reported to be excreted intact and as the glucuronide in urine and in bile in rats (Hanson, 1952; Webb et al, 1962). Fluorescence has been reported in the gall bladder of dogs after inhalation of Fluorescein (Calderwood et al, 1974).

Figure 6.1 illustrates the chemical structure of Fluorescein disodium (I) and Fluorescein⁼ (II).

In order to be able to determine drug input functions (amount absorbed versus time profiles) after aerosol administration, it is first necessary to establish the pharmacokinetics of the compound in the experimental animal to be used. Moreover, the compound must be shown to be absorbed via the lungs. The primary purpose of this chapter is to describe the results of an intravenous dose ranging study in a Beagle dog in order to delineate I's intrinsic pharmacokinetics. With a view to administering I in inhalation aerosols, intratracheal instillation of I in aqueous solution was used to show its absorption from the lungs. These experiments are described and discussed in the light of possible use of inhalation aerosols of I as a means of investigating the effects of formulation and respiratory variables upon the systemic availability of I in Beagle dogs.

6.2 EXPERIMENTAL

6.2.1 Determination of Fluorescein⁼ (II) in Plasma and Urine

Throughout this chapter concentrations and amounts are expressed in terms of the anhydrous fluorescein anion, Fluorescein⁼ (II) (see Figure 6.1). Calibration curves of relative fluorescent intensity (with reference to a standard of known concentration) versus concentration were constructed for concentrations of II ranging from 1 to 12 ng of II per ml in 10% v/v Beagle plasma, 1% v/v Beagle plasma and 0.01% v/v centrifuged (1000g for 15 minutes, Christ bench top centrifuge, type 0300) Beagle urine diluted in pH 12.0 Sorensens glycine buffer (Sorensen, 1909). Excitation and emission wavelengths of 486 and 516nm respectively were employed in an Aminco Bowman spectrofluorimeter (Type 4-8202, American Instrument Company Inc) using 10mm spectrophoto-fluorimeter cells (transmission matched) with lids (Type 6010, code colour green, Helma (England) Ltd). The standard reference solution contained a known concentration of II in the centre of the examined concentration range. Relative intensity, (RI), with reference to the standard solution was calculated according to the following equation

$$RI = \frac{Z}{Z_s} \quad \text{Equation 6.1.}$$

where Z_s is the % transmission of the standard solution and Z the % transmission of the test solution.

6.2.2 The Pharmacokinetics of Fluorescein⁼ (II)

This section describes the methods employed in the delineation of the intrinsic pharmacokinetics of II. It is possible when compounds have proven linear pharmacokinetics, to compute the amount of drug absorbed from an extravascular site, $[A]_{ex}^{\infty}$, using (Gibaldi and Perrier 1975a)

$$[A]_{ex}^{\infty} = \frac{[Do]_{iv} [AUC]_{ex}^{0 \rightarrow \infty}}{[AUC]_{iv}^{0 \rightarrow \infty}} \quad \text{Equation 6.2}$$

where the amount absorbed at time, $t = \infty$, can be calculated by reference to the total areas under the plasma concentration, C_p , versus time profiles for extravascular, $[AUC]_{ex}^{0 \rightarrow \infty}$, and iv bolus, $[AUC]_{iv}^{0 \rightarrow \infty}$, administrations. The term $[Do]_{iv}$ refers to the amount of drug administered as an intravenous bolus which provides an area, $[AUC]_{iv}^{0 \rightarrow \infty}$, under its C_p versus time profile.

When compounds display non-linear pharmacokinetics however, Equation 6.2 does not hold and more sophisticated procedures are necessary in order to compute the amount absorbed. It is essential therefore to establish II's pharmacokinetics prior to its administration by extravascular routes. This is normally performed by administering the compound in a range of doses as intravenous solution boli. For a compound to have linear pharmacokinetics $[AUC]_{iv}^{0 \rightarrow \infty}$ should be directly proportional to $[Do]_{iv}$ (Notari, 1980a). Under these circumstances, Equation 6.2 holds and enables the computation of the amount absorbed from extravascular sites.

6.2.2.1 Preparation of intravenous solutions for injection

The water content of the batch of disodium fluorescein (analytical grade, Koch Light) used in these in vivo experiments was determined as 21.6% w/w (ICI Pharmaceutical Division, Analytical Group, Mereside, Alderley Park). Aqueous solutions containing the desired dose of II were prepared in double distilled water and sterilised by positive pressure filtration through a 0.22 μ m pore size filter (Millipore (UK) Ltd) into a previously sterilised container. The concentration of the final solution was determined on the residual solution after sterile removal of the dose using the analytical technique documented in section 6.2.1 after appropriate dilution in pH 12 Sorensens glycine buffer.

6.2.2.2 Intravenous dose ranging study

Doses of fluorescein (II) ranging 0.43 to 123mg were administered as intravenous boli to a Beagle dog. The 12.6kg Beagle was anaesthetized using a Boyles' apparatus with O₂ at 500ml min⁻¹, N₂O at 2000ml min⁻¹ and halothane (Fluorothane, ICI Ltd) at concentrations ranging 1.5 to 4.0% of the inspired oxygen. The right or left saphenous vein was cannulated using a 35cm indwelling iv cannula (Intravenous cannula set, 17g needle, internal diameter 0.60mm, Pink luer fitting, Type 200/500/030, Portex Ltd). This cannula had a void volume of 0.15ml. The potency of the cannula was maintained during the course of each experiment by filling the cannula with a heparin (The Boots Company Ltd., Nottingham) solution of

5 I.U. per ml in 0.9% w/v sodium chloride solution for injection B.P. (Polyfusor, The Boots Company Ltd. Nottingham). The first 1ml of blood taken at each sample time was discarded.

In experiments involving urine collection the bladder was catheterized using a 2.0mm x 50cm dog catheter with a Luer fitting (A Cox (Surgical) Ltd.).

In most experiments the dog was allowed to regain consciousness and initial blood and urine sample taken before the dose was administered as an intravenous aqueous solution bolus via the intravenous cannula. After dose administration the cannula was rinsed with at least 10 void volume changes of heparinized saline. The luer fitting of the cannula was further rinsed externally with 10ml of heparinized saline. Three ml blood samples were taken at regular time intervals and mixed in previously heparinized containers (Brunswick, LH 10 tubes, Sherwood Medical Ltd). At the end of the experiment after centrifugation (1000g for 15 minutes in Christ Centrifuge, type 03400), the plasma was removed and assayed for fluorescein (section 6.2.1). Urine samples (the bladder was emptied at each sampling time) were stored on ice during the experiment and subsequently assayed for fluorescein⁼ after centrifugation (1000g for 15 minutes in Christ Centrifuge, type 03400). The product of urine concentration and volume enabled construction of cumulative urinary excretion of II versus time curves. Data for plasma concentration versus time was subjected to kinetic analysis as detailed in section 6.3.2.

6.2.3.3 Intratracheal administration

After catheterization and cannulation as previously described, halothane/ N_2O anaesthesia was deepened by increasing the inspired halothane concentration. A cuffed endotracheal tube (110mm, Magill cuff, BOC Medical Supplies Ltd) was introduced. Initial blood and urine samples were taken prior to administration of II. One ml of sterilized fluorescein aqueous solution containing intratracheal doses of II, $[Do]_{it}$, ranging 8.2 to 30.5mg, were instilled into the lungs of the 12.6kg Beagle used previously. Instillation was via a sterile polythene tube inserted into the endotracheal tube so that the end of the inner tube projected beyond the termination of the endotracheal tube. The polythene and endotracheal tube were removed and washed to estimate the amount of II not administered to the Beagle's respiratory tract. The animal was allowed to recover consciousness. Blood samples were taken at various time intervals (see section 6.3.3) and assayed for II as described in section 6.2.1.

6.3 RESULTS AND DISCUSSION

6.3.1 Quantitative determination of fluorescein⁺ (II) in plasma and urine

Calibration curves of relative intensity (Equation 6.1) versus concentration of II in all plasma and urine dilutions could not be distinguished from calibration curves obtained in the absence of plasma or urine (Figure 6.2) provided the instrument was first zeroed using the appropriate reference solution without fluorescein⁺. Thus for plasma concentrations $\leq 10\%$ v/v and urine concentrations $\leq 0.01\%$ v/v in buffer (pH 12), purification of body fluids to extract II was unnecessary in that interference with the assay for II, was proven to be negligible. Calibration curves for II of the type shown in Figure 6.2 were rectilinear for concentrations up to concentrations of 55ng per ml. The solid line shown in Figure 6.2 is the best fit by linear regression to the data for RI versus concentration of II in buffer alone. Repetitions of the experiment in buffer alone enabled $\geq 5\%$ errors to be ascribed to concentrations $\leq 1.75\text{ng}$ per ml of II. This limit was determined by the method of accuracy of coefficients of the line of regression (Topping, 1962) using data from an experiment performed in quintuplicate. More than 5% errors are incurred in concentrations determined for relative intensity ≤ 0.3 (Equation 6.1). Thus an accurate, sensitive assay procedure for II in the presence or absence of soluble biological 'contaminants' was successfully developed.

6.3.2 The Pharmacokinetics of Fluorescein⁻ (II)

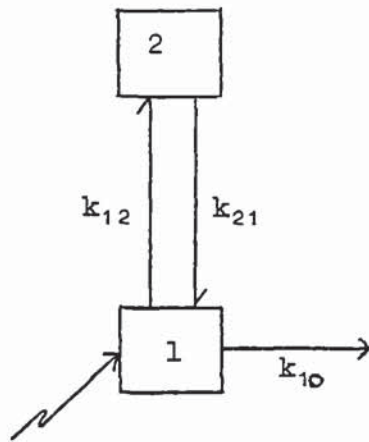
The results of the iv dose ranging study are presented as the discrete data points for plasma concentration, C_p , versus time in Figures 6.3 to 6.8. Each of the experiments provides apparently biexponential data where C_p at any time, t , appears to be described by an equation of the form

$$C_p = A e^{-\alpha t} + B e^{-\beta t} \quad \text{Equation 6.3}$$

where A , B , α and β are constants in discrete experiments. The area under the C_p versus time curve between time, $t = 5$ minutes and $t = 60$ minutes ($[AUC]_{iv}^{5 \rightarrow 60}$) was computed trapezoidally (Gibaldi and Perrier, 1975b) for each individual dose. The results are presented in Figure 6.9 and clearly show that for iv bolus doses greater than 11.4mg the pharmacokinetics may be approximated by a linear model. That is, $[AUC]_{iv}^{5 \rightarrow 60}$ is directly proportional to dose when $[Do]_{iv} \leq 11.4\text{mg}$.

6.3.2.1 Linear Pharmacokinetics

The simplest intravenous pharmacokinetic model which is capable of producing an analytical expression for plasma concentration as a function of time of the type shown by Equation 6.3 is illustrated by Scheme 6.1.



Scheme 6.1 Two compartment open body model

Drug is administered as a bolus to the sampled compartment (1) and simultaneously distributed to a peripheral compartment (2) and eliminated according to the apparent first-order rate constants k_{12} , k_{21} and k_{10} . Equation 6.3 can be rewritten according to Scheme 6.1 as (Gibaldi and Perrier, 1975c).

$$C_p = \frac{[Do]_{iv}}{V_1 (\alpha - \beta)} \left[(\alpha - k_{21}) e^{-\alpha t} + (k_{21} - \beta) e^{-\beta t} \right]$$

$\alpha > \beta$ Equation 6.4.

where $[Do]_{iv}$ is the iv dose and V_1 , the apparent volume of compartment 1. The apparent first order rate constants α and β are functions of k_{12} , k_{21} and k_{10} according to

$$\alpha = \frac{(k_{12} + k_{21} + k_{10}) + \sqrt{((k_{12} + k_{21} + k_{10})^2 - 4k_{10}k_{12})}}{2}$$

Equation 6.5

and

$$\beta = \frac{(k_{12} + k_{21} + k_{10}) - \sqrt{((k_{12} + k_{21} + k_{10})^2 - 4 k_{10} k_{12})}}{2}$$

Equation 6.6

The pharmacokinetics of II have been shown to be apparently linear when $[Do]_{iv} \leq 11.4\text{mg}$ by the direct proportionality between $[AUC]_{iv}^5 \rightarrow 60$ and dose in Figure 6.9. Under these circumstances Scheme 6.1 and Equation 6.4 describe the C_p versus time data. Values for the apparent rate constants k_{12} , k_{21} and k_{10} (Scheme 6.1) should therefore be fluorescein⁼ dependent constants, as should α , β (Equations 6.5 and 6.6) and V_1 . Rearranging Equation 6.4 by dividing both sides by $[Do]_{iv}$ should enable normalised data to be expressed as $C_p/[Do]_{iv}$ versus time when $[Do]_{iv} \leq 11.4\text{mg}$ and the pharmacokinetics of II are linear. Thus

$$\frac{C_p}{[Do]_{iv}} = \frac{1}{V_1 (\alpha - \beta)} \left[(\alpha - k_{21}) e^{-\alpha t} + (k_{21} - \beta) e^{-\beta t} \right]$$

Equation 6.7

Accordingly plasma concentrations determined by fluorescence after iv administration of II of doses less than or equal to 11.4mg were divided by dose in each case and thereby normalised. The results of this procedure are shown in Figure 6.10. This data was subjected to least mean squares non-linear regression analysis (Metzlar, 1969) based on Equation 6.7.

The computer was allowed to float values for k_{12} , k_{21} , k_{10} and V_1 in order to provide their 'best estimates' based upon minimised least mean square deviations of the theoretical curve from the experimentally determined values for $C_p/[Do]_{iv}$ versus time. The solid curve in Figure 6.10 shows the best fit determined by this procedure. The best estimates and standard deviations of the rate constants k_{12} , k_{21} , k_{10} (Scheme 6.1) and the apparent volume of the sampled compartment, V_1 , are documented in Table 6.1.

The total area under the plasma concentration versus time profiles, $[AUC]_{iv}^0 \rightarrow \infty$, for $[Do]_{iv} \leq 11.4\text{mg}$ were calculated trapezoidally (Gibaldi and Perrier 1975b) from the raw data of C_p versus time for each administered dose. In order to perform this calculation it was necessary to ascribe values to C_p at $t = 0$ and $[AUC]_{iv}^x \rightarrow \infty$, for each of the doses (where $t = x$ was the final sampling time in each case). These values were computed according to

$$C_p \text{ at } t=0 = Do \frac{(\alpha - k_{21})}{V_1 (\alpha - \beta)} + \frac{Do (k_{21} - \beta)}{V_1 (\alpha - \beta)} \quad \text{Equation 6.8}$$

and

$$[AUC]_{iv}^x \rightarrow \infty = \frac{C_p \text{ at } t=x}{\beta} \quad \text{Equation 6.9}$$

Values for α , β were calculated according to Equations 6.5 and 6.6. Values for the rate constants and V_1 were assigned according to their best estimates when $[Do]_{iv} \leq 11.4\text{mg}$ (Table 6.1). Equation 6.8 can be derived by taking Equation 6.4 to its limit at $t = 0$. The derivation of Equation 6.9 is shown below.

If Equation 6.4 is taken to its limit as $t \rightarrow \infty$ then because $\alpha > \beta$, the apparently monoexponential decay of C_p versus time (see Figure 6.10) is described by

$$C_p \rightarrow \frac{D_0 (k_{21} - \beta)}{V_1 (\alpha - \beta)} e^{-\beta t} \quad \text{Equation 6.10}$$

Integration of Equation 6.10 between $t = x$ and $t = \infty$ with respect to time and observing that

$$\frac{D_0 (k_{21} - \beta)}{V_1 (\alpha - \beta)} = B \quad (\text{compare Equations 6.3 and 6.4})$$

gives

$$\begin{aligned} [AUC]_{iv}^{x \rightarrow \infty} &= \int_{t=x}^{\infty} C_p dt \\ &= B \int_{t=x}^{\infty} e^{-\beta t} dt \\ &= B \left[\frac{e^{-\beta \infty}}{-\beta} - \frac{e^{-\beta (t=x)}}{-\beta} \right] \\ &= \frac{B e^{-\beta (t=x)}}{\beta} \\ &= \frac{C_p t=x}{\beta} \quad \text{Equation 6.11} \end{aligned}$$

Thus Equation 6.9 can be used to compute the terminal area of the iv plasma concentration versus time profile provided that the data at $t = x$ is apparently monoexponential. Given $C_{p,t=0}$ (Equation 6.8), the remaining area can be computed trapezoidally and $[AUC]_{iv}^{0 \rightarrow \infty}$ determined by summation.

Figure 6.11 shows a plot of $[AUC]_{iv}^{0 \rightarrow \infty}$ versus dose for $[D_0]_{iv} \leq 11.4\text{mg}$. Figure 6.11 may be adequately described by the rectilinear relationship

$$[AUC]_{iv}^{0 \rightarrow \infty} = 6.0 \text{ (ml}^{-1}\text{min)} \cdot [Do]_{iv} \text{ (}\mu\text{g)} + 0.24 \text{ (}\mu\text{g ml}^{-1}\text{min)}$$

$$[AUC]_{iv}^{0 \rightarrow \infty} \leq 70 \mu\text{g ml}^{-1}\text{min} \quad \text{Equation 6.12.}$$

Thus, provided $[AUC]_{iv}^{0 \rightarrow \infty} \leq 70 \mu\text{g ml}^{-1}\text{min}$, the iv pharmacokinetics of II in this Beagle dog were apparently linear.

The maximum plasma concentration attained with $[Do]_{iv} = 11.4\text{mg}$, that is $C_{p_{t=0}}$ computed according to Equation 6.8 was $7.5 \mu\text{g}$ of II per ml of plasma. A plasma concentration, $C_p = 7.5 \mu\text{g ml}^{-1}$ was therefore chosen as a threshold concentration beneath which linear pharmacokinetics were assumed.

Given this definition of linear pharmacokinetics then under circumstances when doses of II are administered extravascularly, provided C_p at any time t after administration $\leq 7.5 \mu\text{g per ml}$, then the amount absorbed can be determined from Equation 6.2.

6.3.2.2 Non-Linear Pharmacokinetics

It is clear from Figure 6.9 that no single Scheme 6.1 with first order rate constants is capable of describing the intrinsic pharmacokinetics of II at all iv doses. If it were, then $[AUC]_{iv}^{0 \rightarrow \infty}$ would be a rectilinear function of intravenous dose over the whole range of doses studied (Notari, 1980a). At doses $> 11.4\text{mg}$ however the $[AUC]_{iv}^{5 \rightarrow 60}$ versus $[Do]_{iv}$ data in Figure 6.9 shows a clear deviation from the linear kinetics observed when $[Do]_{iv} \leq 11.4\text{mg}$ (Figure 6.11). Such a non-proportionality is typical of a compound with saturable elimination kinetics (Notari, 1980b). A more complex model must therefore be postulated in order to describe the apparent dose-dependent kinetics of II when $[Do]_{iv} > 11.4\text{mg}$.

Figure 6.12 shows the cumulative amount of II eliminated in the urine as a function of time after an iv bolus of 18mg (see also Figure 6.7 for the corresponding plasma concentration versus time profile). Estimated values for the renal clearance of II, Cl_r , were calculated from (Gibaldi and Perrier, 1975d)

$$Cl_r = \frac{U(x \rightarrow y)}{[AUC]_{iv}^{x \rightarrow y}} \quad \text{Equation 6.13}$$

where $\bar{U}(x \rightarrow y)$ is the total amount of II excreted in the urine during the time interval $t = x$ to $t = y$ and $[AUC]_{iv}^{x \rightarrow y}$ is the area under the plasma concentration versus time profile during the same interval. The estimated values for Cl_r at various time intervals after $[Do]_{iv} = 18\text{mg}$ are presented in Table 6.2. Renal clearance in all cases was greater than literature values for glomerular filtration rate in 10 to 25kg mongrel dogs ($30 \pm 2\text{ml min}^{-1}$) and tend to Rosenblatt's reported values for renal blood flow of $176 \pm 32\text{ml}^{-1}$. The renal clearance variations presented in Table 6.2 are probably due to difficulties encountered in complete withdrawal of urine at a given time after administration. Clearance values greater than glomerular filtration rate may be taken as evidence for active tubular secretion (Notari, 1980a). This observation is directly supported by Figure 6.13 which shows the effect of halothane anaesthesia upon plasma concentration versus time profiles for II. This figure shows data collected from a conscious dog (1 occasion) and the same animal maintained under halothane anaesthesia (mean of 2 experiments) after an iv bolus of II = 0.43mg. Anaesthesia is known to reduce renal blood flow significantly (Bonvalet et al. 1977), and would be expected to produce a greater change in the elimination kinetics of an

actively secreted compound than would be the case when a compound was eliminated only by simple filtration. These observations in the Beagle would indicate that elimination of II in the urine is primarily by active tubular secretion. The remaining fraction of II to be eliminated could be by metabolism and biliary secretion (Webb et al, 1962). Fluorescence has been observed in the gall bladder of Beagle dogs after administration of aerosols of I (Calderwood et al, 1974). Biliary secretion of II in rats was reported to be via a non-specific anion carrier mechanism (Hanson, 1952) probably similar to the non-specific mechanism involved in its active tubular secretion in the kidney (Mudge and Weiner, 1963).

An appropriate model to describe the dose dependent kinetics of II when $[Do]_{iv} > 11.4\text{mg}$ must therefore show at least one capacity-limited elimination process from the central compartment. In Scheme 6.1 the elimination process is represented by the apparent first order constant, k_{10} . If this process is saturable then Equation 6.4 will only hold when $[Do]_{iv} \leq 11.4\text{mg}$ and C_p at any time $t \leq 7.5\mu\text{g ml}^{-1}$ (Section 6.3.2.1). Irrespective of dose, the rate of change of the amount of drug in the central sampled compartment (1) must be given by

$$\frac{dX_1}{dt} = \text{rate in} - \text{rate out} \quad \text{Equation 6.14.}$$

Provided the distribution process to the peripheral compartment is apparently first order (Scheme 6.1; k_{12} and k_{21}) then the rate out due to distribution must be given by the products $k_{21} X_2$ and $k_{12} X_1$ respectively (where X_1 and X_2 are the amounts of II in the sampled (1) and peripheral compartment (2)).

The elimination process, which also contributes to the rate of output from the central compartment should be described by a term at least as complex as the Michaelis-Menten term, $V_m X_1 / (K_m + X_1)$ where V_m is the maximum rate of elimination and K_m , the amount of drug in the central compartment at which the rate of elimination equals $V_m/2$ (Gibaldi and Perrier, 1975e). In enzyme kinetics X_1 and K_m would more conventionally be written as concentrations. This assumes for simplicity, that the elimination process of II is only by a single saturable route. If this is assumed then Equation 6.14 can be rewritten as

$$\frac{d X_1}{dt} = -k_{12} X_1 + k_{21} X_2 - \frac{V_m X_1}{(K_m + X_1)} \quad \text{Equation 6.15}$$

Although Equation 6.15 can be integrated with respect to time, the resultant equation cannot be solved explicitly for X_1 at any time t (cf Equation 6.4). However, at low doses (producing low values for X_1), where $K_m \gg X_1$, the Michaelis-Menten term simplifies to $V_m X_1 / K_m$. Under these circumstances V_m / K_m provides an apparent first order rate constant, k_{10} such that the final term in Equation 6.15 could be rewritten as $k_{10} X_1$. If the pharmacokinetics of II are correctly described by Equation 6.15, the estimates for k_{10} found in section 6.3.2.1 would more correctly be termed estimates for V_m / K_m (see Table 6.1 for $[Do]_{iv} \leq 11.4\text{mg}$). At very high doses when X_1 is much larger than K_m , the Michaelis-Menten term will tend to V_m , an apparent zero-order constant, k_0 , such that Equation 6.14 will become

$$\frac{d X_1}{dt} = -k_{12} X_1 + k_{21} X_2 - k_0 \quad \text{Equation 6.16}$$

$$X_1 \gg K_m.$$

In this limiting case, after an initial distributive phase, the fall in plasma concentration should be rectilinear with respect to time until the plasma concentration falls below a saturation value. The plasma concentration versus time profile after a 123mg iv bolus (Figure 6.14) however, provides no evidence that elimination from the sampled compartment ever tends to complete saturation. Moreover, all intravenous experiments described in this chapter provide C_p versus time profiles which apparently conform to Equation 6.4. In the absence of complete saturation it is difficult to estimate $k_0 = V_m$ (Equations 6.15 and 6.16).

Although further intravenous studies may enable II's kinetics to be completely delineated at all doses, this was felt to be beyond the scope of this Chapter whose primary purpose was to describe the development of an experimental system capable of providing information on the systemic availability of a compound administered in various inhalation aerosols.

Because all iv experiments described in this Chapter provided data consistent with Equation 6.4, it proved possible to ascribe an apparent value of k_{10} (Scheme 6.1), a first order elimination rate constant for II at $123 \gg [Do]_{iv} > 11.4\text{mg}$. At $[Do]_{iv} > 11.4\text{mg}$ the pharmacokinetics of II however, have been proven to be non-linear. Thus, although the data for each individual iv experiment is apparently described by Equation 6.4, the elimination constant, k_{10} , should be a dose-dependent apparent first order rate constant when $[Do]_{iv} > 11.4\text{mg}$. Under these circumstances if the first order distribution rate constants k_{12} and k_{21} (Scheme 6.1) are held constant at their

best estimates for $[Do]_{iv} \leq 11.4\text{mg}$ (Table 6.1) then the apparent values for k_{10} would be expected to all with increasing $[Do]_{iv} > 11.4\text{mg}$. An equation describing the rate of change of X_1 with respect to time is given by $d X_1 / dt = \text{rate in} - \text{rate out}$ as

$$\frac{d X_1}{dt} = k_{21} X_2 - k_{12} X_1 - k_{10} X_1 \quad \text{Equation 6.17}$$

Dividing both sides of Equation 6.17 by the volume of the central compartment, V_1 , and observing that $C_p = X_1 / V_1$ gives

$$\frac{d C_p}{dt} = k_{21} \frac{X_2}{V_1} - k_{12} C_p - k_{10} C_p \quad \text{Equation 6.18}$$

An analog computer programme was designed to generate C_p versus time profiles according to Equation 6.18 (Appendix 4). Data for C_p versus time profiles of II at $[Do]_{iv} > 11.4\text{mg}$ were plotted on a linear basis. Values for k_{12} , k_{21} , and V_1 were held constant at their mean values as documented in Table 6.1 for $[Do]_{iv} \geq 11.4\text{mg}$. The programme described in Appendix 4 was established on an EAI 180 analog computer connected to a Bryans 26000 X Y recorder. The circuitry enabled the generation and recording of C_p versus time curves according to Equation 6.18. Values for k_{10} were varied in order to produce curves of C_p versus time profiles to provide good fits of the data obtained from individual iv experiments for $[Do]_{iv} > 11.4\text{mg}$. Thus distribution and the apparent volume of the sampled compartment were assumed to be dose independent. A comparison of Equation 6.17 and 6.15 reveals (if Scheme 6.1 is assumed to hold at all doses) that as $[Do]_{iv}$ is increased the apparent values of k_{10} (Equation 6.17) should decrease as the rate of elimination ($V_m X_1 / (K_m + X_1)$, Equation 6.15) increases non-linearly with increasing X_1 .

The 'best' fits obtained as presented as the solid profiles of C_p versus time in Figures 6.6 to 6.8. Table 6.3 documents the values of k_1 as a function of $[Do]_{iv}$ and clearly displays the decreasing values of this apparent first-order constant with increasing iv dose .

6.3.2.3 Intratracheal Instillation

In order for II to be a suitable model compound for studying the systemic availability of aerosols, this compound must be shown to be absorbed from the respiratory tract. Aqueous solutions of II were therefore introduced into the respiratory tract. Ensuing plasma concentration versus time profiles were determined. These profiles are shown in Figure 6.15 to 6.18. The maximum plasma concentrations of II (1.1 to $3.3 \mu\text{g ml}^{-1}$) following these administrations were always substantially less than $7.5 \mu\text{g ml}^{-1}$. The pharmacokinetics of II after its administration were therefore assumed linear according to Equation 6.7 with the variables k_{12} , k_{21} , k_{10} and V_1 as documented in Table 6.1. Equation 6.2 was used therefore to determine the amount absorbed after intratracheal administration from the area under the plasma concentration versus time profile following intratracheal administration of II, $[AUC]_{it}^0 \rightarrow \infty$. The bioavailable fraction, Bf, of the administered it dose, $[Do]_{it}$, was then determined from

$$Bf = \frac{[AUC]_{it}^0}{[Do]_{it}} \quad \text{Equation 6.19}$$

Log-linear plots of plasma concentration versus time following intratracheal administration provide apparently monoexponential data when $t \gg 200\text{mins}$.

A typical example is shown as Figure 6.19 for $[Do]_{it} = 28.2\text{mg}$. From plasma concentration versus time profiles following iv administrations for $[Do]_{iv} \leq 11.4\text{mg}$, β was determined to be $0.039 \pm 0.11 \text{ min}^{-1}$, giving a half life ($t_{0.5}$) of $17.9 \pm 4.9 \text{ min}$. The values for the terminal log-linear slopes estimated from least mean square regression of the apparently monoexponential portion of the data (Table 6.4) following intratracheal instillation are $< \beta$ and fall outside this range. Byron and Notari (1976) have observed that the terminal slopes of log-linear plots of plasma concentration versus time after extravascular administration, S^1 , will only tend to β estimated after iv administration if the input from the depot is some three times faster than output from the whole body. Similarly, S^1 will only approach k_a , a first order absorption rate constant for drug input, if $S^1/\beta < 0.5$. The results obtained following intratracheal administration reveal that S^1 (Figure 6.19) should provide an estimate for first-order absorption rate constants following i.t. administration if it is valid to assume that input from the depot is first order. There is some tentative evidence therefore that values for S^1 (Table 6.4) are in fact estimates for input rate constants after i.t. administration. If this is the case then input is possibly rate determining. Such rate determination would be expected to become more and more apparent if fluorescein was administered in formulations with properties likely to delay its release prior to absorption. Under these circumstances, when II is administered in aerosol form, and absorption is slow, the bioavailability of II may be expected to fall due

to parallel mucociliary clearance to the gastrointestinal tract (Byron, 1980).

It was necessary to calculate the values of S^1 (see Figure 6.19) for all of the intratracheal instillations performed in order to be able to calculate the terminal areas under the C_p versus time profiles following each dose. In a similar fashion to that described in the derivation of Equation 6.9 the area under the curve of the terminal mono-exponential portion of data can be determined from

$$[AUC]_{it}^{x \rightarrow \infty} = \frac{C_p_{t=x}}{S^1} \quad \text{Equation 6.20}$$

Bioavailable fractions were therefore calculated in a step-wise fashion $[AUC]_{it}$ following i.t administration up to and including the last sampling time were calculated trapezoidally. The final portion (from the last sampling time to time ∞) was estimated from Equation 6.20 using the appropriate value of S^1 from Table 6.4 and $C_p_{t=x}$ from figures 6.15 to 6.18. The calculated bioavailable fractions for the various values of $[Do]_{it}$ are presented in Table 6.5. These results indicate that II is well absorbed from the respiratory tract.

It is unlikely that administration of aerosols of I would results in plasma concentration versus time profiles which are described by non-linear pharmacokinetics. This can be illustrated by considering the likely deposited dose from an administered monodisperse aerosol of I. Cuddihy et al (1974) have shown that the particle size for optimum pulmonary deposition in Beagle dogs would have an aerodynamic diameter of 2 to $3\mu\text{m}$. However, the expected aerodynamic growth ratio of dry particles to equilibrium droplets, assuming complete

hygroscopic growth in the respiratory tract, is 2.77. It would thus be expected that approximately 30% of a monodisperse aerosol of 1 μ m dry particles of I would deposit in the pulmonary region. Assuming an aerosol concentration, N^1 , of 1×10^6 particles per ml, the mass of I per ml of inspired air will be

$$\frac{4}{3} \pi r^3 \cdot \rho \cdot N^1 = 0.0008 \text{mg per ml.}$$

The reported tidal volume in resting Beagles is 204 ± 2 ml and the respiratory rate 23 ± 2 respirations per minute (Park et al, 1970). Thus the expected deposited dose, assuming 30% deposition, would be approximately 1mg per minute. Without extended administration times, it is thus unlikely that aerosols of I would result in plasma concentration versus time profiles which are described by non-linear pharmacokinetics .

Thus II is a suitable model compound for studying the systemic availability of aerosols. It should therefore be possible to investigate differences in systemic availability of different particle sizes of fluorescein aerosols under constant physiological conditions. Control of physiological parameters such as tidal volume, respiratory rate and breathing pattern (for example, the breath holding manouvre) may be achieved by the use of intermittent positive breathing apparatus. Thus the effect of physiological parameters on the systemic availability of fluorescein aerosols could be investigated.

The data presented in this chapter forms a base enabling the determination of systemic availability of II subsequent to its administration in various inhalation aerosol formulations. A sensitive assay for fluorescein⁻ (II) in Beagle plasma and urine was developed enabling estimation of concentrations of II $\geq 20\text{ng ml}^{-1}$ with $< 5\%$ error. The intrinsic pharmacokinetics of II at iv. doses ranging 0.43 to 123mg are documented. The results presented clearly indicate that the intrinsic pharmacokinetics of II cannot be described by linear pharmacokinetics at all values of C_p . However, for $C_p \leq 7.5\text{ng per ml}$ the data may be adequately described by a two-compartment open body model. It is suggested that non-linear pharmacokinetics occur at higher i.v. doses due to the presence of saturable elimination routes. Nevertheless, when II is administered as an extravascular depot provided $C_p \leq 7.5\text{ng per ml}$, the existence of non-linear pharmacokinetics can be excluded and the area under the plasma concentration versus time profiles may be used as an indicator of available dose. Intratracheal doses of II $\leq 30.5\text{mg}$ produced maximum plasma concentrations $\leq 3.3\text{ng per ml}$.

In order for II to be used as a model system for systemic availability of aerosols, it was necessary to estimate the magnitude of II's absorption from the respiratory tract. There was an indication that the absorption of II from aqueous intratracheal instillation may be rate determining relative to its elimination from the body.

Good systemic availability ($B_f > 0.90$) has been shown for intratracheal instillations of 8.2mg to 30.5mg of II in aqueous solution. It is unlikely that inhalation aerosol administration of II will result in a need to delineate its more complex non-linear kinetics at high doses. Fluorescein would thus appear to be a suitable model compound for investigating the systemic availability of drugs administered in inhalation aerosols. It is envisaged that following administration of characterised monodisperse aerosols of II the amount available systemically may be determined from the ensuing plasma concentration versus time profile. By comparison of the amount of inhaled aerosol and that exhaled and retained in the apparatus the bioavailable fraction of the dose retained in the respiratory tract can be estimated. This can be investigated as a function of formulation variables and variation in the methods and modes of administration.

6.5

TablesTable Captions

Table 6.1 Best estimates for the fitted parameters k_{12} , k_{21} , k_{10} and V_1 from non-linear least means square regression analysis after i.v. administration of II for $[Do]_{iv} \leq 11.4\text{mg}$.

Table 6.2 Estimates for renal clearance of an 18mg i.v. bolus of II according to Equation 6.13.

Table 6.3 k_{10} values estimated by analog computation of C_p versus time profiles according to Equation 6.18 for $[Do]_{iv} \geq 11.4\text{mg}$.

Table 6.4 Terminal slope, S^1 , values following intratracheal administration, estimated by least mean square regression of the apparently monoexponential portions of the plasma concentration versus time profiles.

Table 6.5 Bioavailable fraction of II after intratracheal administration of an aqueous bolus, determined using Equation 6.19.

Table 6.1 Best estimates for the fitted parameters k_{12} , k_{21} , k_{10} and V_1 from non-linear least mean square regression analysis after iv administration of II for $[Do]_{iv} \leq 11.4\text{mg}$

Parameter	Estimate	Standard Deviation
k_{12}	0.064 min ⁻¹	0.023 min ⁻¹
k_{21}	0.075 min ⁻¹	0.028 min ⁻¹
k_{10}	0.108 min ⁻¹	0.016 min ⁻¹
V_1	1.62 l.	0.26 l.

Correlation coefficient = 0.990 (n = 30)

Table 6.2 Estimates for renal clearance of an 18mg iv bolus of II according to Equation 6.13.

Time interval (mins)		Cl_r (ml min ⁻¹)
t = x	t = y	
6	11	60
11	16	109
16	22.5	132
22.5	54	160
54	80	200
80	102	152
102	140	152

Table 6.3 k_{10} values estimated by analog computation of C_p versus time profiles according to Equation 6.18 for $[Do]_{iv} \gg 11.4\text{mg}$.

Dose (mg)	k_{10} (min^{-1})
123	0.030
33.6	0.055
18	0.070
13.95	0.090
13.6	0.098
11.4	0.107

Table 6.4 Terminal slope, S^1 , values following intra-tracheal administration, estimated by least mean square regression of the apparently monoexponential portions of the plasma concentration versus time profiles.

β , for $[Do]_{iv} \gg 11.4\text{mg} = 0.0387 \pm 0.0105 \text{ min}^{-1}$

Administered dose (mg)	S^1 (min^{-1})	S^1/β
8.2	0.0090	0.23
19.0	0.0151	0.39
28.2	0.0059	0.15
30.5	0.0093	0.24

Table 6.5 Bioavailable fraction of II after intratracheal administration of an aqueous bolus, determined using Equation 619..

Administered dose (mg)	Bioavailable fraction
8.2	1.05
19.0	1.01
28.2	0.90
30.5	1.15

Figure Captions

Figure 6.1 The chemical structure of Fluorescein disodium (I) and Fluorescein⁻ (II).

Figure 6.2 Relative Intensity (Equation 6.1) versus concentration for Fluorescein⁻ (II) in plasma and urine. Fluorescein in buffer (pH 12) (●); Fluorescein⁻ with 10% v/v plasma in buffer (○) Fluorescein⁻ with 1% v/v plasma in buffer (▲); Fluorescein⁻ with 0.001% v/v urine in buffer (Δ). The solid line is the best fit by linear regression to the data for relative intensity versus concentration of II in buffer alone.

Figure 6.3 Plasma concentration versus time profiles for II after iv administration as solution boli. $[Do]_{iv}$ was 0.43mg (○) and 3.4mg (x). The curves are the 'best fits' according to non-linear least mean square (lms) regression analysis based on Equation 6.7 (section 6.3.2.1).

Figure 6.4 Plasma concentration versus time profile of II after iv administration as solution boli, $[Do]_{iv}$ was 8.2mg (●) and 10.8mg (⊙). The curves are the 'best fits' according to non-linear lms regression analysis based on Equation 6.7 (section 6.3.2.1).

Figure 6.5 Plasma concentration versus time profile of II after iv administration as solution bolus. $[Do]_{iv}$ was 11.4mg. The curve is the 'best fit' according to non-linear lms regression

analysis based on Equation 6.7 (section 6.3.2.1)

Figure 6.6 Plasma concentration versus time profiles for II after iv administration as solution boli. $[Do]_{iv}$ was 13.6mg (\bullet); 13.95mg (1st experiment) (\times) and 13.95 (2nd experiment) (\circ). The curves are the 'best fits' obtained using an analog computer programme according to Scheme 6.1 (section 6.3.2.1)

Figure 6.7 Plasma concentration versus time profiles for II after iv administration as solution boli. $[Do]_{iv}$ was 18.0mg (\bullet) and 33.0mg (\circ). The curves are the best fit obtained using an analog computer programme according to Scheme 6.1 (section 6.3.2.1).

Figure 6.8 Plasma concentration versus time profiles for II after iv administration as solution bolus. $[Do]_{iv}$ was 123mg (\bullet). The curve is the best fit obtained using an analog computer programme according to Scheme 6.1 (section 6.3.2.1).

Figure 6.9 Area under iv plasma concentration $[AUC]_{iv}^5 \rightarrow 60$ versus time profiles ($t = 5$ to $t = 60$) versus dose, $[Do]_{iv}$.

Figure 6.10 Plasma concentration divided by dose ($C_p/[Do]_{iv}$) versus time for $[Do]_{iv} \leq 11.4\text{mg}$ (data from Figure 6.3 to 6.5) The curve is the 'best fit' according to non-linear lms regression analysis based on Equation 6.7.

Figure 6.11 Total area $[AUC]_{iv}^0 \rightarrow \infty$ under plasma concentration versus time profile as a function of iv dose $[Do]_{iv}$ when $[Do]_{iv} \leq 11.4\text{mg}$.

Figure 6.12 Cumulative amount of II excreted in urine after 18mg iv bolus.

Figure 6.13 Plasma concentration time profile after 0.43mg iv bolus to anaesthetised and conscious dog. Anaesthesia maintained throughout the experiment (o), dose administered to the conscious dog (●).

Figure 6.14 Plasma concentration of II (linear scale) versus time profile after administration of 123mg iv bolus. Experimentally determined concentrations (●), the curve is the 'best fit' obtained using an analog computer programme to model Scheme 6.1.

Figure 6.15 Plasma concentration versus time profile for II after $[Do]_{it} = 8.6\text{mg}$ intratracheal instillation. The curve illustrated shows the trapezoidal approximation used to calculate the area under the curve.

Figure 6.16 Plasma concentration versus time profile for II after $[Do]_{it} = 19.0\text{mg}$ intratracheal instillation. The curve illustrated shows the trapezoidal approximation used to determine the area under the curve.

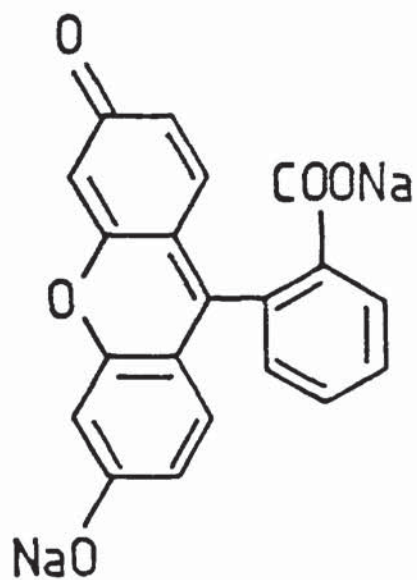
Figure 6.17 Plasma concentration versus time profile for II after $[Do]_{it} = 28.2\text{mg}$ intratracheal instillation. The curve illustrated shows the trapezoidal approximation used to determine the area under the curve.

Figure 6.18 Plasma concentration versus time profile for II after $[Do]_{it} = 30.5\text{mg}$ intratracheal instillation. The curve illustrated shows the trapezoidal approximation used to determine the area under the curve.

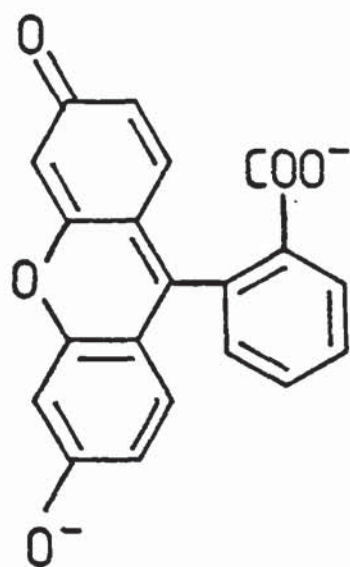
Figure 6.19 Log-linear plot of plasma concentration versus time for II after intratracheal instillation of an aqueous bolus of 28.2mg. The terminal slope, S^t , determined by linear regression is illustrated by the solid line.

Figure 6.1 The chemical structure of Fluorescein disodium

(I) and Fluorescein⁻ (II)



I



II

Figure 6.2 Relative Intensity (Equation 6.1) versus concentration for fluorescein⁼ (II) in plasma and urine. Fluorescein in buffer (pH 12) (●), fluorescein⁼ with 10% v/v plasma in buffer (○), fluorescein⁼ with 1% v/v plasma in buffer (▲), fluorescein⁼ with 0.01% v/v urine buffer (△). The solid line is the best fit by linear regression to the data for relative intensity versus concentration of II in buffer alone.

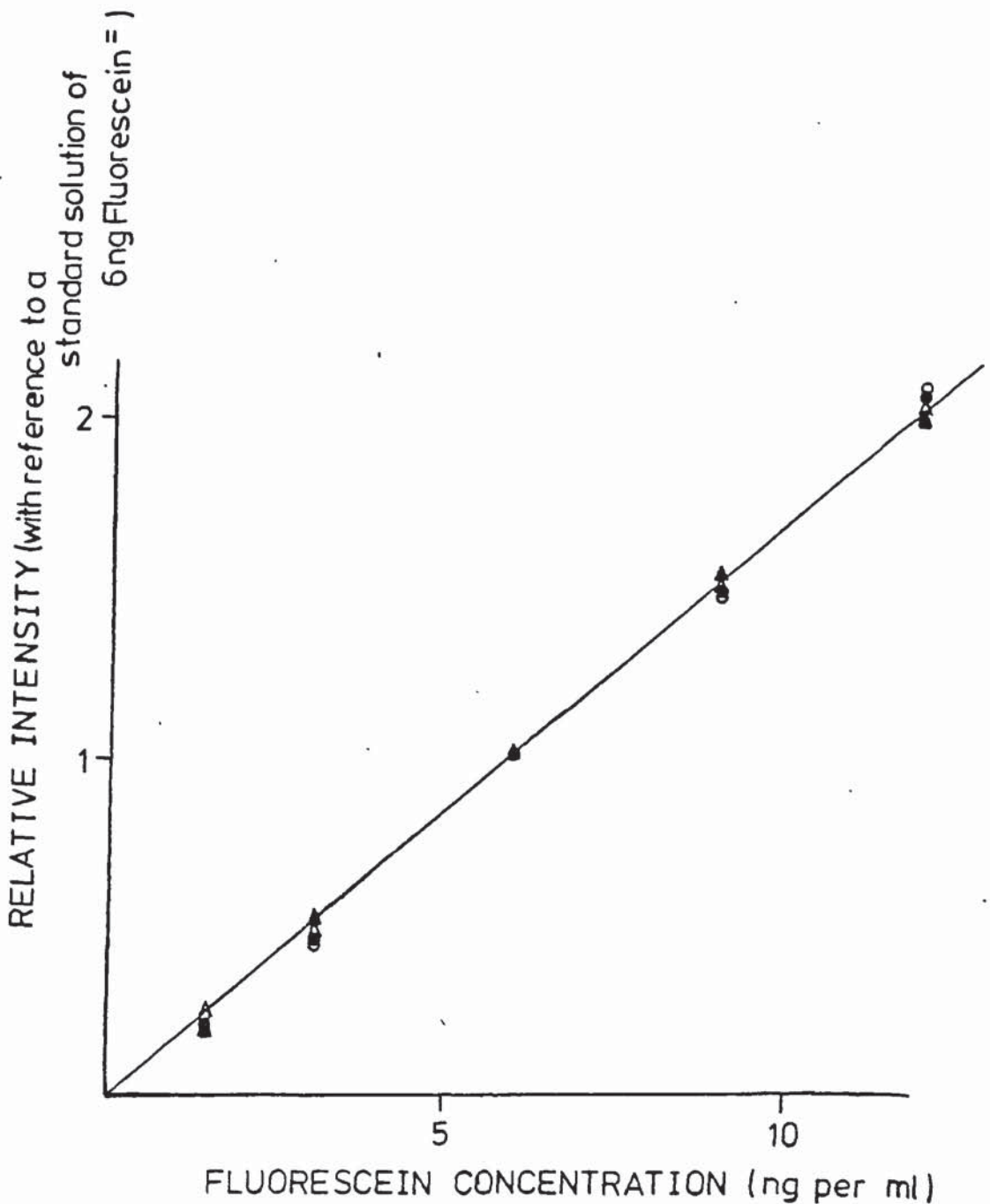


Figure 6.3 Plasma concentration versus time profiles for II after iv administration as solution boli $[Do]_{iv}$ was 0.43mg (o) and 3.4mg (x). The curves are the 'best fit' according to non-linear least mean square (lms) regression analysis based on Equation 6.7 (Section 6.3.2.1).

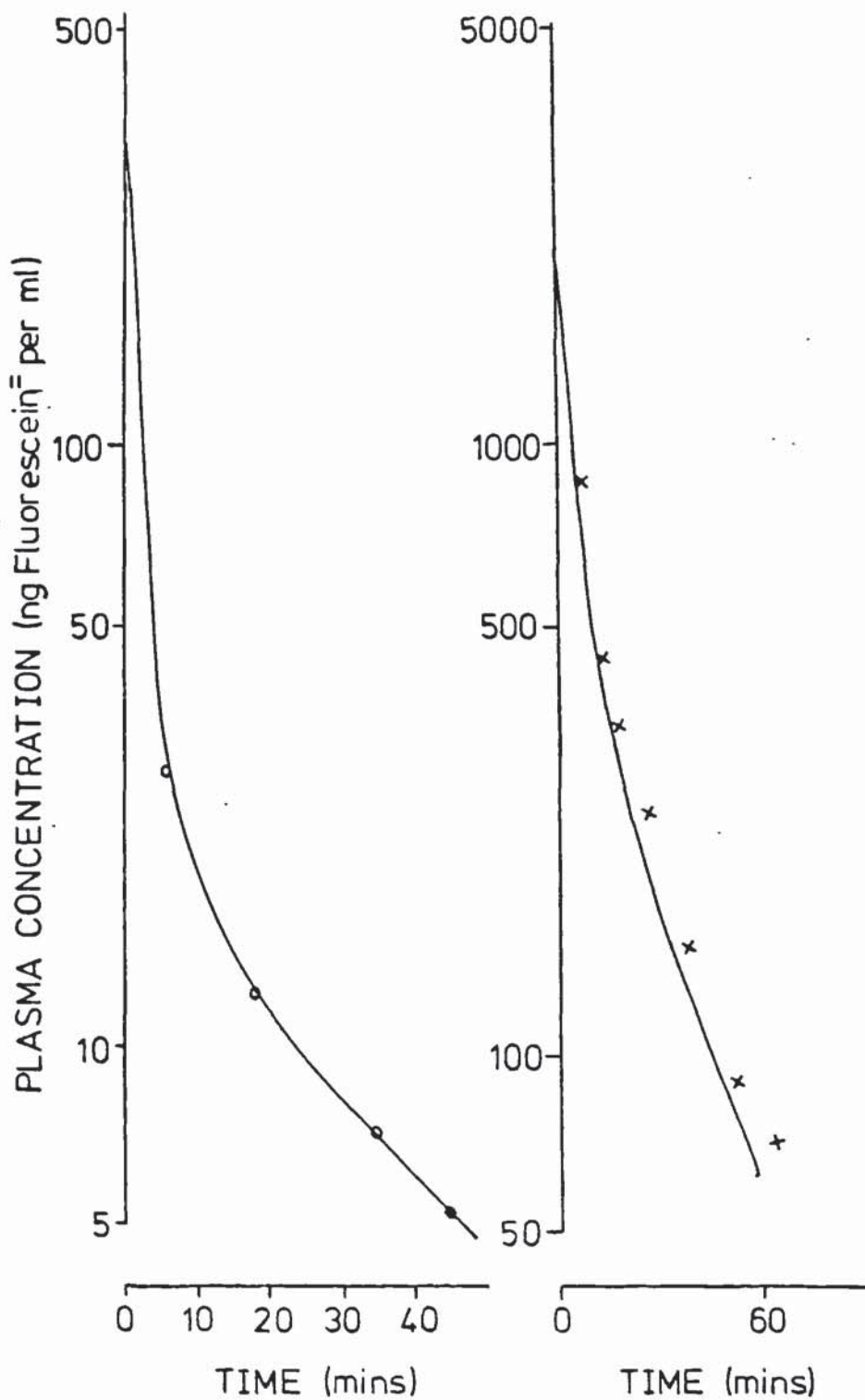


Figure 6.4 Plasma concentration versus time profiles for II after iv administration as solution boli. $[Do]_{iv}$ was 8.2mg (●) and 10.8mg (○). The curves are the 'best fits' according to non-linear lms regression analysis based on Equation 6.7 (section 6.3.2.1).

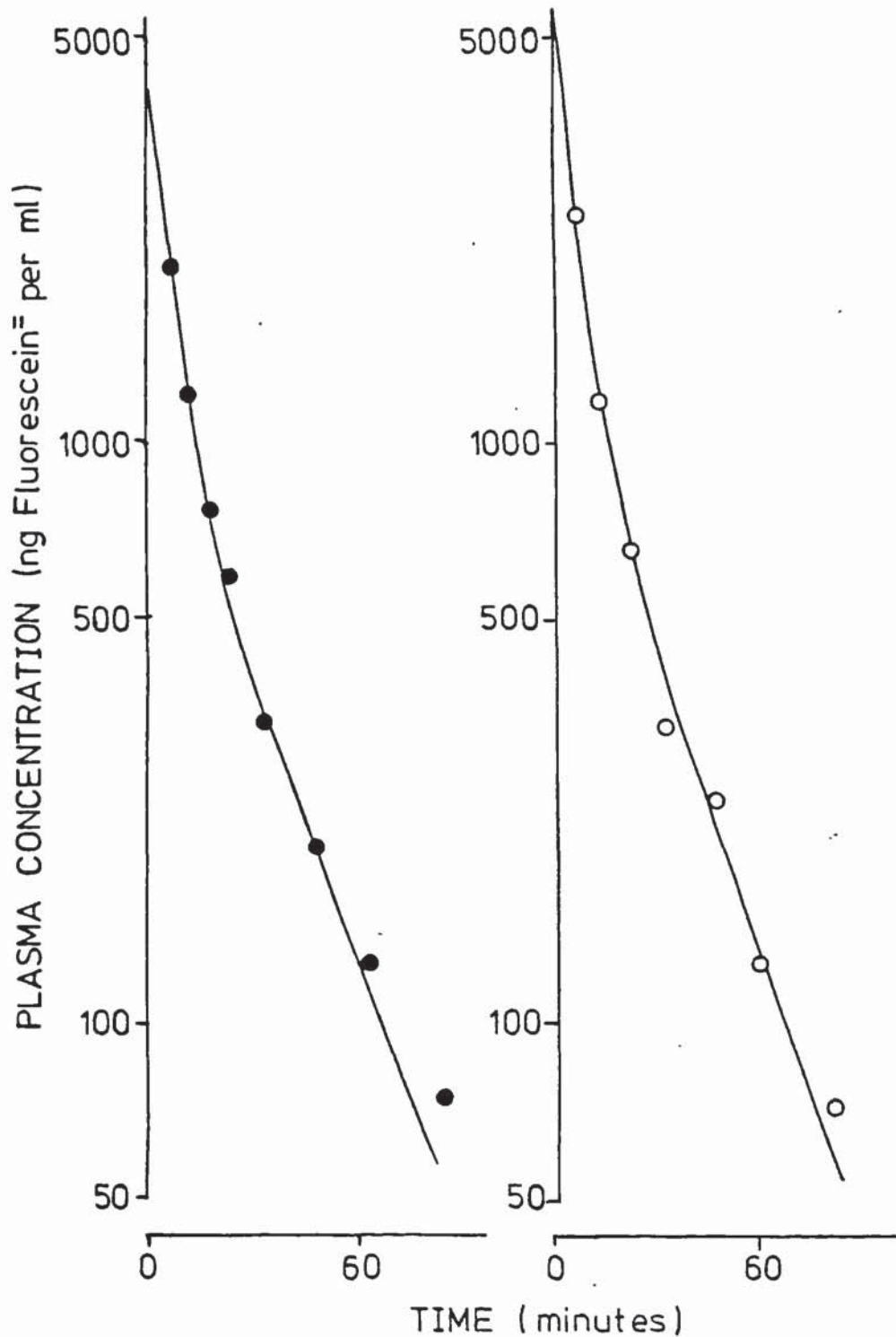


Figure 6.5 Plasma concentration versus time profile for II after iv administration as solution bolus. $[Do]_{iv}$ was 11.4mg (x). The curve is the 'best fit' according to non-linear lms regression analysis based on Equation 6.7 (section 6.3.2.1).

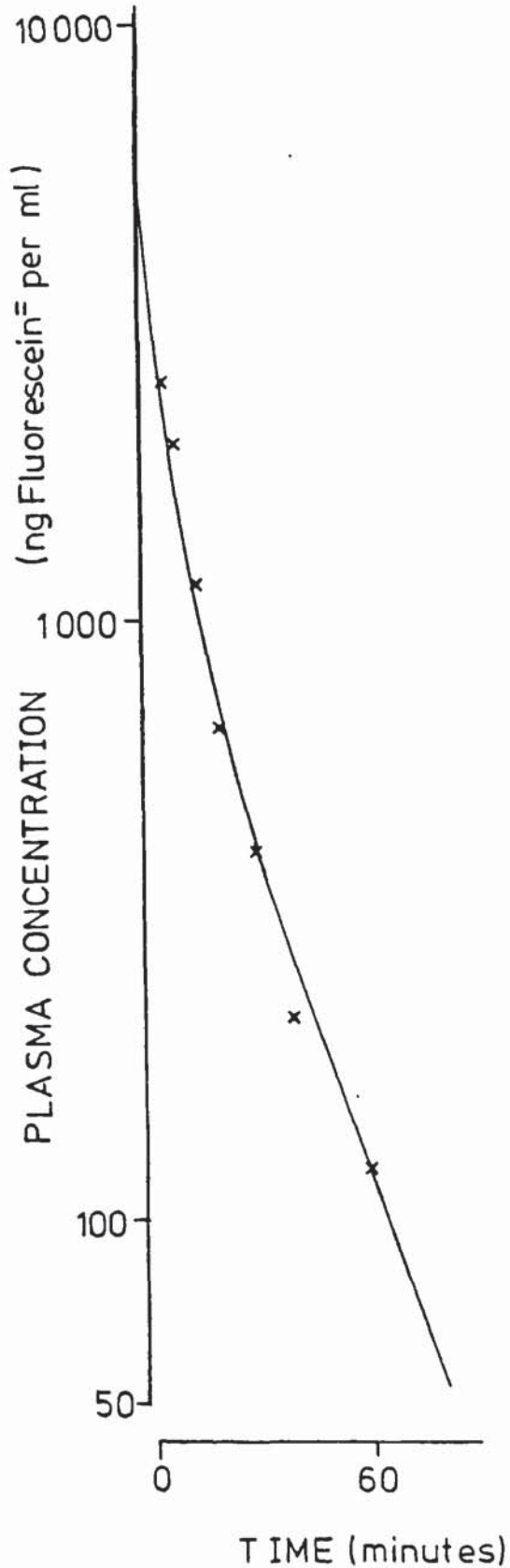


Figure 6.6 Plasma concentration versus time profiles for II after iv administration as solution bolus. $[Do]_{iv}$ was 13.6mg (●), 13.95mg (1st experiment (x) and 13.95mg iv bolus, 2nd experiment (○). The curves are the best fits obtained using an analog computer programme according to Scheme 6.1 (section 6.3.2.1).

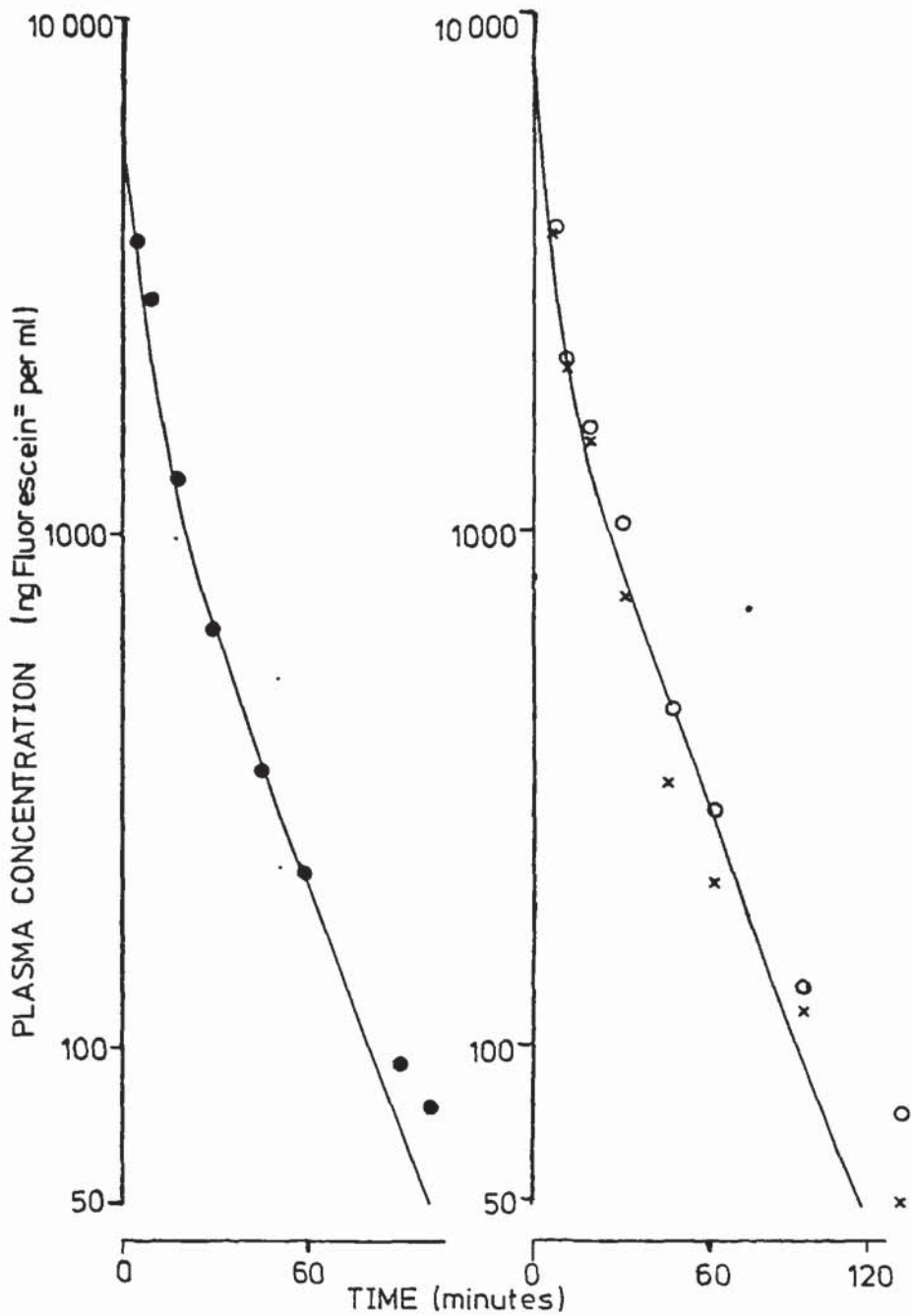


Figure 6.7 Plasma concentration versus time profile for II after iv administration as solution boli. $[Do]_{iv}$ was 18.0mg (●) and 33.0mg (○). The curves are the best fit obtained using an analog computer programme according to Scheme 6.1 (section 6.3.2.1).

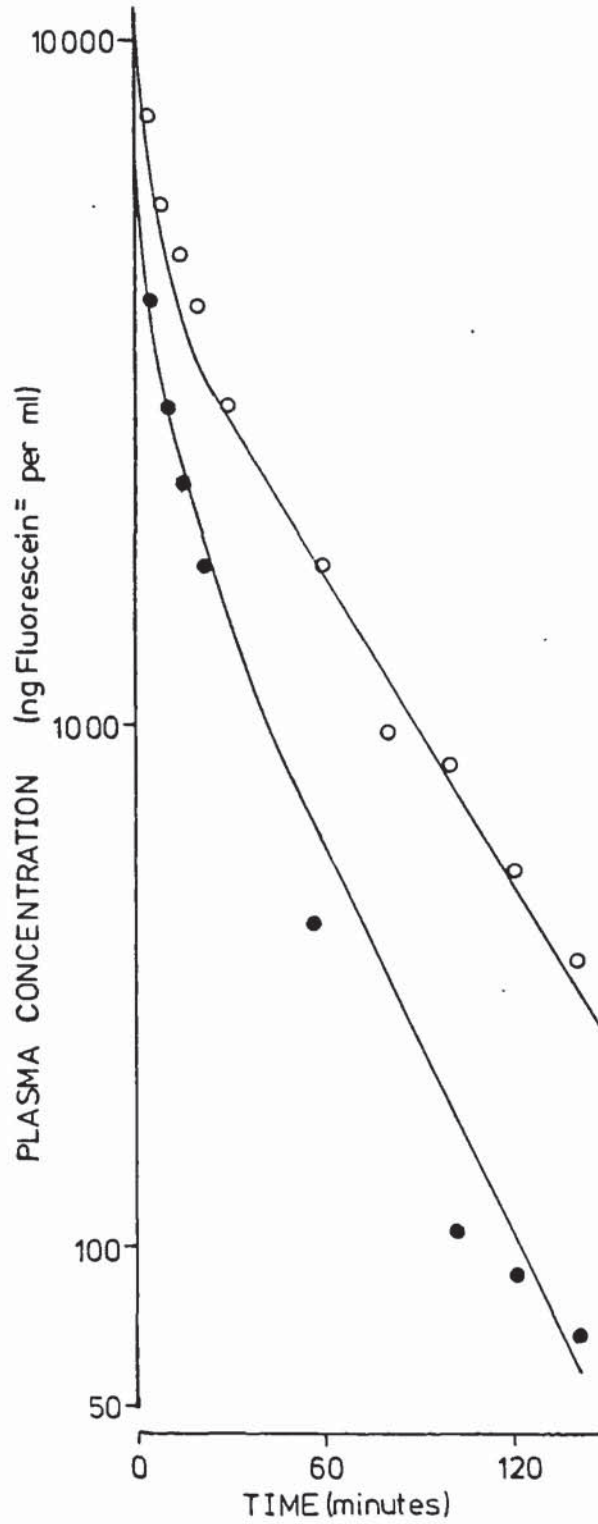


Figure 6.8 Plasma concentration versus time profiles for II after iv administration as solution bolus $[Do]_{iv}$ was 123mg (●). The curve is the best fit obtained using an analog computer programme according to Scheme 6.1 (section 6.3.2.1).

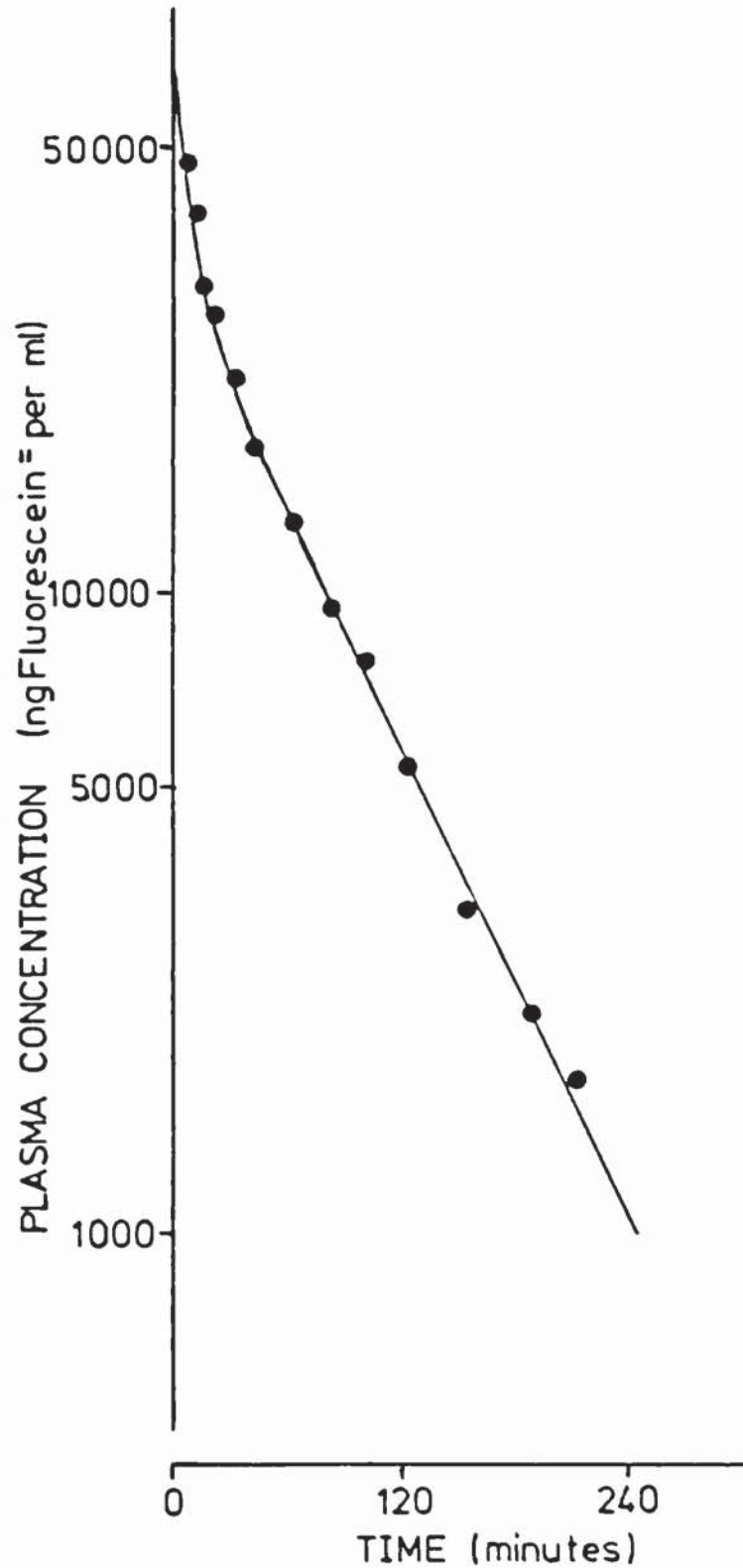


Figure 6.9 Area under iv plasma concentration $[AUC]_{iv}^{5 \rightarrow 60}$ versus time profiles ($t = 5$ to $t = 60$) versus dose $[Do]_{iv}$

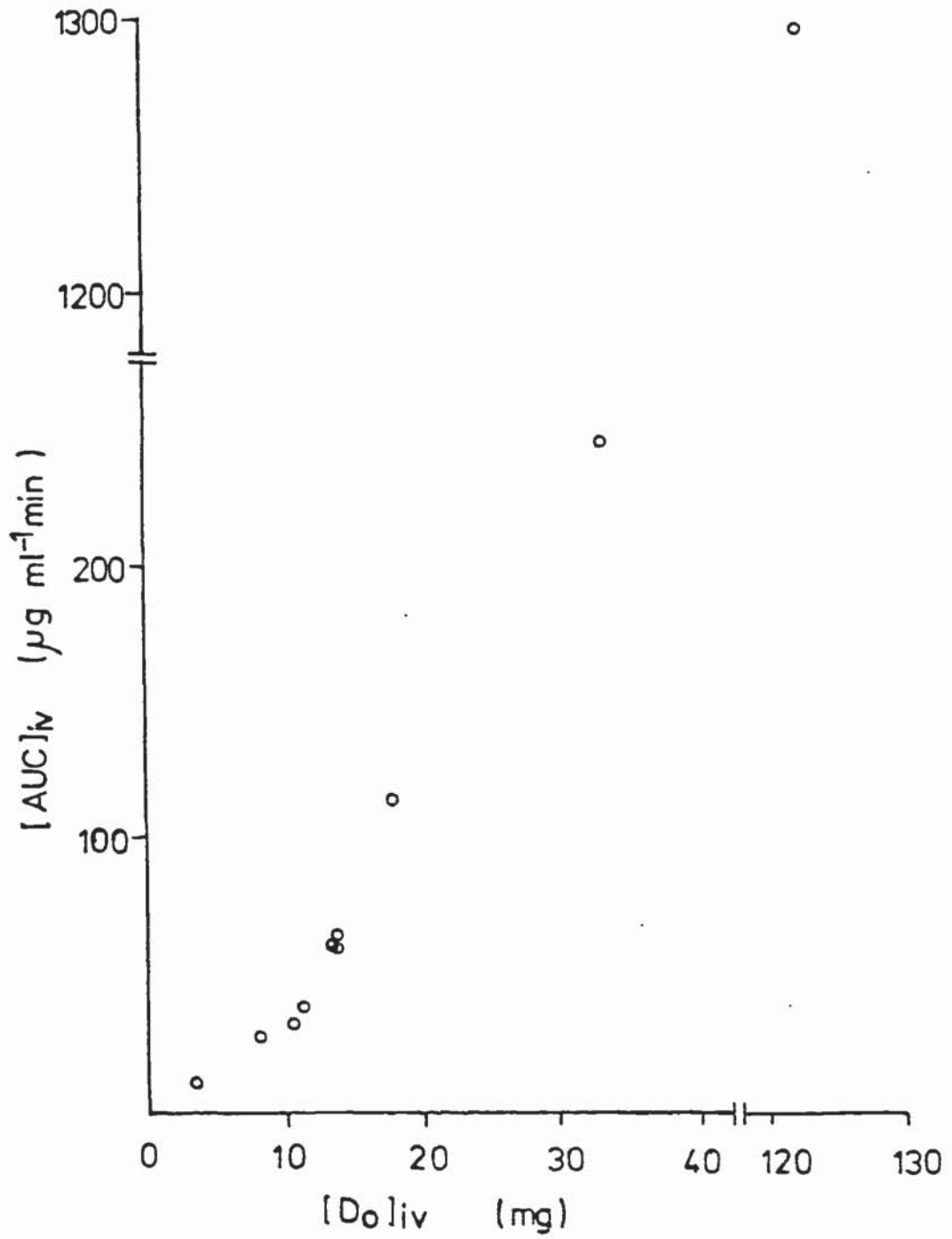


Figure 6.10 Plasma concentration divided by dose ($C_p/[Do]_{iv}$) versus time for $[Do]_{iv} \leq 11.4\text{mg}$ (data from Figure 6.3 to 6.5). The curve is the 'best fit' according to non-linear least mean square regression analysis based on Equation 6.7.

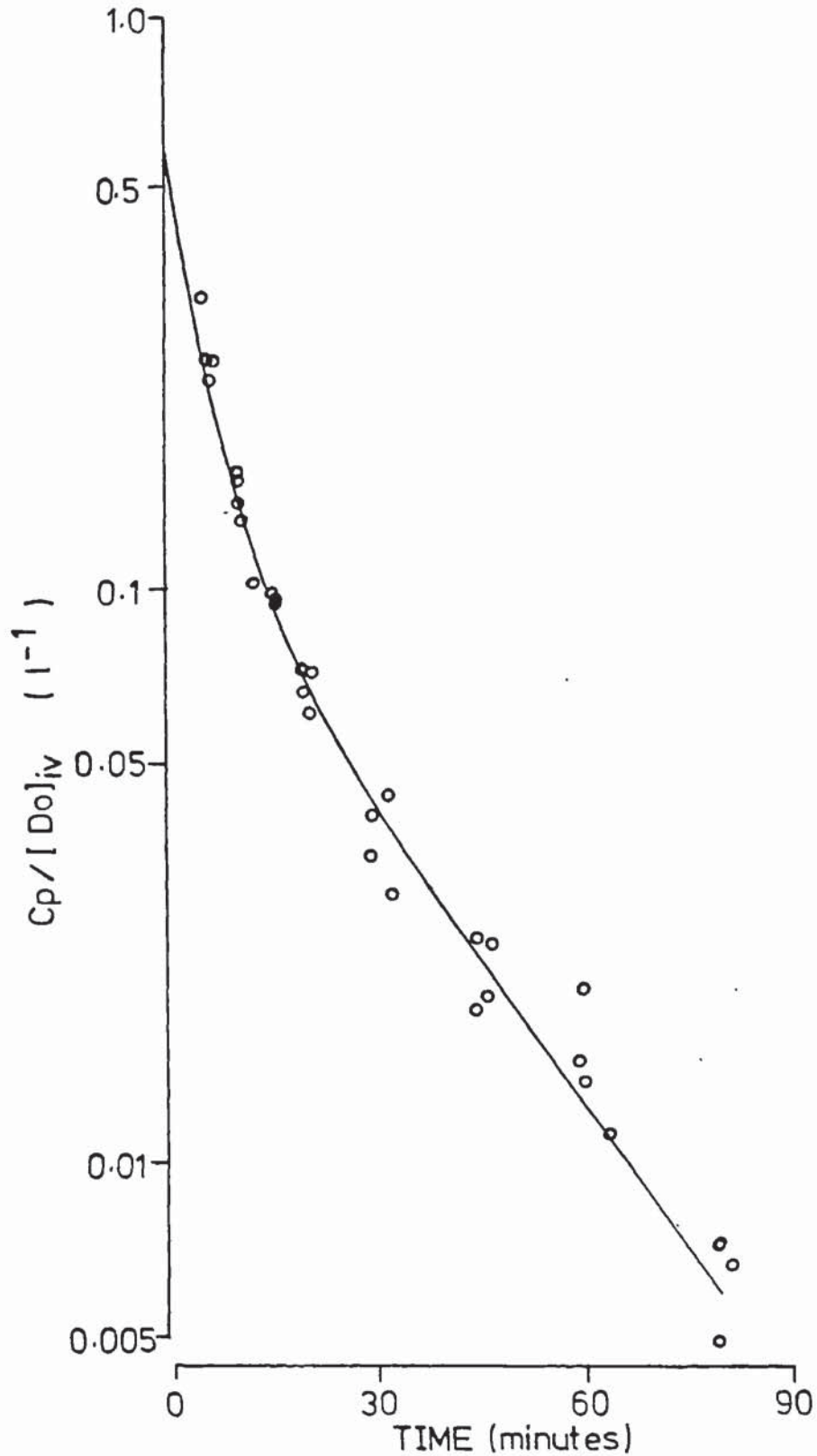


Figure 6.11 Total area, $[AUC]_{iv}^{0 \rightarrow \infty}$ under plasma concentration versus time profiles as a function of iv dose, $[Do]_{iv}$ when $[Do]_{iv} \leq 11.4\text{mg}$.

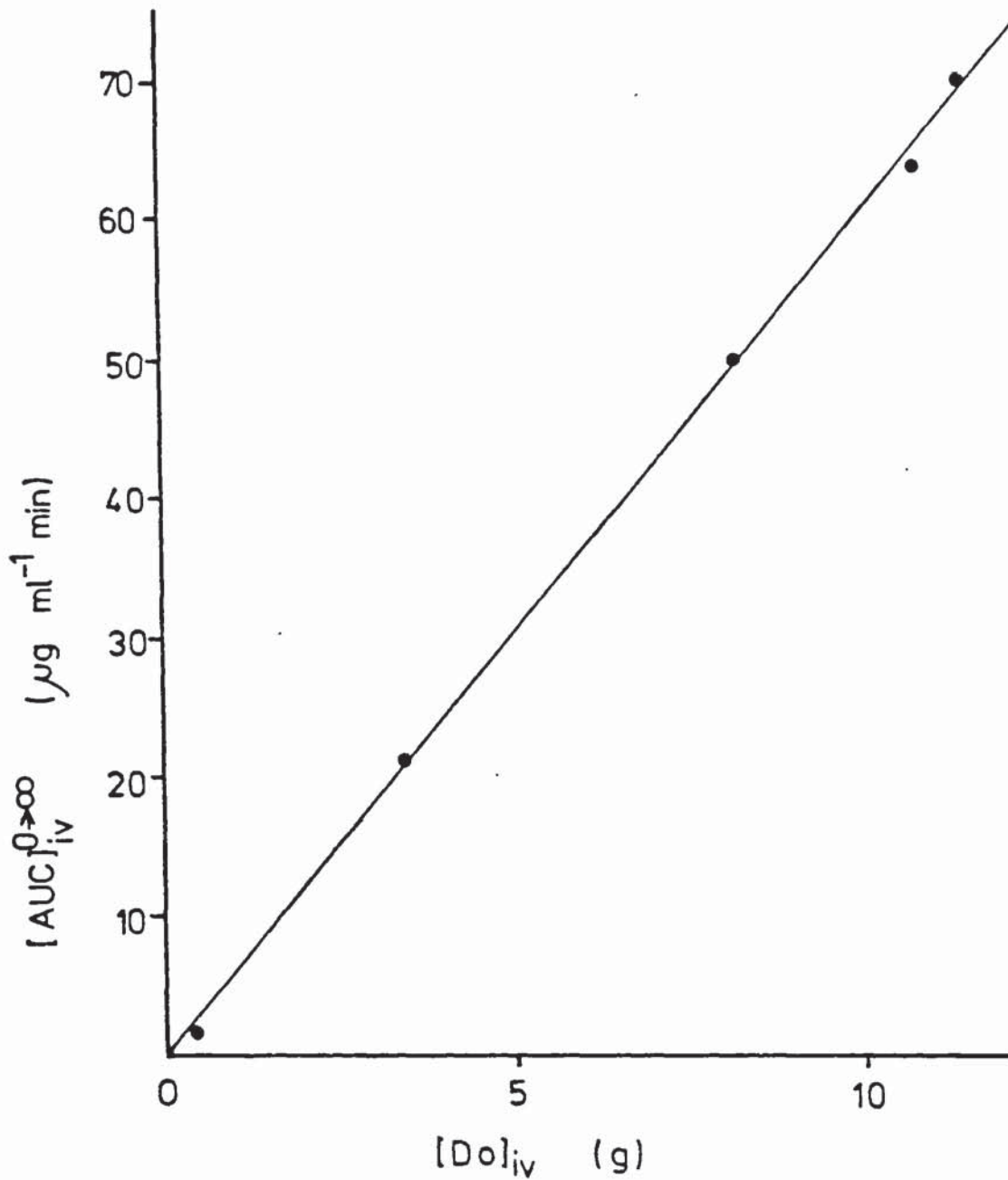


Figure 6.12 Cumulative amount of II excreted in urine after 18mg iv bolus.

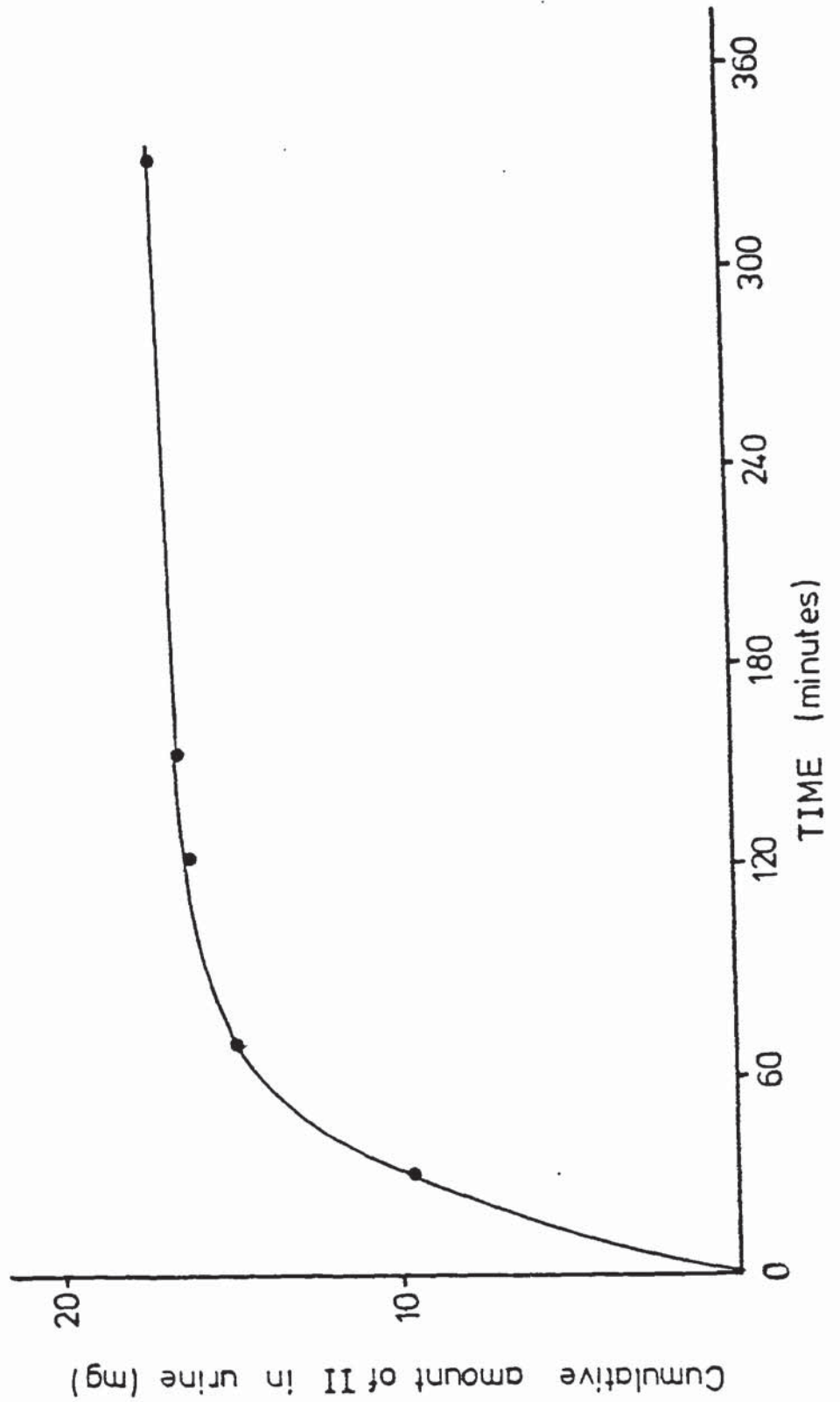


Figure 6.13 Plasma concentration time profile after 0.43mg iv bolus to anaesthetised and conscious dog, o anaesthesia maintained throughout the experiment, ● dose administered to the conscious dog.

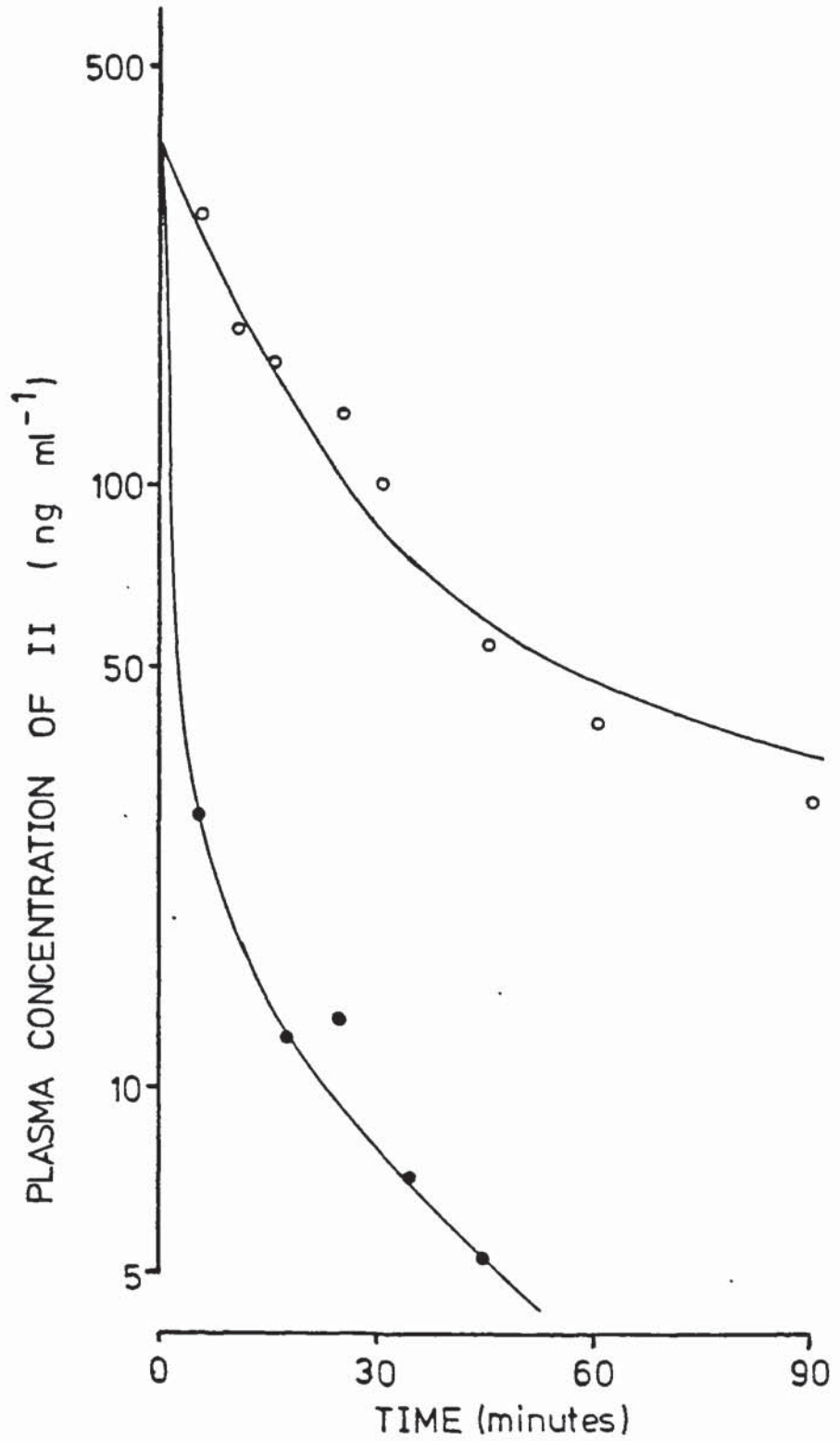


Figure 6.14 Plasma concentration of II (linear scale) versus time profile after administration of 123mg iv bolus. experimentally determined concentrations, the curve is the best fit obtained using an analog computer programme to model Scheme 6.1.

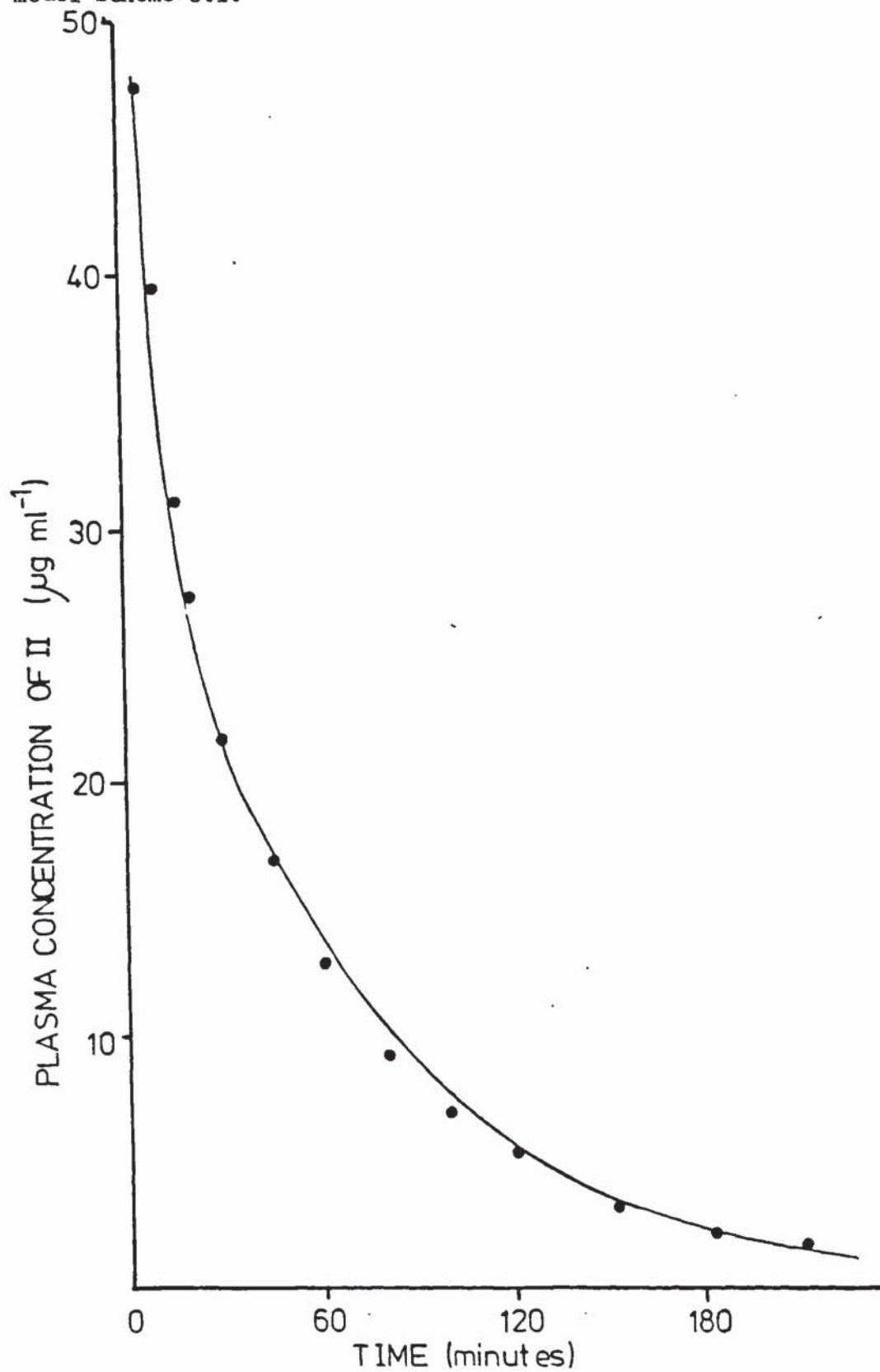


Figure 6.15 Plasma concentration versus time profile for II
[Do]_{it} = 8.6mg intratracheal instillation. The curve illustrated shows the trapezoidal approximation used to calculate the area under the curve.

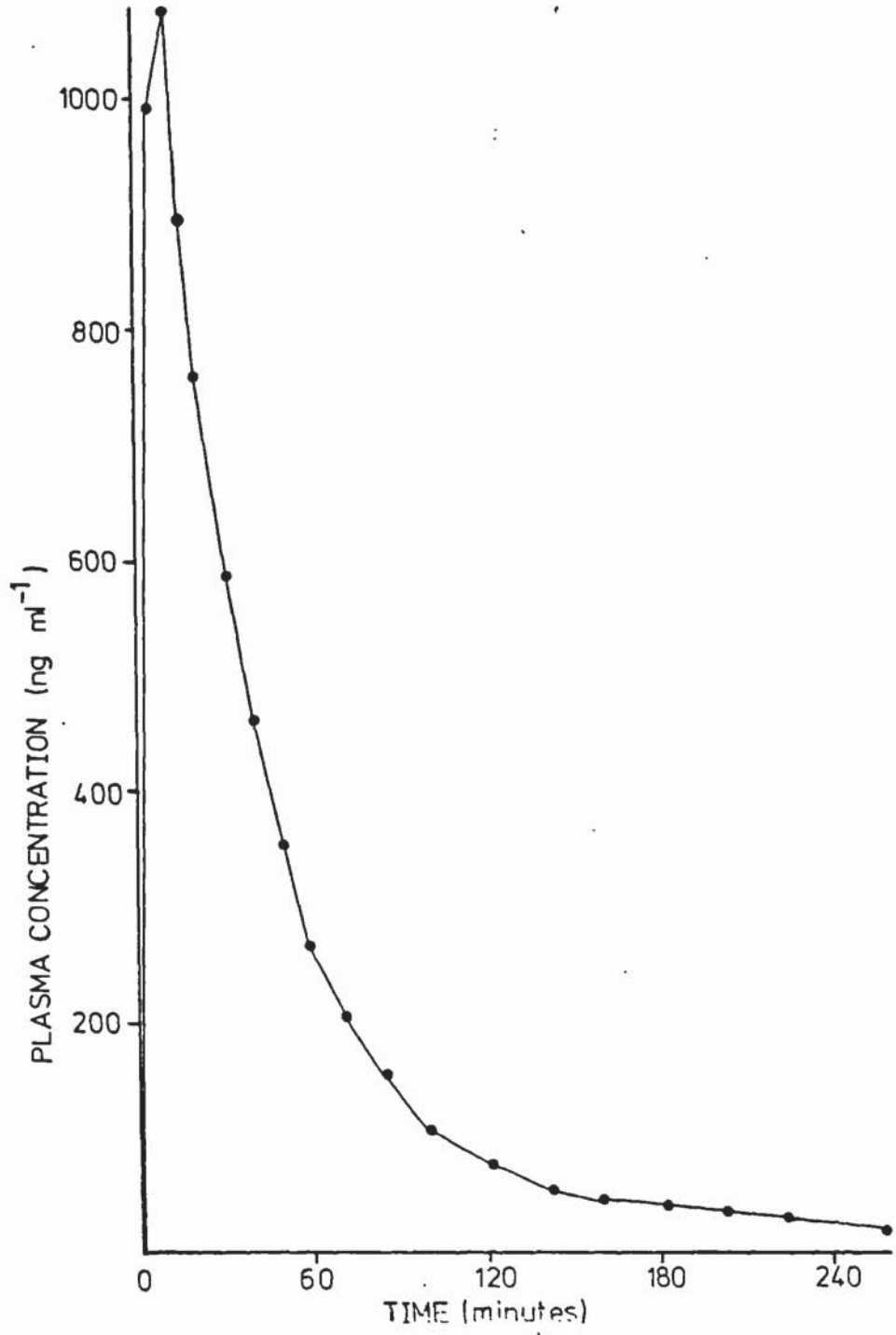


Figure 6.16 Plasma concentration-versus time profile for II after $[Do]_{it} = 19.0\text{mg}$ intratracheal instillation. The curve illustrated shows the trapezoidal approximations used to determine the area under the curve.

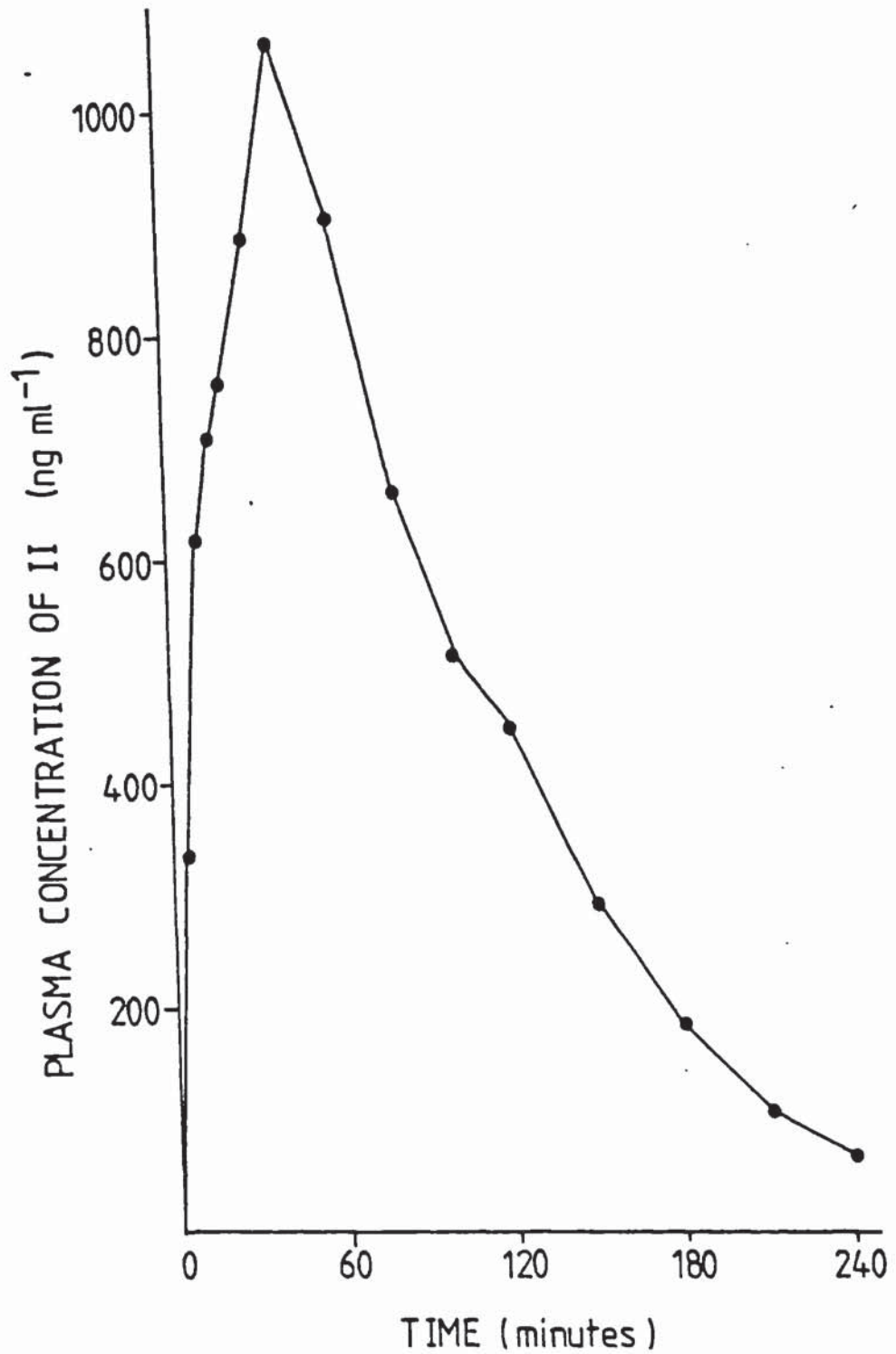


Figure 6.17 Plasma concentration versus time profile for II after $[Do]_{it} = 28.2\text{mg}$ intratracheal instillation. The curve illustrated shows the trapezoidal approximations used to determine the area under the curve.

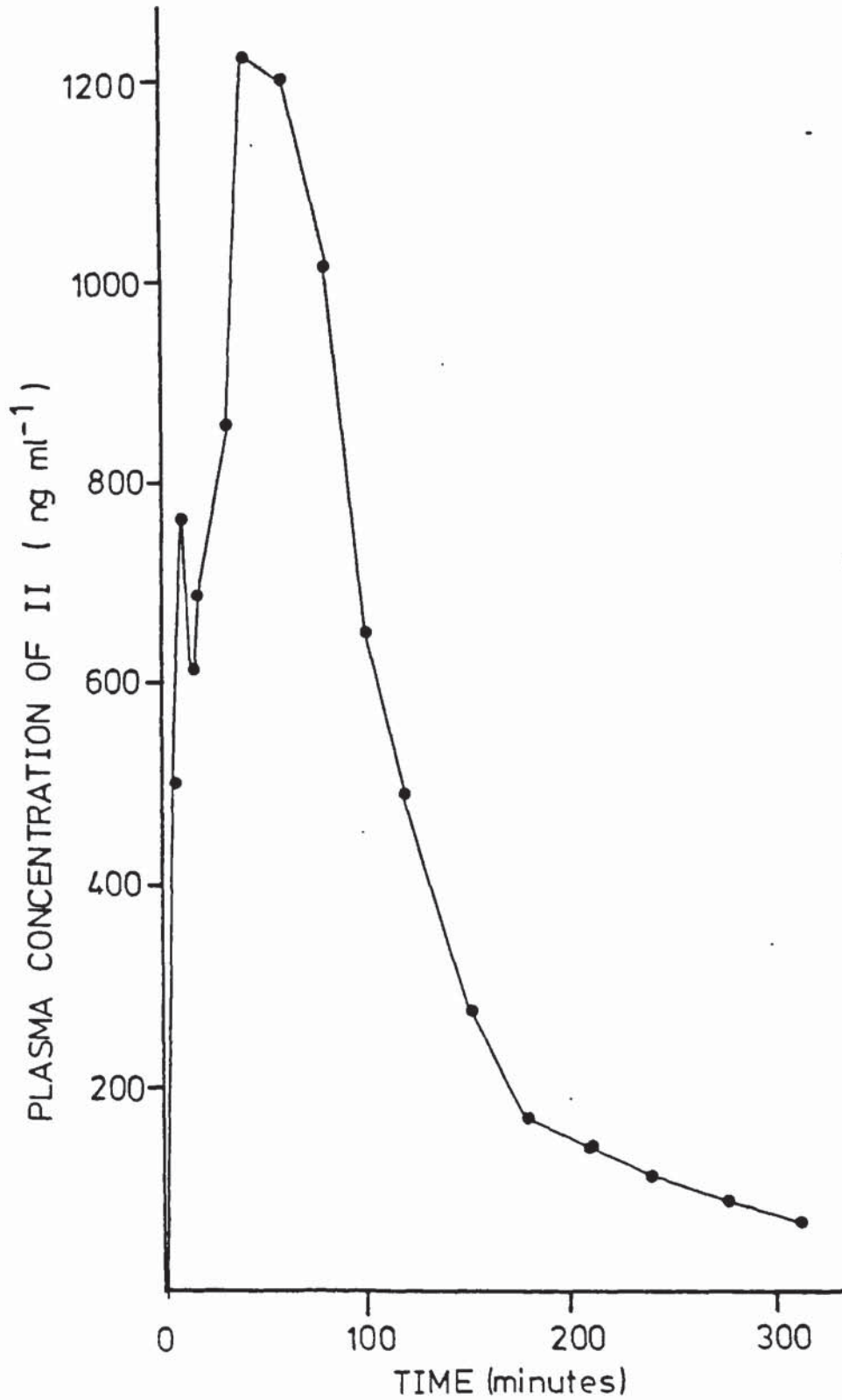


Figure 6.18 Plasma concentration versus time profile for II after $[Do]_{it} = 30.5\text{mg}$ intratracheal instillation. The curve illustrated shows the trapezoidal approximations used to determine the area under the curve.

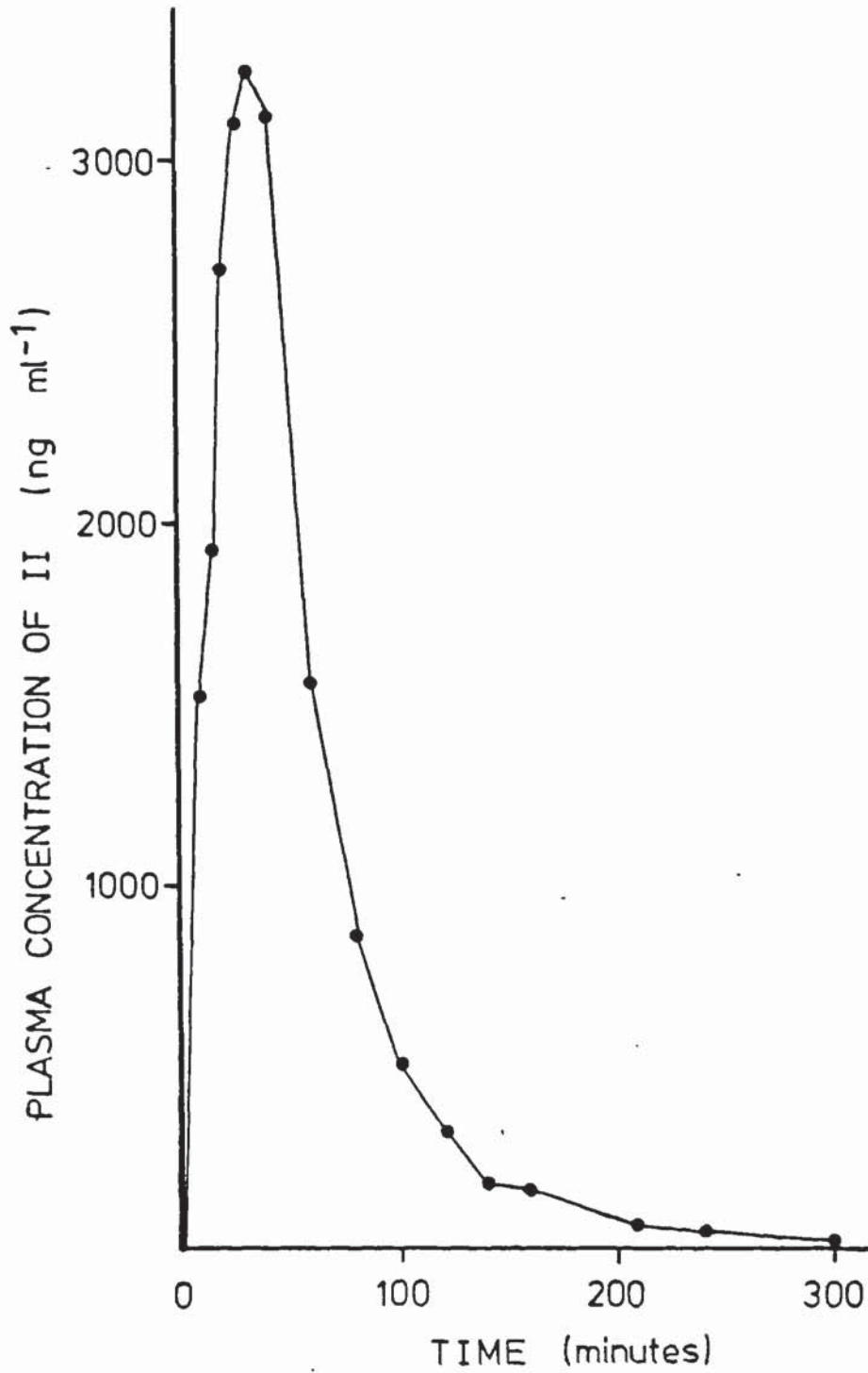
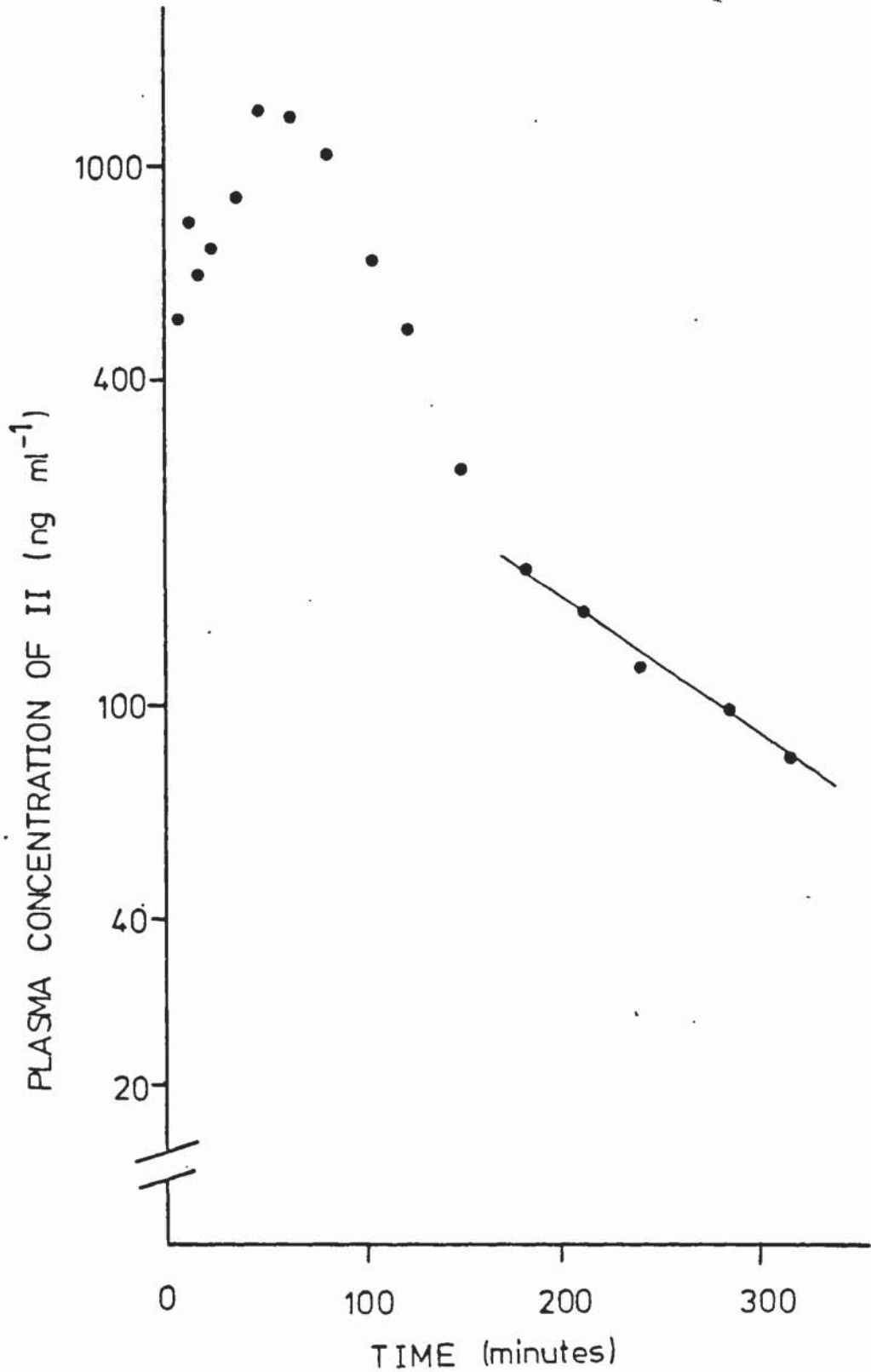


Figure 6.19 Log-Linear plot of plasma concentration versus time for II after intratracheal instillation of an aqueous bolus of 28.2mg. The terminal slope S^1 , determined by linear regression is illustrated by the solid line.



Chapter 7 DISCUSSION AND SUGGESTED FUTURE WORK

In these studies an attempt has been made to quantify the effects of relative humidity on inhalation aerosols. A technique for calculating the change in aerodynamic diameter of particles containing a single water-soluble compound from the physico-chemical characteristics of aqueous solutions of the compound has been described. The results for sodium cromoglycate, isoprenaline sulphate, and isoprenaline hydrochloride and salbutamol sulphate indicate that there are significant deviations from 'ideal' solution behaviour. This was most marked for disodium cromoglycate which undergoes a phase transition from solution to mixed solution and mesophase. This phase change is indicated by a plateau in water activity. The concentration at which this phase change occurs has been shown to be temperature dependent (Cox et al, 1971). Furthermore the water activity at the plateau is higher than the value for isotonic saline at 25° C whereas the converse is true at 37° C. In the light of this observation it is advisable that determinations of isotonic equivalents should be made at physiological temperatures.

The most exact expression for calculating aerodynamic growth ratios takes into account the increased vapour pressure above curved surfaces, the Kelvin effect. For the compounds examined the over estimation in growth ratio if the Kelvin effect is neglected is less than 5% for particles initially greater than 1µm in diameter. As submicron particles are unlikely to occur in appreciable quantities in most currently employed inhalation aerosols reasonable estimates for the

aerodynamic growth ratios may be obtained neglecting the Kelvin effect.

The magnitude of the effect of condensation growth on the site and amount of deposition may be determined by the use of computer models for deposition. The results obtained in this study indicate that for different salts of the same compound the site and amount of deposition may occur even if the initial particle size distribution of the dry particles is the same because of differing physicochemical properties. This type of study may be useful in preformulation studies to identify potential problems of poor pulmonary and systemic availability of pharmaceutical aerosols. (Gonda and Byron, 1978).

For more complex inhalation aerosol formulations comprising of water-soluble and insoluble components the behaviour of the aerosol under high humidity conditions cannot be predicted from the physicochemical measurements for pure drug alone. In this instance direct measurement of size changes with varying humidity is desirable. The cascade impactor is a useful sizing tool for polyphasic aerosols, in that by chemical or radio-chemical assay of the deposits it is possible to examine changes in the size distribution of the species of interest i.e. drug.

The experiments described in Chapter 4 have confirmed the observations of other researchers (Rao and Whitby, 1977a, 1977b, Cushing et al, 1979) that a suitable coating on the collection surface is necessary in order to obtain collection efficiency curves that approach 100% collection efficiency. Even with the most efficient slide coating there was some evidence of a decline in collection efficiency after reaching

a maximum value approaching 100%, presumably through rebound and re-entrainment of the larger particles. In the light of these observations it would be wise to avoid overburdening of the cascade impactor and only collect amounts in the order of the loading limits suggested by Mercer (1966).

Appreciable differences were observed between the experimental calibration performed at operating flow rates and the calibration supplied by the manufacturer. These observations indicate the necessity of calibration at the operating flow rates.

In practise it is difficult to achieve the degree of temperature control required to maintain the relative humidity experienced within the respiratory tract. For example in order to obtain the growth ratio of a single water-soluble compound with an accuracy of 5% at 99.5% relative humidity would require temperature control within $\pm 0.015^{\circ}\text{C}$ at 37°C (Gonda et al, 1981). Correspondingly, studies on the effect of relative humidity on the particle size of aerosol are performed at sub-physiological humidities. The temperature in the controlled temperature and humidity cabinet used in these studies could be controlled to $\pm 0.05^{\circ}\text{C}$ at 37°C . The major problem in the use of this apparatus arises from the addition of carrier gas bringing aerosol into the equilibrium chamber perturbing the previously established humidity. However good correlation was observed between the observed growth ratio for fluorescein disodium aerosols and that predicted from physicochemical measurements of aqueous fluorescein disodium solutions. A more constant humidity level could be achieved by the use of a

continuous mixing system and a reduction in carrier gas entering the equilibrium chamber.

It may be possible to retard condensation growth by the inclusion of water-insoluble films on aerosols. Surface active films have been found to retard droplet evaporation rates by several orders of magnitude (Snead and Zung, 1968; Eisner et al, 1960). The compounds used to potentially retard condensation growth on pharmaceutical aerosols must be carefully considered on toxicological grounds. The lungs are coated with a natural surfactant, lecithin, which may prove satisfactory from both a physical and toxicological view point in preventing or retarding condensation growth. The effect of humidity on coated particles could be examined using a controlled temperature and humidity apparatus. Differences in growth ratios will however only be observed if the coat retards the rate of condensation growth by at least an order of magnitude.

Using the data presented in chapter six the systemic availability of fluorescein disodium subsequent to its administration in various inhalation aerosol formulations *maybe estimated*. There is some evidence that the rate of absorption may vary with the site of deposition (Schanker, 1978), it would therefore be expected that the systemic availability of fluorescein disodium effectively coated with a condensation retarding agent will differ from the untreated dry powder.

Appendix 1

Water activity of solutions used to calibrate the vapour pressure osmometer.

Sodium Chloride

Concentration mol kg ⁻¹	Water activity at 25° C	Reference	Water activity at 37 C	Reference
0.0064	.9997757	1	-	
0.0256	.9991204	1	-	
0.0576	.9980498	1	-	
0.1	.996646	2	.9966 4(9)	
0.2	.993360	2	.9933 6(6)	
0.3	.99009	2	.9900 9(5)	
0.4	.98682	2	.9868 (15)	
0.5	.98355	2	.9835 (3)	
0.6	.98025	2	.9802 (2)	
0.7	.97692	2	.976(8 8)	
0.8	.97359	2	.9735 (3)	
0.9	.97023	2	.970 (1 6)	
1.0	.96686	2	.9667	3
2.0	.9316	2	.9312	3
3.0	.8932	2	.8926	3
4.0	.8515	2	.8510	3
5.0	.8068	2	.8068	3
6.0	.7598	2	.7606	3

linear interpolation
between data from
references 2 and 3 (50° C
data)

Potassium Chloride

Concentration (mol kg ⁻¹)	Water activity at 25° C	Reference
0.1	0.996668	2
0.2	0.993443	2
0.3	0.99025	2
0.4	0.98709	2
0.5	0.98078	2
0.6	0.98078	2

Calcium Chloride

Concentration (mol kg ⁻¹)	Water activity at 25° C	Reference
0.1	0.99540	2
0.2	0.99073	2
0.3	0.98590	2
0.4	0.98086	2

Sucrose

Concentration (mol kg ⁻¹)	Water activity at 25° C	Reference
0.1	0.99819	2
0.2	0.99635	2
0.3	0.99449	2
0.4	0.99260	2
0.5	0.99068	2
0.6	0.98874	2
0.7	0.98676	2
0.8	0.98475	2
0.9	0.98272	2
1.0	0.98065	2

References

1. Robinson and Stoke 1959a
2. Robinson and Stoke 1959b
3. Gibbard et al 1974

Appendix 2

Calibration curves for the Knauer vapour pressure osmometer Percentage full scale deflection versus negative natural logarithm of water activity

<u>Temperature</u>	<u>Sensitivity setting</u>	<u>Slope</u>	<u>Intercept</u>	<u>Correlation coefficient</u>
25	2	337	+ 1.29	0.998
25	16	3329	- 0.8	0.998
25	32	6754	- 0.4	0.998
25	64	14506	- 1.2	0.999
37	2	412	+ 1.8	0.999
37	32	8434	- 1.5	0.999

Proportional Power Controller

Proportional controllers are those which deliver a variable fraction of their maximum power output. The actual amount of power depends upon an error voltage - the larger the error, the greater the power output. The power output corresponding to zero error voltage can usually be adjusted over a range from 1 to 99% of full power, though the ideal state would be near 50%.

The magnitude of the error voltage is compared with a ramp (sawtooth) waveform. In the case of the L121 zero voltage switch, which is the control element in this design, the ramp waveform started about 1 volt (referenced to mains NEUTRAL), and increases to about 6 volts before being reset to 1 volt and starting again. The time taken for one ramp cycle determines the resolution of the power control - when the error voltage is less than the ramp voltage, the power is on, and when the error voltage is greater, the power is off. With a one second ramp cycle time, the smallest amount of power that can be let through is one half mains cycle, the largest amount being 99 half cycles out of the 100 occurring in that second. The other alternatives are that the power is fully off, or fully on - so no control is possible.

External components determine the gain properties of the operational amplifier that is used to produce the error voltage, and the frequency of the ramp oscillator. These components, together with a detector for turning the parameter to be controlled into a suitable current or voltage, make up the control part of the circuit. The two other parts of the circuit are the power supply for the zero voltage switch, comprising one power resistor as a mains dropper and two smoothing capacitors, and the triac protection which comprises a R-C network which limits the maximum rate of rise of voltage on the triac terminals. The triac itself, is a semiconductor switch which, once triggered, stays on until the current passing through it drops below the holding current. Since mains power is alternating, the current should change polarity every 20 milliseconds or so, and this turns the triac off. The R-C network is also intended to make sure that the triac does turn off. The zero voltage switch will then turn the triac on again while the voltage is close to zero in accordance with the error signal/ramp voltages. This technique reduces the amount of radio frequency interference reflected into the mains supply, and also reduces the amount of switching

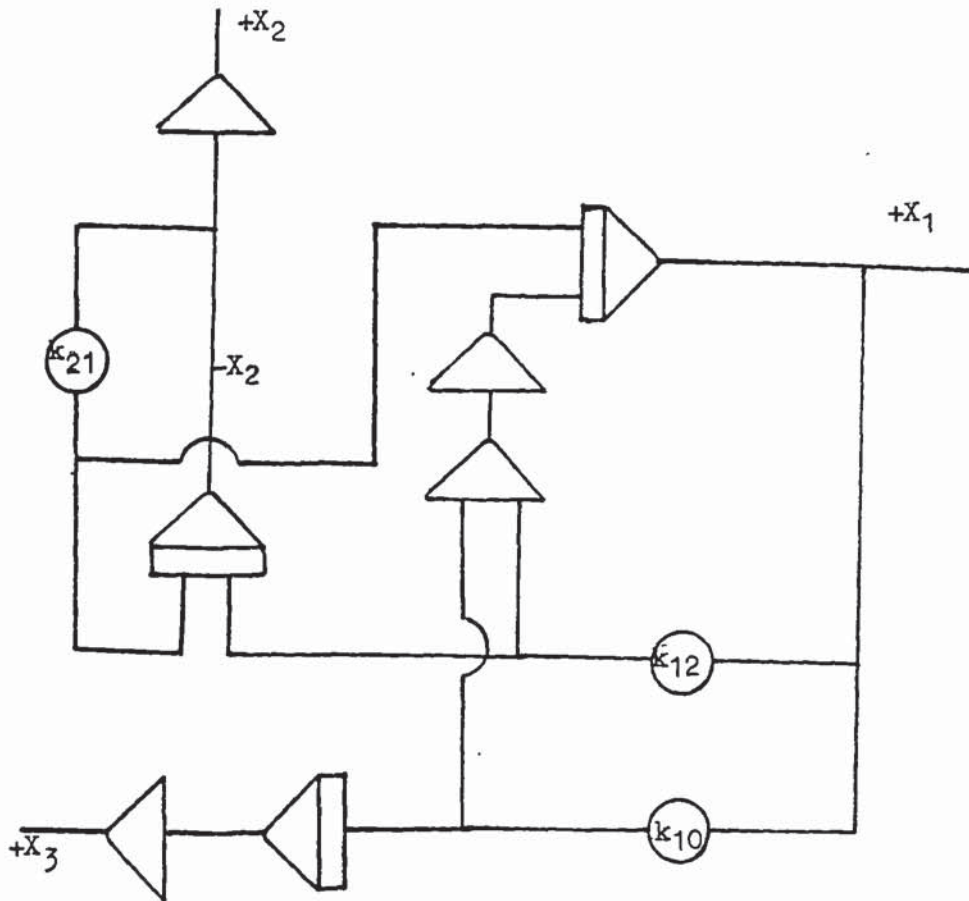
work that the triac has to do- giving a lower power dissipation and better reliability.

In this design, a thermistor is used to detect temperature in such a way that an error voltage varying from 1 volt at 70°C to 6 volts at about 28°C. This determines the range of the controller. It is important to realise that an alteration in the temperature will produce an alteration in the output power. This will tend to bring the temperature back towards its control value, but an alteration in the amount of power required to maintain a given temperature - say a draught - will alter the control setting required to maintain the desired temperature. It is only possible to adjust the range between fully on and fully off by adjusting the gain of the operational amplifier. A high gain will give a narrow range, but any drift in component values will be accentuated as well. If in doubt, - use a thermometer!

WARNING: This device is not isolated from the mains. Thermistor connected to mains NEUTRAL. Heater power output is mains LINE and switched NEUTRAL.

Appendix 4

Analog computer circuitry to model two-compartment open body model
(Scheme 6.1)



Potentiometer



Operational Amplifier



Integrator

Appendix 5 Publications

C.V. Groom, I. Gonda and F J T Fildes

'Prediction of equilibrium aerodynamic diameters of inhalation aerosols'
2nd Int. Conf. Pharm. Technol., APGI, Paris 5 p 124-131, 1980

C .V. Groom and I. Gonda

'Equilibrium diameters of inhalation aerosol droplets'
J. Pharm. Pharmacol. 32 (Suppl) 1P, 1980

C.V. Groom and I. Gonda

'Cascade impaction: the performance of different collection surfaces'
J. Pharm. Pharmacol. 32 (Suppl) 93P, 1980

I, Gonda and C.V. Groom

A data inversion method for sizing using a calibrated cascade impactor
in International symposium on Deposition and clearance of Aerosols in the
Human Respiratory Tract' GAF and IGAeM, Bad Gleichenberg, Austria, 22/23
May, 1981.

I. Gonda, JB Kayes, C.V. Groom and FJT Fildes

'Characterisation of hygroscopic inhalation aerosols'
to be presented at Particle sizing conference, Loughborough September,
1981.

A.R. Clark, PR Byron and C.V. Groom

'Fluorescein pharmacokinetics in the beagle'
to be presented at British Pharmaceutical Conference September 1981.

Page removed for copyright restrictions.